PATTERNS OF TOTAL STRAIN IN THE WALLS OF TWO GREENSTONE ASSEMBLAGE BOUNDARIES, WESTERN BIRCH-UCHI (CONFEDERATION LAKE) BELT, NW ONTARIO

by

MICHAEL JAMES CREWS

A Thesis submitted in conformity with the requirements
for the degree of Master of Science
Graduate Department of Geology
University of Toronto

PATTERNS OF TOTAL STRAIN IN THE WALLS OF TWO GREENSTONE ASSEMBLAGE BOUNDARIES, WESTERN BIRCH-UCHI (CONFEDERATION LAKE) BELT, NW ONTARIO

Master of Science, 1999
Michael James Crews
Department of Geology, University of Toronto

Abstract

The boundaries between the Balmer-Woman and Woman-Confederation assemblages are well exposed in western central parts of the Birch-Uchi belt. Based on zircon dates for the felsic metavolcanics, age gaps of *ca.* 100 Ma between the assemblages were recognized by others. The results of the present structural analysis suggest that boundary slip was kinematically insignificant during regional ductile deformation, and did not lead to omission of rock strata or production of large age gaps. Nothing can be said, however, about the possible effects of (i) brittle faulting at early stages of tectonism or (ii) discomformable deposition of the basal strata of the assemblages. Detailed study of effects of total strain furnishes structural data that permit qualitative and quantitative assessments of the displacement field associated with ductile deformation. Applying the stretching-fault concept to the study area, distributed tangential-shear strain at the Balmer-Woman assemblage boundary proves to have the sense of thrust faults (hanging wall of Woman assemblage rocks to the NW). By contrast, the distributed tangential-shear strain at the Woman-Confederation assemblage boundary has the sense of sinistral faults (hanging wall of Confederation rocks to the north). This result is compatible with elements of the northward transportation hypothesis for the Birch-Uchi belt.

ACKNOWLEDGMENTS

The author would like to thank Dr. W.M. Schwerdtner for his research guidance and all-around supervision of the M.Sc. project. Dr.'s A.R. Cruden and E.T.C. Spooner are thanked for their scientific help and constructive criticism of thesis drafts. Grants from NSERC and LITHOPROBE were used to finance the thesis research, and the Ontario Geological Survey provided equipment to carry out the fieldwork. G. Filomene acted as field assistant in 1996 and his contribution is gratefully acknowledged. Thanks are due to B. Atkinson and C. Storey at the Resident's Geologist office in Red Lake for facilitating the field activity. Mike and Julie Hoffman of Canada North Lodge are thanked for their hospitality and logistic support. Dr. P-Y.F. Robin and Doug Ciceri are thanked for their assistance with part of the thin section analysis. The help provided by Chris Rancourt is appreciated. Andrew Conly assisted with pagination, while Karyn Gorra helped with plate preparation at the University of Toronto. I would like to thank my parents, Cy and Jane, for their loving support and finally, I would like to thank my Fiancé, Kathy, for her love, patience and support during the long preparation of the thesis.

TABLE OF CONTENTS

LIST OF TABLES

LIST OF PLATES

LIST OF FIGURES

APPENDICES

CHAPTER I

INTRODUCTION

PATTERNS OF TOTAL STRAIN IN THE WALLS OF TWO GREENSTONE ASSEMBLAGE BOUNDARIES, WESTERN BIRCH-UCHI (CONFEDERATION LAKE) BELT, NW ONTARIO

I. INTRODUCTION

1.1 Tectonic Models and Principal Objectives

Greenstone assemblages make up the greenstone belts of the northwestern Superior Province (Figure 1). The three assemblages of the Birch-Uchi belt, whose felsic rocks differ greatly in absolute age (Figure 2, Stott & Corfu 1991), were initially considered as in-situ products of successive volcanic cycles (Thurston 1985). However, recent structural, geochemical, and geochronological evidence suggests to some workers that the assemblages have been juxtaposed tectonically (Williams *et al.* 1991). Results of the present study will help in discriminating whether the apparent jumps in protolith age at the assemblage boundaries resulted mainly from dislocation of rock masses in the ductile realm or brittle type faulting/long breaks in deposition of volcanics and sediments. This information will help in gaining a better understanding of Archean tectonics in the Uchi subprovince.

Williams *et al.* (1991) proposed a conceptual model of Archean accretionary tectonics for the Superior Province. They envisaged a hypothetical series of tectonic events as recognized in modern collisional orogeny. Davis (1997) formulated a different accretionary model compatible with results of detailed geochronological studies. He suggested that the Wabigoon and Wawa subprovinces are parts of one extensive island arc complex. Accordingly, only the Uchi-English River subprovince boundary is a collisional suture (Davis 1997, 1998). This is supported by new U-Pb zircon dates and petrologic data that point to a continuous system of volcanic and sedimentary rocks between the English River subprovince and the Wabigoon subprovince (Cruden *et al.* 1997, 1998). In agreement with Davis'(1997, 1998) model, Cruden *et al.* (1997,

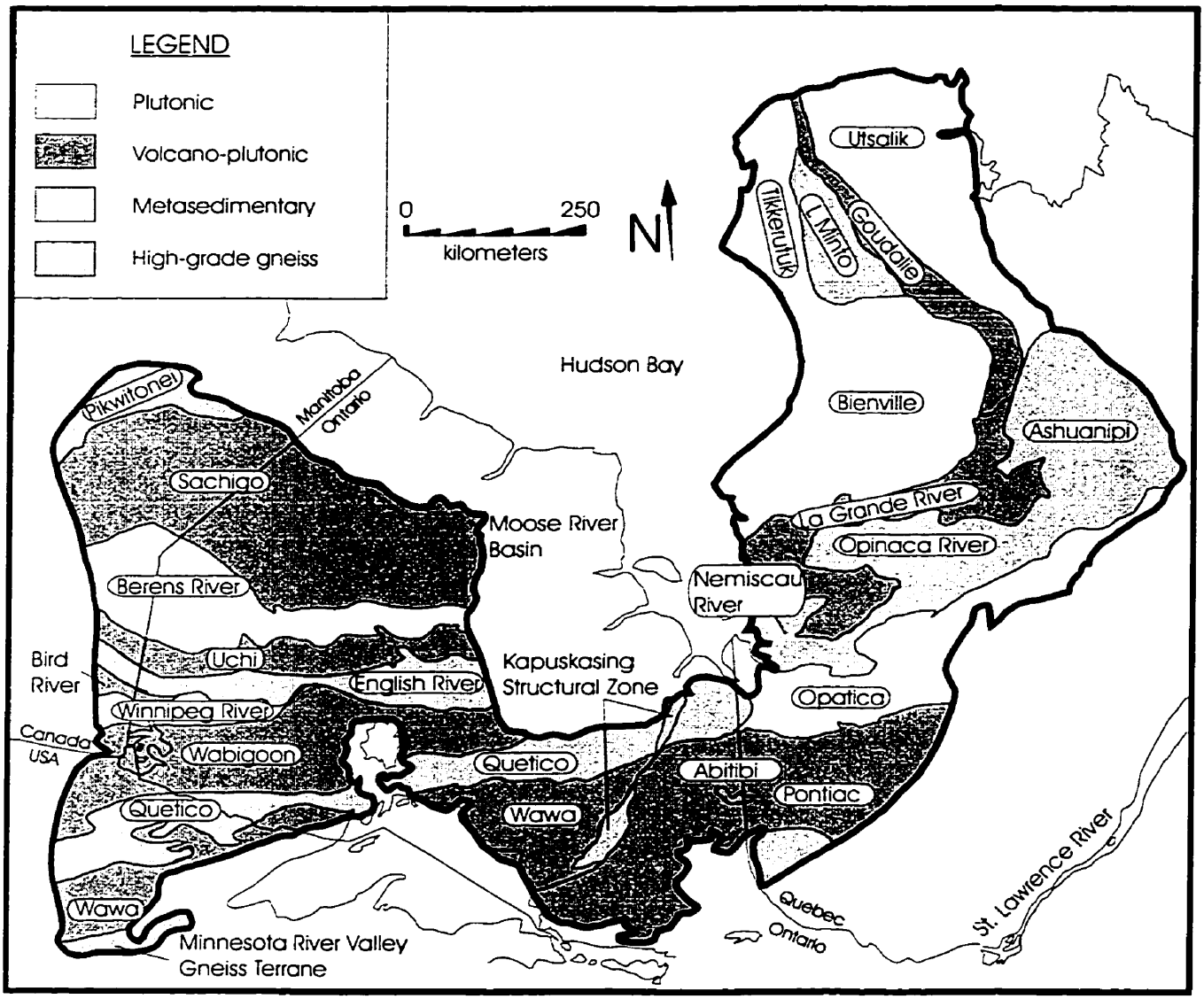

Generalized geology of the Superior Province (modified from Card & Ciesielski 1986, Stott 1991, Thurston 1991, Percival et al. 1992).

Figure 1

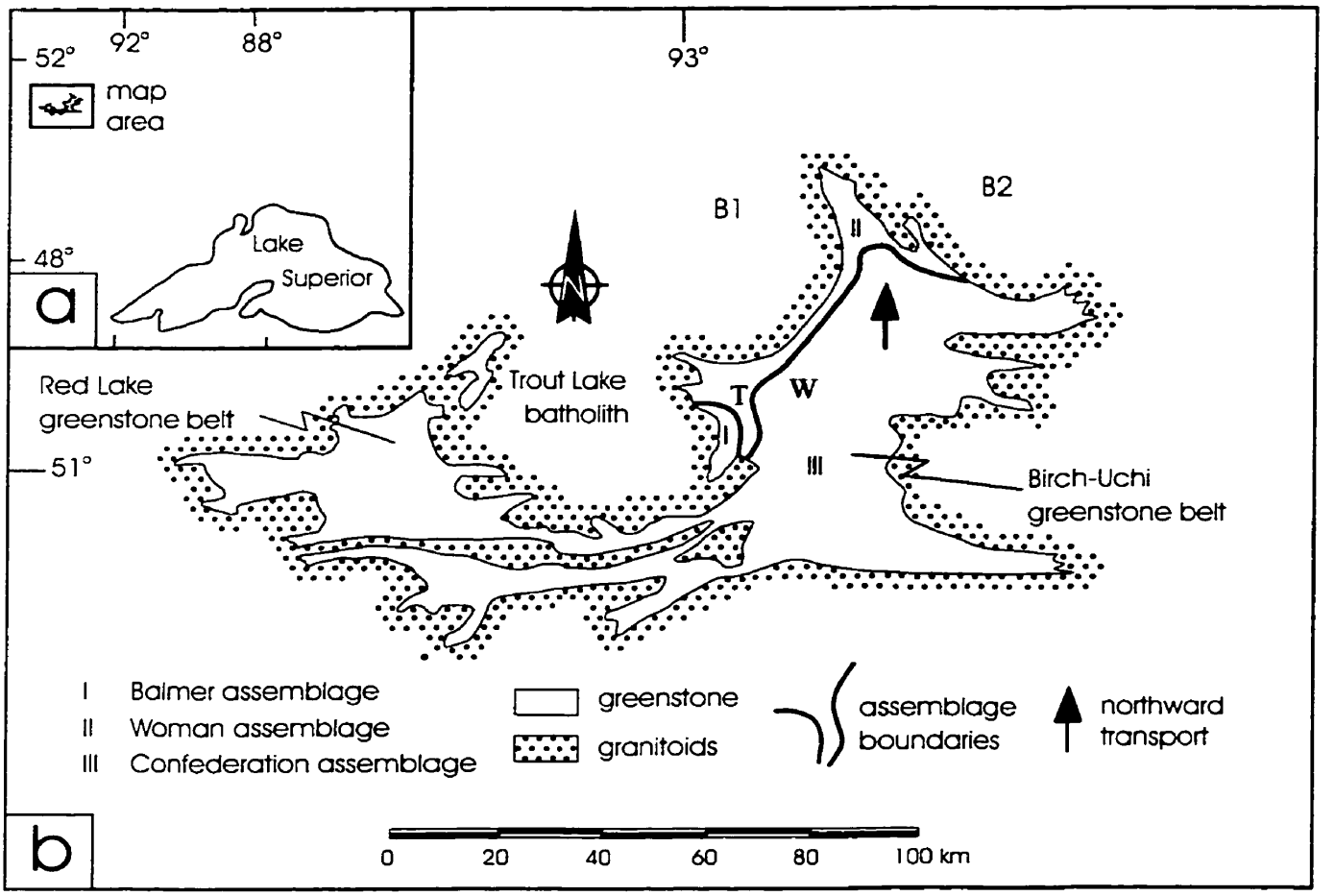

Red Lake-Birch-Uchi greenstone belts and vicinity; B1, B2 granitoid batholiths
T = centre of triple junction in foliation (schistosity) pattern and the strain field
W = Washagomis Lake

Figure 2

1998) conclude that the English River, Winnipeg River and Wabigoon subprovinces had a common tectonic history from at least 2717 Ma. onwards. The present geometry of greenstone-granite systems is attributed to horizontal tectonics and associated emplacement of tabular plutons (Cruden & Robin 1998). Other geologists, however, interpret the Archean granite-greenstone map pattern as a product of vertical granite diapirism, without significant horizontal tectonism in the upper crust (e.g. Macgregor 1951, Hamilton 1998a & b).

The main objective of this thesis is to assess the structural significance of two greenstone assemblage boundaries within the Uchi Subprovince, and provide a better understanding of the mechanical behaviour of such boundaries during ductile deformation. Available structural models such as the northward transportation hypothesis (Stott & Corfu 1991) will be tested in the Birch-Uchi greenstone belt by deriving the local sense and magnitude of total shear strain in wall segments of the two lithotectonic boundaries (LTBs; Crews & Schwerdtner 1997, Schwerdtner 1998). The northward transportation hypothesis (Figure 2; Stott & Corfu 1991) is part of an accretionary model for the Uchi and Wabigoon subprovinces of NW Ontario. Structural field and laboratory data gathered in the present study of assemblage boundary walls will form the basis for the structural testing of this hypothesis in the western Birch-Uchi belt.

1.2 Structural Models and New Concepts

Stott and Corfu (1991) hypothesized that the northward transport of the Confederation assemblage mass (Figure 2) was accomplished by two heterogeneous deformations (D_1, D_2), on the scale of the Birch-Uchi belt. D_1 created the N-S structural grain in the greenstone belt mainly by northward translation and rotation of rock strata. These displacements were thought to

> "have accompanied the aggregation of the assemblages after 2730 Ma, during collision between the Uchi-Sachigo and Wabigoon-Winnipeg River superterranes. The northward

> transport is conceived to have been in the form of a fist-like, northward closing protrusion of the [Confederation] assemblage, which overrode part of the Woman assemblage. Conceivably associated with this northward transportation event in the Birch-Uchi greenstone belt is the second deformation. D_2 schistosity strikes eastward and dips moderately to steeply southward carrying a shallowly plunging stretching lineation which is generally masked by the steeper D_1 lineation" (Stott and Corfu 1991, p. 198).

Crews and Schwerdtner (1997) found that in western central parts of the Birch-Uchi belt that the trajectories of schistosity and total strain are markedly curved, i.e. the local strike changes gradually from E to NNE. On the kilometre scale, the walls of both assemblage boundaries are ductilely deformed by multi-order folding and passive straining (Schwerdtner *et al.* 1997, 1998a, 1998b).

The assemblage boundaries may have been incoherent at some stages of ductile deformation, but were probably more akin to three-dimensional stretching faults (Means 1989) than to brittle type dislocations. To underline this vital point and guide the reader's thinking away from the image of classical translational structures, Means emphasized on page 893 of his article that stretching faults are "entirely embedded in flowing rock masses." Such faults "may be old or new fractures of any kind, bedding planes or other interfaces between rock masses. The flow [of wall rocks] associated with the faulting is not a response to slip, but an independent process driven by the same remote loads as are causing the slip." By contrast, Stott and Corfu (1991) seem to emphasize rigid-body displacements (translation and rotation) in formulating the northward transportation hypothesis. To compare the results of the present study with chief elements of the hypothesis, it will be necessary to change emphasis from rigid-body displacements to strain-related displacements (cf. Ramsay and Huber 1983, p.55-72).

1.3 Research Program and Recent Ideas

The study area includes most of Bear Lake, southern and central parts of Woman Lake and adjacent smaller lakes (Figure 3, 4). Here the assemblage boundaries are folded on various scales and well exposed on Spot and Woman Lakes. However, the locus of the Woman-Confederation assemblage boundary may differ from that proposed by Thurston (1985) and Stott & Corfu (1991). New geological and geochemical evidence suggests that the Woman-Confederation boundary may lie east of Woman Narrows and partly coincide with the Rowe Lake shear zone (RLSZ, Rogers *et al.* 1999; Figure 3). Further to the north, the boundary may depart from the RLSZ and follow the stratigraphic base of a folded metasedimentary unit composed partly of metaconglomerate (Crews *et al.* 1998). Opinions differ as to what the Balmer-Woman and Woman-Confederation assemblage boundaries may represent. Thurston (1985) suggests that both assemblage boundaries are disconformities that formed as a result of a long pause in volcanic deposition and were later folded during ductile deformation. Stott & Corfu (1991) propose that the boundaries acted as major thrust surfaces. Alternatively the boundaries may have formed through a combination of both mechanisms leading to an apparent gap in the stratigraphic record. In other words, the "missing strata" were either not deposited or removed tectonically. Recently, van Staal (1998) and Rogers *et al.* (1999) have ruled out any type of major faulting at the assemblage boundaries.

Metagabbroic bodies occur in all three assemblages (Rogers *et al.* 1999), and appear to be parallel to mineral schistosity at many localities (Pryslak and co-workers 1970, 1971). In the Spot Lake area (Figure 3) metagabbroic bodies transect the Balmer-Woman (I-II) assemblage boundary trace without being offset or deflected. Metagabbro sheets appear to be largely unstrained at most localities (Crews & Schwerdtner 1997), but may have accumulated a few

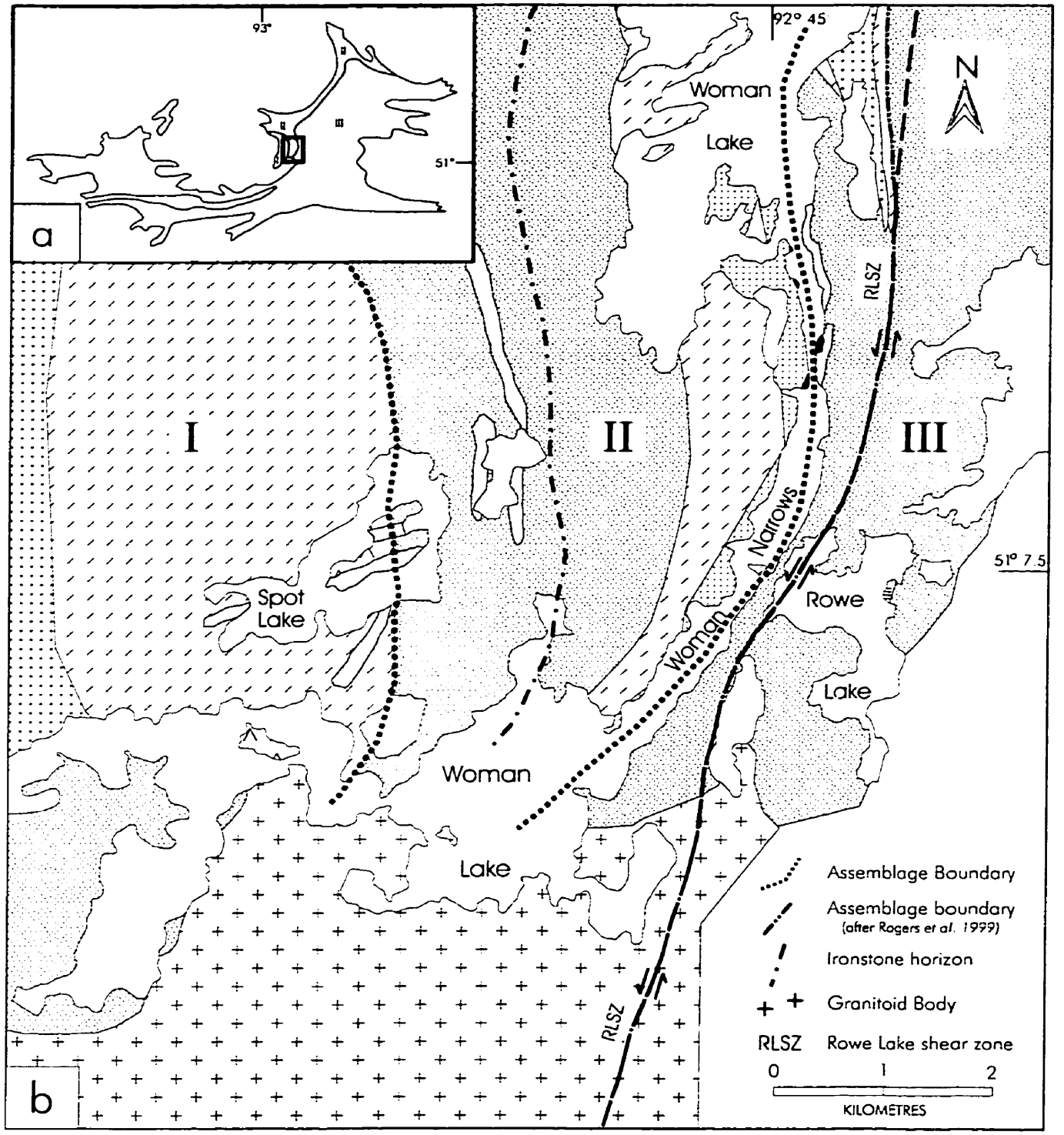

Mafic metavolcanics

Intermediate meta-volcanics/pyroclastics

Felsic metavolcanics & pyroclastics

Metasediments

Granites

Qtz-feldspar porphyry

Marble

Metagabbros

Figure 3
(modified from Pryslak 1971, Thurston 1985, Rogers et al. 1999)

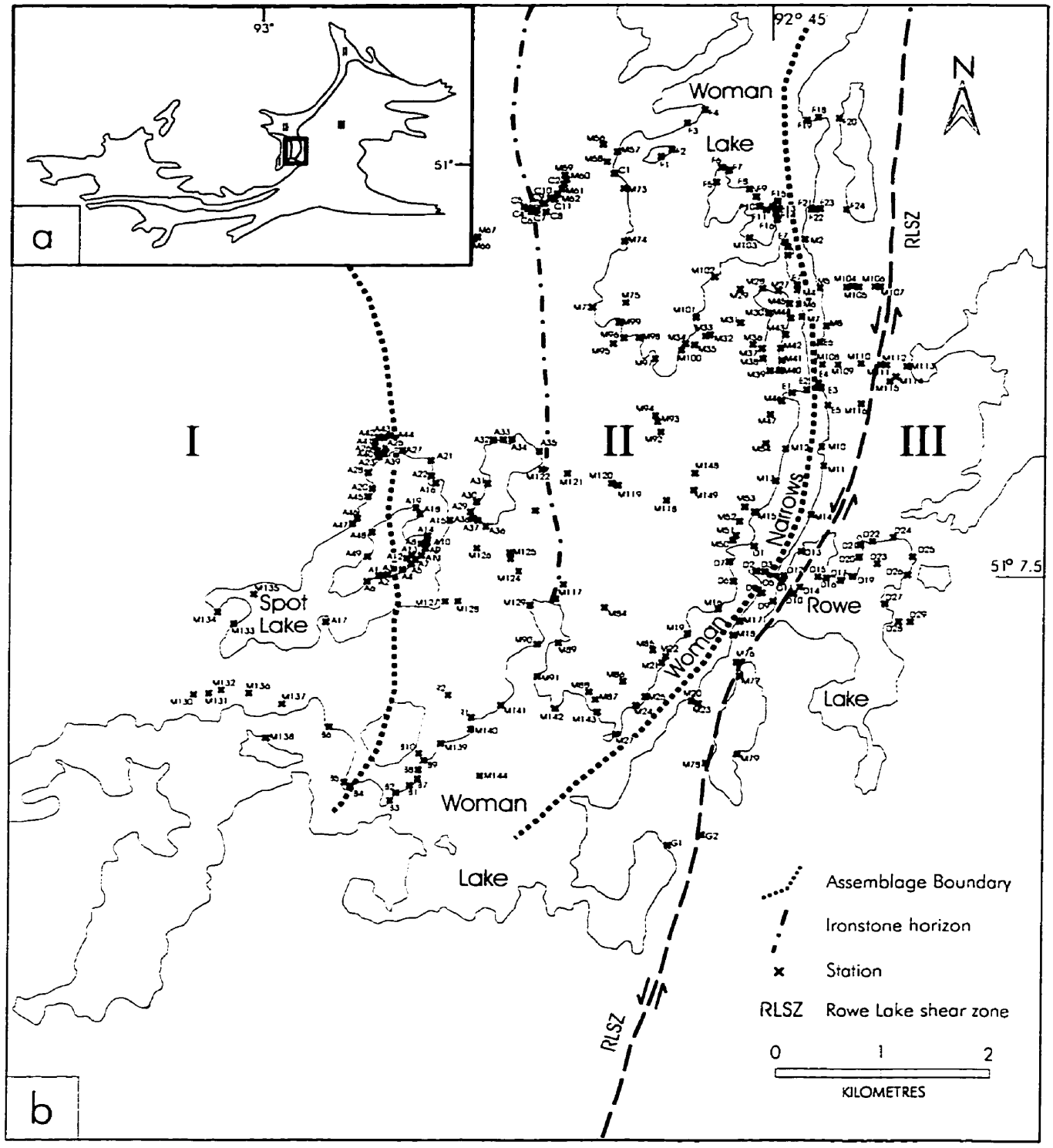

Figure 4
Station location map
(modified from Stott & Corfu 1991, Rogers et al. 1999)

percent of strain. To elucidate the strain and fabric pattern in metagabbro, the anisotropy of magnetic susceptibility (AMS) was analysed in parts of a well-exposed, leucogabbroic sheet with relict igneous textures. The main purpose of this AMS study was to detect subtle fabric changes and associated strain gradients across the Spot Lake segment of the Balmer-Woman assemblage boundary (Figure 3).

The total strain is a net result of the entire ductile deformation of a rock volume. Principal magnitudes of total strain are generally estimated by using deformed primary features such as ductile pebbles, lapilli or igneous mafic clots. To aid in determining the local sense of total shear strain in the boundary walls, foliation (S) and mineral lineation (L) attitudes were gathered throughout the study area. The map pattern of L-S attitudes aids greatly in the determination of shear strain magnitude in the walls of the two assemblage boundaries (Schwerdtner *et al.* 1997). Preliminary field evidence had shown that, like the shape fabric of primary features, the mineral fabric resulted from the total ductile deformation of the supracrustals in the western Birch-Uchi belt (Crews & Schwerdtner 1997). Additional data were obtained in 1998 (Crews *et al.* 1999, Borowik *et al.* 1999), and are included in this thesis.

CHAPTER II

BACKGROUND INFORMATION

II. BACKGROUND INFORMATION

2.1 Introduction

Despite over 100 years of geological research, the structural evolution of greenstone belts is still controversial (de Wit & Ashwal 1997, Hamilton 1998a). The controversy results partly from differences in thinking amongst two rival groups. The first group focuses on the similarities between Archean and Phanerozoic rock assemblages and the second dwells on the differences between these assemblages (e.g. Windley 1993, Burke 1997, De Wit & Ashwal 1997, Hamilton 1998a).

This chapter provides a summary and discussion of two end-member models of greenstone belt genesis put forward by the rival groups, and outlines the geological history of the Uchi subprovince in general (Figure 1) and western Birch-Uchi greenstone belt in particular (Figure 2).

2.2 Rock Types and Tectonostratigraphic Correlation

2.2.1 Introduction

The Birch-Uchi greenstone belt is located within the Uchi-subprovince (Figure 1, 2, Ayres *et al.* 1971), and consists of metavolcanic and metasedimentary rocks locally intruded by Archean granitoids (Nunes and Thurston 1980; Thurston and Fryer 1983, Fyon & Lane 1986, Good 1988, Beakhouse 1989, Williams *et al.* 1991, Devaney 1997). The greenstone belt extends 84 km to the north and is 32 km wide in an E-W direction (Goodwin 1991, Gupta & Wadge 1986). Thurston & Fryer (1983) have computed a total stratigraphic thickness of 8500 to 11240 m, but this amount depends critically on correct interpretation of the regional fold pattern. Metasedimentary English River rocks border the belt to the south, whereas granitic rocks

surround the belt to the east, west, and north (Ayres *et al.* 1971, Thurston and Breaks 1978, Thurston and Fryer 1983).

Three volcano-sedimentary assemblages have been recognized in the Woman-Confederation Lake area (Goodwin 1967, Pryslak & co-workers 1969, 1971, Thurston 1985). The assemblages are called, in order of decreasing depositional age, Balmer (I), Woman (II), and Confederation (III) (Figure 2). The age difference between the top strata of the assemblages is *ca.* 100 Ma (Nunes and Thurston 1980, Thurston & Fryer 1983); however, the duration of individual depositional cycles and the length of the time gaps between the assemblages are unknown (Wallace *et al.* 1986). Each assemblage represents a distinct cycle of volcanism containing tholeiitic pillowed basalts and andesitic flows overlain by intermediate pyroclastics and volcanic flows which are topped by rhyolitic pyroclastics and minor flows (Thurston 1985, Fyon & O'Donnell 1986). Rocks of all assemblages have been metamorphosed to the greenschist facies and locally to lower amphibolite facies as indicated by the Abukuma type regional metamorphic mineral assemblage present, chlorite and tremolite-actinolite (Thurston and Breaks 1978).

Stott & Corfu (1991) interpret Thurston's (1985) depositional cycles in the Birch-Uchi greenstone belt as tectonically juxtaposed assemblages, based on similarities with geologic relations in the Red Lake greenstone belt. The concept of a lithotectonic assemblage was first developed in Phanerozoic plate tectonic terrane analysis and applied to volcanic and sedimentary rock units that share a common depositional environment, structural style and age (Tipper *et al.* 1981, Gabrielse & Yorath 1989, Williams *et al.* 1991). Recent workers (Rogers *et al.* 1999) believe that the application of the lithotectonic assemblage concept in the Uchi Subprovince should be reconsidered. Therefore, the term "greenstone assemblage" will be used in this thesis.

The metamorphic rocks examined in the thesis area during this structural study were identified on the basis of colour. Other studies employ geochemical analysis to provide detailed descriptions of the rock types observed (Goodwin 1967, Pryslak 1971, Thurston 1980, Thurston & Fryer 1983, van Staal 1998, Rogers *et al.* 1999).

The following sections deal with rock types found within the three recognized assemblages of the Birch-Uchi greenstone belt, Balmer, Woman and Confederation assemblages. In addition, the tectono-stratigraphic correlation of these assemblages with other greenstone belt assemblages is discussed.

2.2.2 Balmer Assemblage

The supracrustal rocks of the Balmer assemblage have the oldest protolith ages in the Birch-Uchi greenstone belt and lie adjacent to the Trout Lake batholith (Nunes & Thurston 1980, Rogers *et al.* 1999). The lower portion of the Balmer assemblage consists mainly of pillowed tholeiitic mafic flows and contains some massive basalt. The rocks appear grey-green on fresh surfaces and weather brown-green. Felsic pyroclastic rocks occur as lenses which alternate with the mafic metavolcanics near the southwest end of Narrow Lake. Several diabase and gabbro bodies cut the mafic metavolcanics, which are underlain by layered gabbro near the structural base of the Balmer assemblage (Thurston 1981, Rogers *et al.* 1999). Basaltic to intermediate rocks overlie the mafic metavolcanics and are overlain by coarse intermediate subaqueous pyroclastic breccia of ash flow origin (Thurston 1981). Within the section containing the intermediate breccia are wedges of wacke-argillite metasediments with minor felsic tuffs and fine to medium grained pyroclastic rocks of intermediate composition. At the top of the Balmer assemblage lies a 100-metre unit of siliceous marble with isolated lenses of massive pyrite and pyrrhotite. A unit of chert and sulphide-facies iron formation occurs stratigraphically on strike

(SE) of the marble (Pryslak 1971). Intermediate pyroclastics mark the top of the Balmer assemblage with lithic and crystal tuff, lapilli-tuffs and tuff breccia near narrow Lake and lapilli tuff and tuff at Spot Lake (Plate 1a). However, locally a thin sheet of strongly foliated quartz-feldspar phyric or aphyric dacite/rhyolite forms the structural top of the Balmer assemblage (van Staal 1998).

2.2.3 Woman Assemblage

The Woman assemblage, like the Balmer assemblage, is composed of mafic to felsic volcanics with chemical sedimentary rocks at the top. Tholeiitic pillowed (Plate 1b) and massive mafic flows and their respective coarse-grained intrusive equivalents mark the basal section of the Woman assemblage. On Narrow Lake, these flows lie conformably on the siliceous marble of the Balmer assemblage and are interfingered with intermediate pillowed flows (Thurston 1985). Near the stratigraphic middle of the mafic flows there is a narrow band of oxide-facies iron formation that trends north from medicine rock in the south end of Woman Lake to Narrow Lake (Figure 3). Where exposure is poor the iron formation causes anomalous behaviour of the compass needle. A stratigraphic package containing wacke-argillite sediments continues north along the same trend (Thurston 1984 map, 1985). Rogers *et al.* (1998) discuss the fact that the iron formation implies a pause in volcanism at this stratigraphic position. Varioles/spherules are observed stratigraphically below the iron formation in both pillowed and massive mafic metavolcanics. Varioles/spherules are spherical, mm- to cm-sized felsic bodies that commonly occur in the mafic metavolcanic rocks of most Archean greenstone belts (Gelinas *et al.* 1976). They are commonly termed "ocelli". Overlying the mafic metavolcanics is a succession of intermediate pyroclastic rocks with lapilli and other tuffs containing units of sediments (conglomerate, argillite and wackes). Thurston's (1980) Woman Lake Tuffs, a felsic sequence of

Plate 1

Representative rock types from the Birch-Uchi greenstone belt:
a) contact of weakly deformed lapilli tuff horizon,
b) pillow lava with top direction shown on birch bark,
c) subvertically folded primary layering and foliation in felsic pyroclastics.

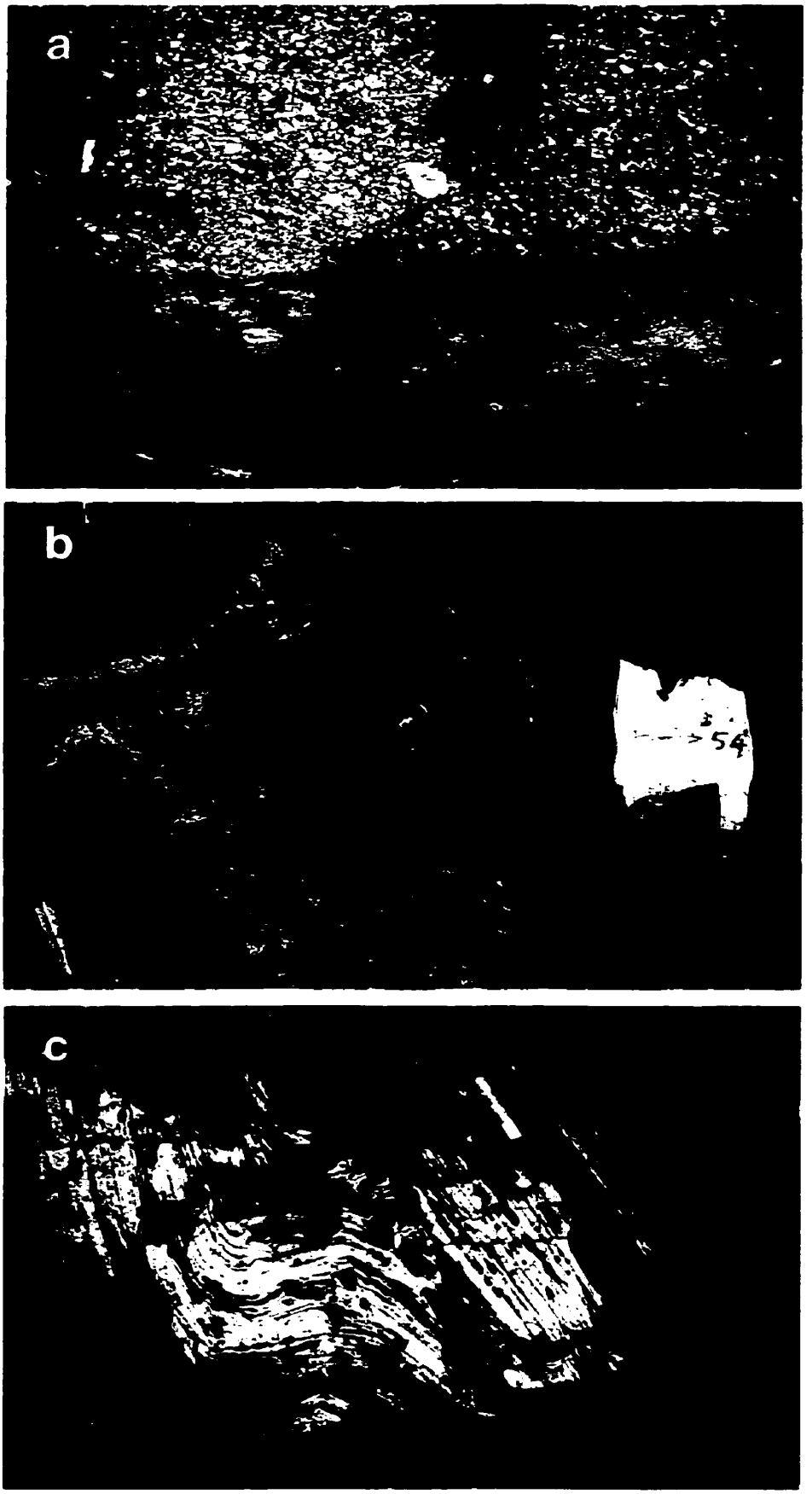

Plate 1

volcanic rocks cap this. These rocks contain felsic lapilli tuff, other tuff and minor tuff-breccia and represent two ignimbrite flow units. The ignimbrite units document a brief period of subaerial volcanism (Thurston 1980). A ~100 metre thick unit of strained stromatolitic marble (indicative of shallow water sedimentation) with minor cherty lenses marks the Woman-Confederation assemblage boundary and overlies the Woman Lake tuffs (Hofmann *et al.* 1985). Although Thurston (1985) mapped the Woman assemblage as a single eastward-facing mafic to felsic sequence, Rogers *et al.* (1999) consider that the Woman assemblage may be a complex of two or more relic greenstone masses. U-Pb age determinations suggest that part of the Woman assemblage can be correlated with an older suite of volcanic rocks (Rogers *et al.* 1999). Geochemical evidence indicates that what was previously mapped as the lower Confederation assemblage may actually be part of the Woman assemblage rocks. This is suggested by similarities between volcanics of the Woman assemblage and the unit in question (Rogers *et al.* 1999).

In 1981, Thurston (1981) completed a stratigraphic correlation between volcanic units in the Birch-Uchi and Red Lake greenstone belts using two lines of evidence, 1) stromatolitic marble units and 2) similar felsic sequences capped by bands of iron formation. U-Pb age determinations gathered to test a tectonostratigraphic model for the Red Lake greenstone belt confirm the correlation (Wallace *et al.* 1986). Thurston (1981) noticed that the stromatolitic marble unit of the Woman assemblage in the Birch-Uchi greenstone belt is very similar to a dolomitic marble sequence on northern McKenzie Island in the Red Lake greenstone belt. Both units are underlain by felsic metavolcanics that have been dated at 2840 Ma and 2830 Ma for the Birch-Uchi and Red Lake units respectively. This indicates that both carbonate units occupy similar time-stratigraphic positions and since stromatolitic occurrences in Archean rocks are rare

it is reasonable to conclude that the units are tectono-stratigraphic equivalents (Thurston 1981, Wallace *et al.* 1986). A mafic to felsic metavolcanic cycle in the Woman assemblage of the Birch-Uchi greenstone belt is capped by chert and iron formation. Thurston (1981) correlated this sequence with similar units in the Red Lake belt indicating that they both were positioned at comparable stratigraphic intervals. Both lines of evidence suggest that the Woman assemblage of the Birch-Uchi greenstone belt can be correlated and may be genetically related with parts of the Red Lake greenstone belt (Wallace *et al.* 1986).

2.2.4 Confederation Assemblage

The Confederation assemblage has a basal unit of mainly tholeiitic basalt that overlies the upper felsic Woman Lake tuff units and the stromatolitic marble unit of the Woman assemblage. This basal unit is both pillowed and massive and contains a prominent variolitic/spherulitic unit. Variolitic/spherulitic rocks were observed by the author along the north shore of Rowe Lake (Figure 3). Also within the basal unit are metasedimentary rocks containing polymictic conglomerates and siltstones (Thurston 1980, Crews *et al.* 1998). Rogers *et al.* (1999) suggest that the sedimentary rocks mark the top of the Woman assemblage, and infer that the sedimentary unit attests to localised erosion and subsidence of the underlying Woman assemblage units. This inference holds true only if the underlying basalt is in fact part of the Woman assemblage. Pillowed basalts and hyaloclastics with minor andesite flows overlie the massive variolitic flows. Above these are intermediate tuff, lapilli tuff and quartz-feldspar-phyric flows with minor rhyolitic flows and tuffs. Marking the stratigraphic top of the Confederation assemblage are felsic pyroclastic rocks such as lapilli tuff and tuff breccia. The top of the Confederation assemblage is disturbed by a fault-bounded graben containing dominantly felsic and intermediate volcanic rocks and their felsic igneous intrusion equivalents such as quartz-feldspar porphyry

which form endogenous domes (Thurston 1985). Above the graben fill are felsic & mafic flows and pyroclastic rocks derived from material left after the collapse of the dome. Thurston (1985), based on symmetrically distributed ages and opposing stratigraphic top directions, put the Confederation assemblage into the core of a synclinorium with an N-S axis. The eastern half of the Confederation assemblage differs from the western half in that it is composed of multiple mafic to felsic cycles rather than one large single cycle (Stott & Corfu 1991). Stott & Corfu (1991) propose that Confederation assemblage rocks have been thrust northward relative to the underlying Woman assemblage rocks. The stratigraphic pattern and current U-Pb age determinations suggest to Stott & Corfu (1991) that the eastern half of the Birch-Uchi greenstone belt and the unit south of the Red Lake greenstone belt may be composed of tectonically repeated members of a single cycle produced by stacking and crustal thickening due to faulting and later folding. Dates obtained by Noble *et al.* (1989) support the idea that the eastern half of the assemblage may be composed of interleaving rapidly deposited, volcanic cycles.

Further study is required to elucidate the true nature of this tectono-stratigraphy and to ascertain the geologic relations in the structurally complex Birch-Uchi belt (Wallace *et al.* 1986, Stott & Corfu 1991, Rogers *et al.* 1999).

2.3 Tectonic Hypotheses

2.3.1 Introduction

The nature of Archean tectonic styles has long been debated. Tectonic models of greenstone belt genesis have become more complex in recent years. Before 1980, transformist/fixist models dominated the literature. These models envisage tectonic processes driven by granite diapirism in the upper crust.

Two decades ago, similarities between greenstone belts and modern arc settings were recognized (Langford & Morin 1976, Williams *et al.* 1991). In the 1980's, improved geochemical, geochronological, geophysical and structural techniques yielded results that spawned a general consensus for the uniformitarian/mobilist way of thinking (Williams *et al.* 1991, Hamilton 1998b). In particular, many authors applied concepts of mobile, horizontal tectonics to the Archean shields, and envisaged processes similar to modern plate tectonics (Platt 1980, Williams *et al.* 1991).

2.3.2 Transformist/Fixist Interpretation (MacGregor/Hamilton)

MacGregor (1951) has been credited with constructing density-inversion models for greenstone belt genesis. Such models are currently supported by Hamilton (1998a,b), Goodwin (1996), and others. The models are based on work on mantled gneiss domes in Finland (Eskola 1948), and suggestions that supracrustal rocks were deposited on a gneissic basement. According to Eskola, the gneisses were reactivated and rose diapirically into the supracrustal rocks. The diapirism was facilitated by rock ductility and driven by differences in gravity between the greenstones and sialic basement (Condie 1993). MacGregor's (1951) density-inversion model was later perfected by Ramberg (1981), who assumed the existence of a sialic crust (Figure 5a). In Ramberg-type models, volcanic supracrustals erupt and cover the gneisses (Marachal & West 198?). In such models the denser mafic volcanics begin to sink and displace the gneissic basement, which is variably remobilized and moves upward during wholesale diapirism (Figure 5b,c; Ayres *et al.* 1991, Hamilton 1998a & b, Schwerdtner *et al.* 1998). The greenstones are crowded aside and sink between these large diapiric batholiths during sag-tectonics, creating dual source areas for sediment (Figure 5c; Glikson, 1971, 1972, Goodwin 1981). This process forms the typical anastomosing complexes of upright synforms found in

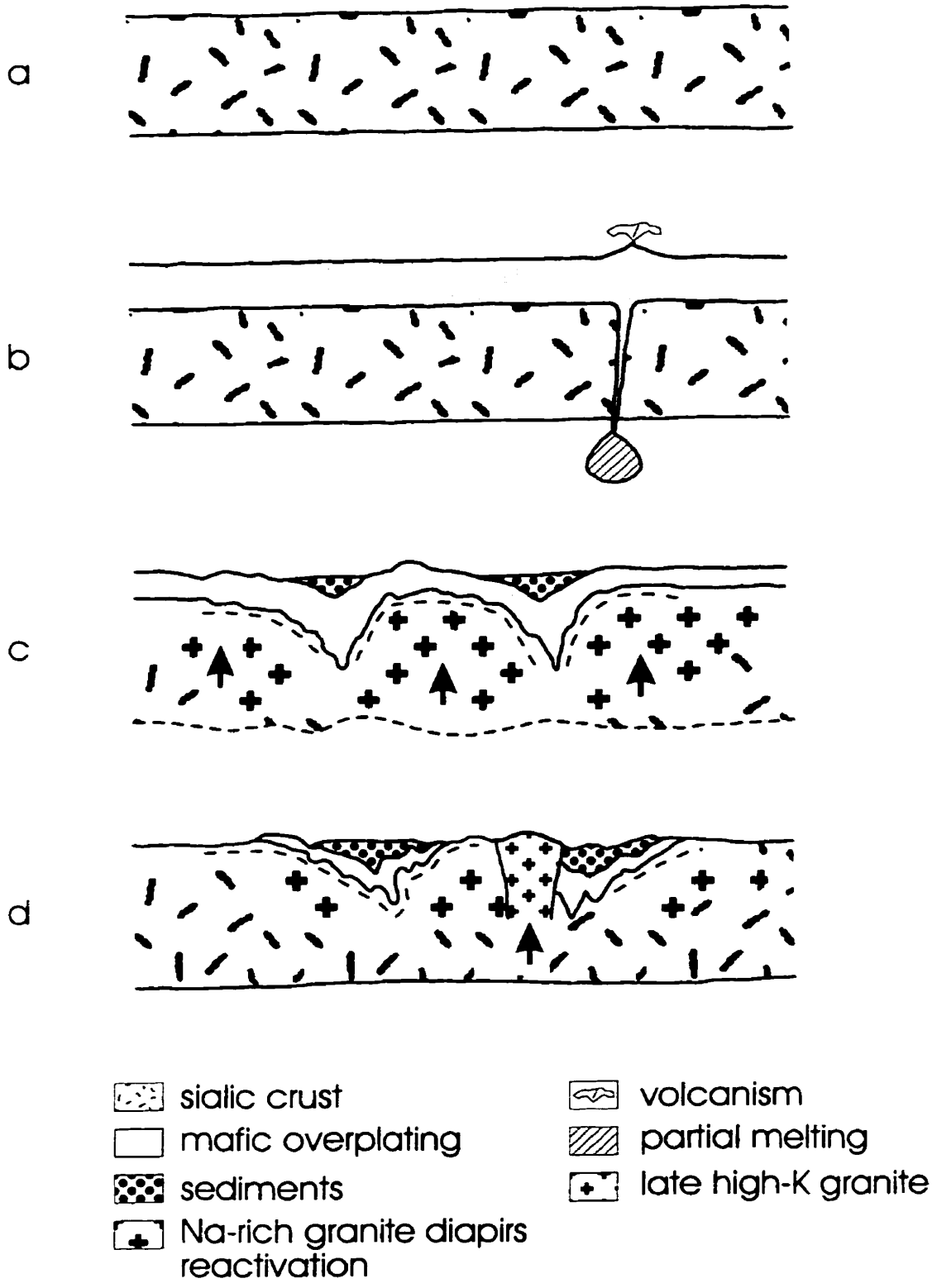

Figure 5
(Modified from Condie 1976)

greenstone belts (Figure 5d; Hamilton 1998a, b). The volcanic rocks of greenstone belts formed as a regional "veneer" and underwent no major deformation before diapirism started (Condie 1981, 1997, Hamilton 1998a,b). The presence of synclines composed of volcanic and sedimentary rocks, between batholiths that are in contact with the stratigraphically lowest units would support such diapirism (Hamilton 1998a). Further support for the concept of diapir tectonism comes from the lack of complementary antiforms between the synforms and separation of adjacent synforms by dislocations (Hunter & Stowe 1997). In general the diapir concept involves a tectonically undisturbed and folded layer-cake stratigraphy and cyclic volcanism within linear basins developed on a granitic substrate (Williams *et al.* 1991). Regional compression is not needed to explain the structures typical of greenstone belts (Anhausser *et al.* 1969). Such belts underwent deformation as a result of granite diapirism, possibly accompanied by horizontal bulk-pure shear shortening and extension. Accordingly, the upper crust was effectively floating on granitoid material beneath (Condie 1997, Hamilton 1998a). The ductile deformation in the greenstone belts is synchronous with contact metamorphism that typically decreases away from the diapirs (Ayres 1978, Hamilton 1998a). Tonalite-trondhjemite-granodiorite (TTG) complexes would later intrude such deformed granite-greenstone terranes (Figure 5d). The nature of the transition from granite-greenstone mode at about 2.6 Ga to the plate-tectonic mode by about 2.0 Ga remains unclear (Hamilton 1998b). However, the transition may have occurred as hydrated, dense Archean crust sank into the mantle resulting in increased levels of water and carbon dioxide allowing plate tectonics to begin (Hamilton 1998a).

2.3.3 Uniformitarian/Mobilist Interpretation (O.G.S/Davis)

The common uniformitarian viewpoint is that plate-tectonic processes dominated the Archean Earth because of perceived similarities with modern plate tectonic processes (Windley

1993). Evidence that horizontal tectonics plays an important role in the evolution of Archean greenstone belts was first provided by Stowe (1974), who studied large-scale thrust imbrication in south-central Zimbabwe. Recent structural geochemical and geochronological evidence supported the consensus that the assemblages and subprovinces of the Superior Province, in particular, have been juxtaposed tectonically (Langford & Morin 1976, Hoffman 1989, Percival & Williams 1989, Williams 1991). This way of thinking brought a change in perspective from autochthonous cyclicity to allochthonous juxtaposition of greenstone masses/assemblages (Williams *et al.* 1991). Mobilist hypotheses invoke an early kind of subduction-driven horizontal accretion of Archean crustal material, typically in convergent plate boundary environments (Talbot 1973, Card 1990). Talbot (1973), Langford & Morin (1976), Williams (1990), Percival & Williams (1989), Card (1990), Williams *et al.* (1991) and Percival *et al.* (1994) invisage 2 stages in the construction of the Archean Superior Province. These stages lead to the aggregation of previously created terranes to form the subprovinces by arc-arc accretion and the assembly of the subprovinces via horizontal thick-skinned tectonics to result in the Superior Province at *ca.* 2.7 Ga during the Kenoran Orogeny.

A single northern terrane existed at the onset of Superior Province development. Autochthonous supracrustal rocks were deposited on the primordial sialic crust forming what is now referred to as the North Caribou terrane. Allochthonous assemblages were then juxtaposed with this terrane including parts of the Uchi subprovince as the North Caribou terrane grew to the south (Figure 6, Stott 1998). It was subsequently deformed and intruded by plutons during suspected collisions with terranes from the south. This resulted in diverse greenstone-dominated terranes to the south, which are considered to represent the remnants of a chain of allochthonous island arcs (Figure 7). During progressive north-directed subduction these terranes collided with

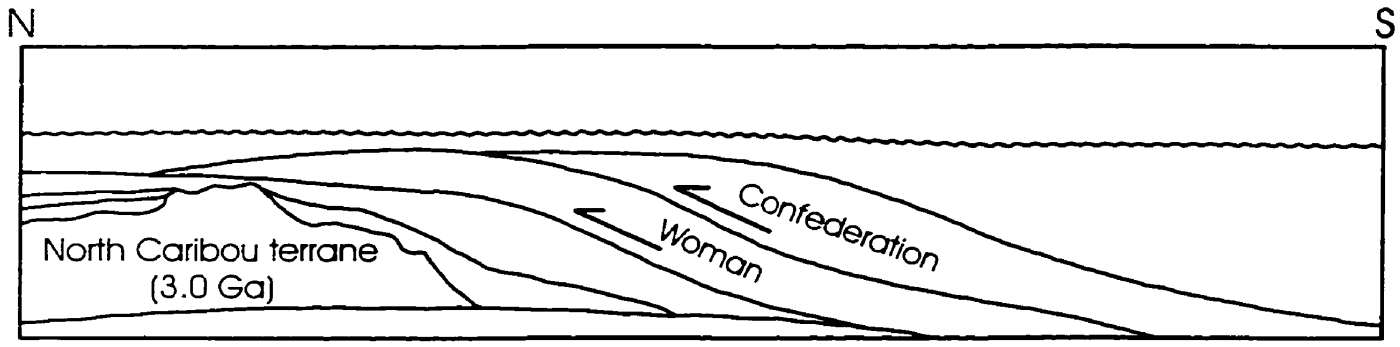

Assemblage accretion stage. Autochthonous supracrustal rocks developed on older sialic crust and allocthonous assemblages were then juxtaposed against North Caribou terrane. (modified from Williams *et al.* 1991).

Figure 6

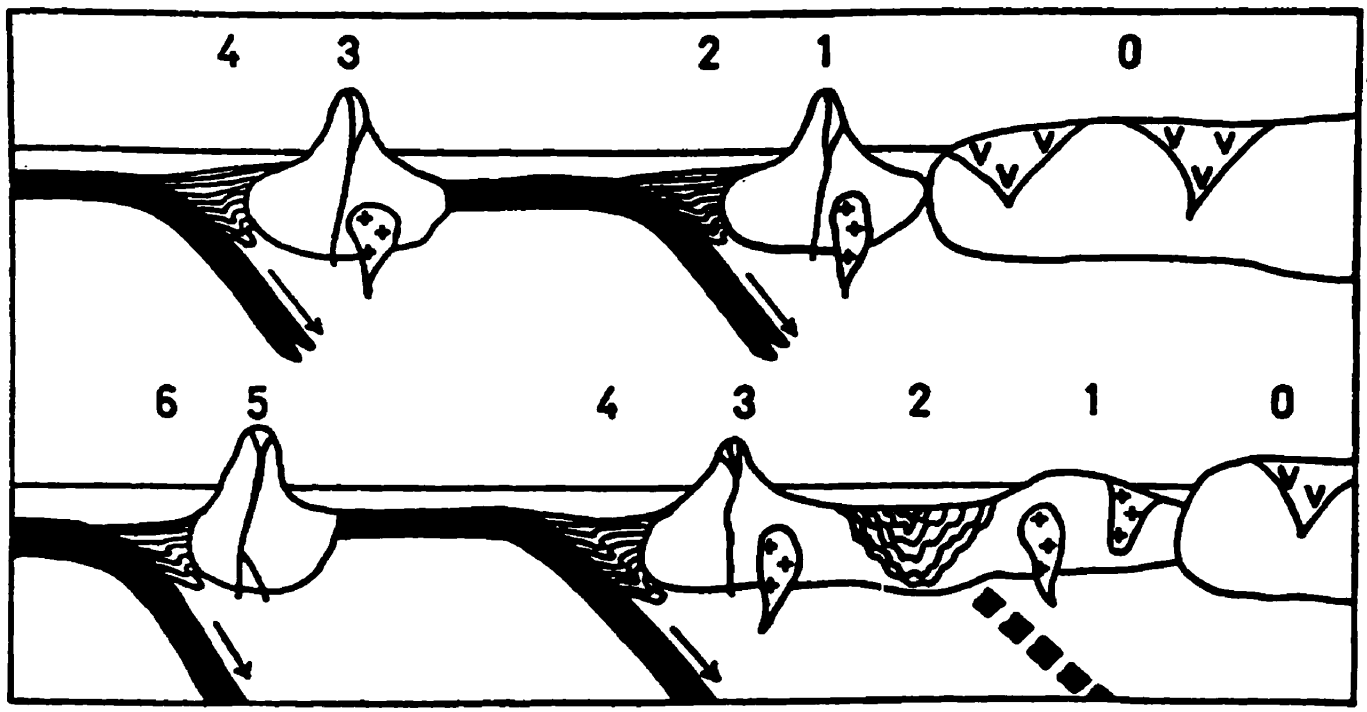

Accretionary model of the development of the Superior province (after Langford & Morin 1976)

Figure 7

the northern craton resulting in a southward migration of the accretionary complex. As subduction progressed the arcs both moved together and continued to evolve until the volcanics became subaerial. Basins on the flanks of the arcs filled with sediment and were trapped as the greenstone-dominated terranes collide with them forming the English River and Quetico subprovinces. Williams (1990) suggested that the Wawa and Wabigoon subprovinces originated and evolved as separate entities but converged during small-scale accretionary processes before the Kenoran orogeny. The greenstone-rich subprovinces were then juxtaposed with the Quetico subprovince. Intrusive activity in each terrane followed each collisional event. The subprovinces acted as stable entities following subprovince aggregation. They accommodated further compressional stress along subprovince boundaries or along newly formed trans-subprovince faults (Stott & Corfu 1991).

Subprovince boundaries may represent the remnants of one or several north-directed subduction zones within the Superior Province (Williams *et al.* 1991, Davis 1997). Results of detailed geochronological studies indicate that there was a continuous cover of sedimentary rocks between the English River and Wawa subprovince, and this suggests that the Wabigoon and Wawa subprovinces are part of one extensive island arc complex (Davis 1997, 1998). Cruden *et al.* (1997, 1998) proposes that the English River-Winnipeg River and Winnipeg River-Wabigoon subprovince boundaries and internal structural patterns were shaped by means of large-scale horizontal deformation and the emplacement of tabular granitoid plutons. This assumes that only the Uchi-English River subprovince boundary represents a collisional suture (Davis 1997, 1998).

2.3.4 Summary & Discussion

Two markedly different tectonic mechanisms constitute end members of models of greenstone belt genesis. The first mechanism envisages a tectonically undisturbed crust in which

rising granitoid diapirs cause intermediate gravitational sagging of denser greenstones (Hunter & Stowe 1997). The second mechanism of producing greenstone belts invokes a convecting mantle similar to that in modern plate tectonics (Hunter & Stowe 1997).

The role of diapirism in producing some of the structural patterns within greenstone belts has not been ascertained. However, petrologists believe that vertical granite diapirism may better explain some of the stratigraphic sequences in greenstone belts (de Wit & Ashwal 1997). Granite-greenstone terranes do not appear to be directly attributable to any plate tectonic activity (Platt 1980). Apparently, the Archean earth lost heat by voluminous magmatism from a mantle supposedly much hotter than the present (Hamilton 1998b). Nonetheless, models that rely on horizontal tectonics for Archean greenstone belt genesis are championed by recent workers (de Wit 1998).

2.4 Uchi Subprovince/Confederation Greenstone Belt

2.4.1 Introduction

The Uchi Subprovince is an east trending zone of granitic, metavolcanic and metasedimentary rocks extending 80km from Lake Winnipeg to the Archean-Paleozoic contact to the east (Figure 1, Thurston & Breaks 1978, Corfu & Stott 1993). Stott & Corfu (1991) interpreted the Uchi Subprovince as a relic of a deformed volcanic island chain. The Uchi Subprovince has a narrow ribbon-like map pattern, which differs from the map pattern revealed by the other volcano-plutonic subprovinces (Stott & Corfu 1991). This pattern is accentuated by the subprovinces that bound it to the north and south, the Berens River and the English River Subprovinces respectively (Card & Ciesielski 1986). At its present erosion level the southern boundary is defined sharply by the Sydney Lake-Lake St. Joseph Fault.

2.4.2 Tectonic History as unraveled by the O.G.S.

Many greenstone belts have tectonic histories supposedly involving several phases of tectonic deformation (Hudleston & Schwerdtner 1997). In the western Superior Province, Schwerdtner *et al.* (1979) concluded that two phases of deformation occurred, respectively, in realms of vertical and horizontal tectonics. The first tectonic deformation is attributed to compression by batholith emplacement (Thurston & Breaks 1978). The second tectonic deformation is driven by regional south-east/north-west compression, and produced large-scale shearing and major transcurrent faults throughout the Uchi Subprovince. Stott & Corfu (1991) and others (Corfu & Stott 1993a) suggest the first deformation resulted in the allochthonous or para-autochthanous northward displacement of the Confederation assemblage and rotation of the strata to a northerly strike during the Kenoran Orogeny. There is an asymmetric distribution of dates in metavolcanic rocks throughout the Uchi Subprovince, with a general younging to the south (Corfu & Stott 1993b, Stott 1998). Local reversals in this pattern indicate tectonic juxtaposition of assemblages during compressional events (Corfu & Stott 1993). Furthermore, the regional distribution of protolith ages reveals that the magmatic arcs and back-arcs of the Uchi Subprovince were accreted to the southern margin of the North Caribou terrane. The North Caribou terrane later collided with the Winnipeg River and Wabigoon subprovinces converging from the south during the Uchian phase of the Kenoran orogeny (Stott 1997). Late-stage faulting and thrust stacking occurred throughout the subprovinces as a result of further compression and regional horizontal shortening. In the later stages of this orogenic event, extensive plutonism occurred within all the subprovinces (Beakhouse 1991, Stott & Corfu 1991, Corfu & Stott 1993). This late syn-tectonic plutonism formed the Berens River Subprovince to the north of the Uchi

Subprovince (Stott 1998). The Kenoran orogeny is interpreted to have ended with regional transpression (Stott & Corfu 1991).

In some regions of the Uchi Subprovince the tectonic history is poorly constrained. Where boundaries are poorly defined the tectonic interpretation is largely inferred from the age determinations and structural relationships observed in the field (Stott & Corfu 1991).

2.4.3 Previous Work in Birch-Uchi belt and vicinity

In 1893, Dowling (1896) undertook the first geological reconnaissance of the Birch-Uchi belt for the Geological Survey of Canada. Major gold discoveries in the 1920's and 1930's prompted geological mapping of the Confederation Lake and Woman & Narrow Lakes area by Burwash (1920) and Greig (1928), respectively. Further work by Bruce (1929), Harding (1936), Thomson (1939) and Bateman (1940a) for the Ontario Department of Mines focussed largely on the newly discovered gold deposits.

The Geological Survey of Canada carried out another reconnaissance survey of the Birch-Uchi Greenstone belt and the surrounding region from 1959 to 1961. Several geochemical studies were conducted as a result of the survey including studies by Holman (1963) and Moxham (1965).

Innes (1960) completed the first regional gravity interpretation in 1960. He suggested that the mafic rocks of the Red Lake area extend to a depth of 1.9 to 4.1 kilometres. In 1967, the Earth Physics branch in Ottawa compiled a series of bouguer anomaly maps of the Red Lake and Birch-Uchi Lakes areas. During the same year, Goodwin (1967) completed his extensive whole-rock chemical analysis and stratigraphic study of the area. He described two cycles of mafic to felsic volcanism in the Birch-Uchi greenstone belt.

Pryslak (1970, 1971) and Thurston (*et al.* 1974; 1978) initiated detailed mapping of the Birch-Uchi Greenstone belt for the Ontario Department of Mines following the discovery of an ore body at the South Bay mine in 1968. During his mapping, Pryslak (1971) identified rocks of a third cycle (cycle I), located stratigraphically lower than those of the two cycles recognized by Goodwin (1967).

Pryslak (1971) and Thurston (1978), estimated that the present stratigraphic thickness of the Birch-Uchi Greenstone belt is approximately 10 km. Barlow *et al.* (1976) and Gupta and Wadge (1978) performed additional gravity surveys in an area including the greenstone belt. In 1986, Gupta and Wadge completed a gravity study and estimated the vertical thickness of the belt to be between 3.5 and 4 km. The authors proposed that the greenstone assemblage boundaries do not exist at depth.

In 1981, Thurston made the earliest attempt at correlating greenstone assemblages between adjacent belts. Volcanological and geochemical studies in 1983 and 1985 by Thurston & Fryer and Thurston, respectively, extended Pryslak's (1971) greenstone assemblages to include the East Side of the belt.

Nunes & Thurston (1980) and Wallace *et al.* (1986) determined the ages of the upper felsic units of the three cycles identified using a U-Pb zircon technique. The dates determined by Wallace *et al.* (1986) helped revise Thurston's (1981) first attempt at regional correlation. Stott & Corfu (1991) reinterpreted greenstone of different cycles as 3 tectonic assemblages since they correlate with assemblage patterns observed in neighbouring greenstone belts.

Recent structural and geochemical work by van Staal 1998 and Rogers *et al.* 1999 indicate that the Woman assemblage is composite. Their findings also suggest that the Woman-Confederation assemblage boundary be shifted slightly to the east from Stott & Corfu's (1991)

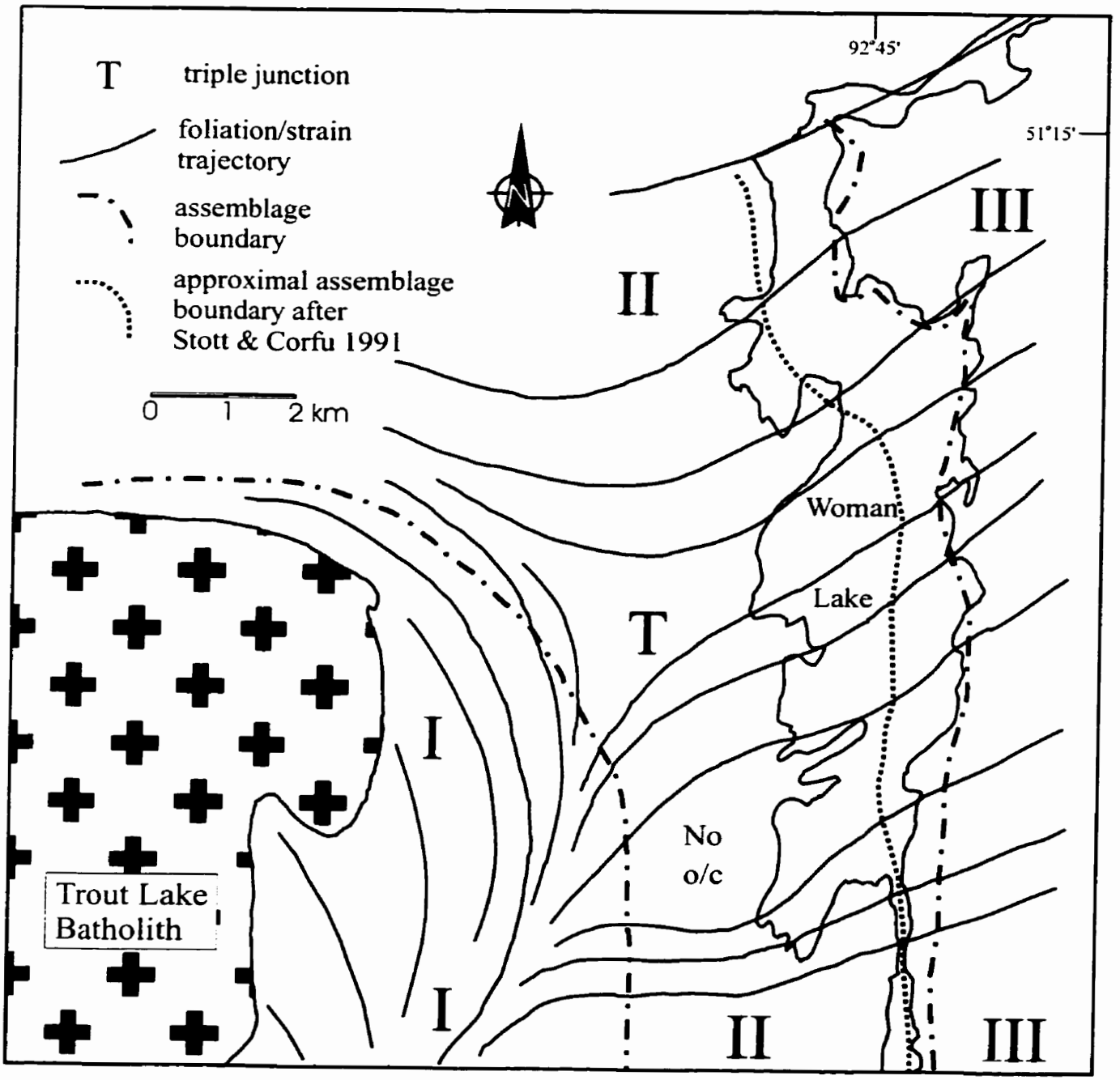

Figure 8
(after Borowik *etal.* 1999)

position to correspond with the Rowe Lake shear zone and metasedimentary unit (Figures 3, 8). Other current work in the belt include Devaney (1997, 1999) whose sedimentological studies resulted in the proposal of two tectonic hypotheses for the late orogenic history of the Birch-Uchi greenstone belt.

2.4.4 Geochronology

A large number of ages have been obtained for rocks of the Uchi Subprovince using the high precision zircon U-Pb method (Nunes & Thurston 1980, Corfu & Stott 1993). Granite-greenstone protoliths of the Uchi Subprovince range in age from *ca.* 3000 Ma to *ca.* 2730 Ma (Nunes & Thurston 1980, Corfu & Wallace 1986, Corfu & Andrews 1987, Noble 1989, Noble *et al.* 1989, Rogers *et al.* 1999). This age range suggests a meso- to neo-Archean magmatic and tectonic development for the Uchi Subprovince (Corfu & Stott 1993b). From U-Pb dates, Corfu & Stott (1993b) deduce the formation of volcano-plutonic complexes between 2900-2800 Ma. Furthermore, at 2750-2710 Ma, magmatic and tectonic accretion promoted the southward growth of the Subprovince (Corfu & Stott 1993b). This southward growth terminated at 2720-2700 Ma during extensive granitoid plutonism and the collisional Kenoran orogeny. Age and duration of tectonic and magmatic events differ across the subprovinces, which indicates a piecemeal tectonic development and an active accretionary complex that moved progressively towards the south (Corfu & Stott 1993b).

Felsic rock units have been dated in the Birch-Uchi greenstone belt and its three distinct assemblages, the Balmer (2959±2 & 2975±1.7 Ma), Woman (*ca.* 2840 Ma) and the Confederation (2735±4·3 - 2739±2 Ma; Figure 9; Nunes & Thurston 1980, Noble 1989, Noble *et al.* 1989, Rogers *et al.* 1999). Two tonalites of the Trout Lake batholith have been dated at 2838±4·3 and 2806±12·2 Ma (Noble *et al.* 1989, Noble 1989). The younger tonalite cuts the

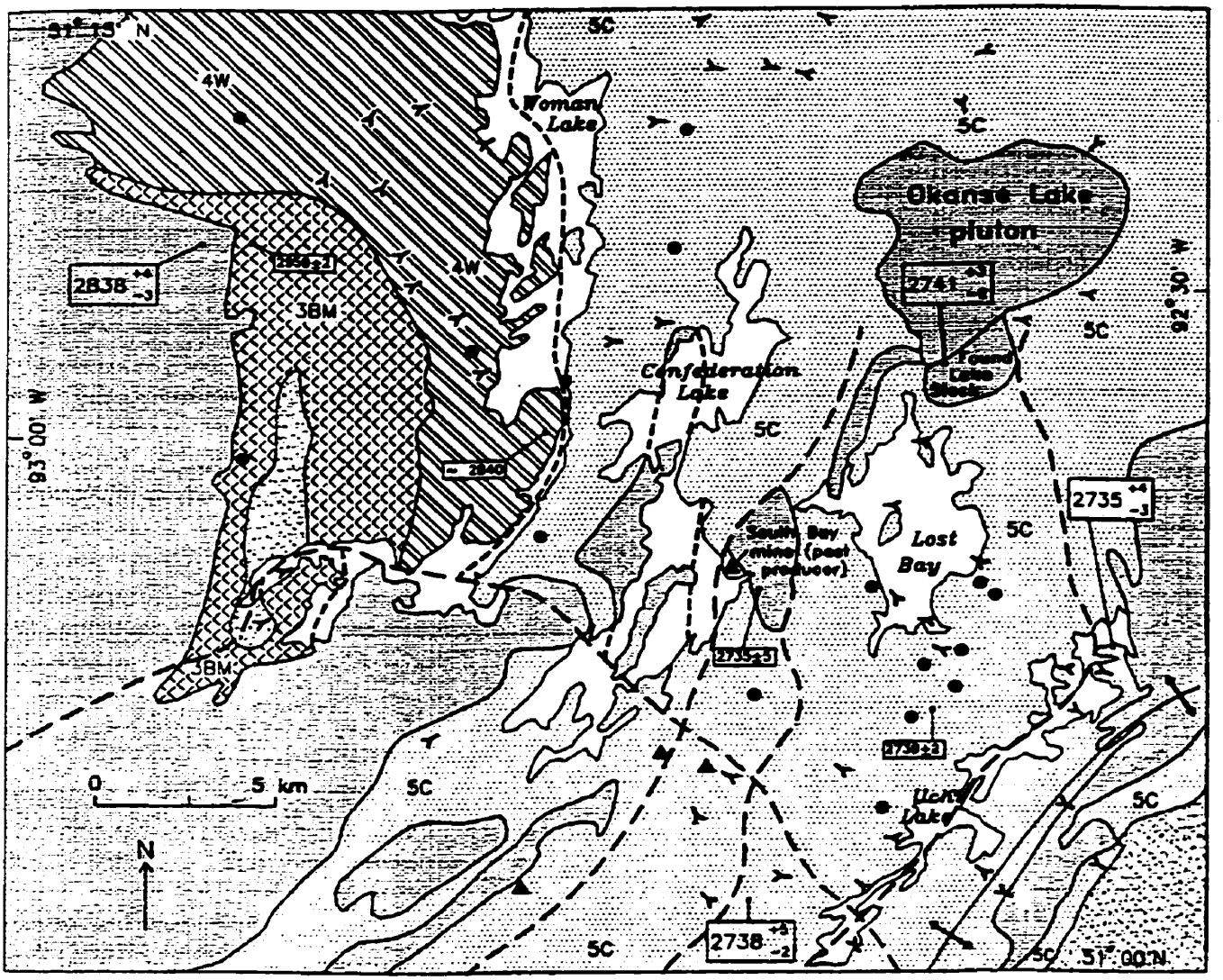

Volcanic Assemblages

Map notation	Assemblage	Age range (Ma)
5C	Confederation	2730–2800
4W	Woman	2800–2900
3BM	Balmer	2900–3000

Sedimentary rocks (age variable)

Intrusive rocks (age variable)

Symbols

- Past gold producers, gold prospects and occurrences
- Copper–zinc past producers and occurrences
- U–Pb zircon age determinations (Ma)
- Tectonic assemblage boundary (observed)
- Tectonic assemblage boundary (assumed)
- Fault
- Anticline
- Younging direction (top in direction of stem)

Figure 9
(from Stott 1997)

Balmer and Woman assemblage contact and is similar in age to the youngest Woman assemblage rocks (*ca.* 2805 Ma, Scharer 1989, Stott & Corfu 1991). This relationship marks both the termination of Woman assemblage volcanic activity and the onset of collision between the Woman and Balmer assemblages (Thurston *et al.* 1991). Stott (1998) argues that the common age between older Woman assemblage (*ca.* 2840 Ma) and the second dated tonalite phase of the Trout Lake Batholith (2838±4·3 Ma) that intrudes the base of the 2959±2 Ma Balmer assemblage reveals that the Woman assemblage developed on or near the margin of the Balmer assemblage. This indicates that the Woman assemblage is either an autochthonous or parautochthonous slice transported northward (Stott & Corfu 1991). The presence of a 2838±4·3 Ma old tonalite body, which is synchronous with Woman assemblage volcanism, provides evidence of a continental arc setting for the Woman assemblage (Noble 1989, Stott & Corfu 1991). Ages of zircons from inhomogeneous Woman-assemblage metavolcanics are *ca.* 2800-2835 Ma (Corfu & Wallace 1986). Wallace *et al.* (1986) propose that the age range of these metavolcanics approximates the duration of Woman assemblage volcanism on a regional scale. Based on U-Pb evidence, they postulate that at *ca.* 2740 Ma the Balmer and Woman masses (Figure 2) were juxtaposed, hence the Woman assemblage lies disconformably over the Balmer assemblage (Stott & Corfu 1991). On Spot Lake a metaleucogabbro sheet, transecting the Balmer-Woman assemblage boundary, has been dated at 2832±2 Ma (van Staal 1998, personal communication). Rogers *et al.* deduce from this age that the gabbro sheets acted as feeders to the Woman assemblage basalts and gabbro sills. At any rate, the new date confirms that the Woman assemblage overlies the Balmer assemblage, above a disconformable boundary (Rogers *et al.* 1999).

Woman and Confederation assemblage masses are separated by a late-stage fault on Woman Lake and the assemblage boundary is marked locally by brittle-ductile shear zones (Fyon

& Lane 1985, Stott & Corfu 1991, Stott 1998). Age relationships indicate that the protoliths to the Confederation assemblage were deposited 2800-2730 Ma ago (Stott & Corfu 1991). The eastern half of the assemblage is thought to be either a series of rapidly deposited cycles of volcanic rocks or a tectonic repetition of a single cycle based on the array of ages 2730-2740 Ma gathered throughout the Confederation assemblage (Noble *et al.* 1989, Stott & Corfu 1991, Stott 1998).

2.4.5 Geophysical Information on Birch-Uchi Belt

Several geophysical studies have been completed for the Birch-Uchi greenstone belt and the surrounding region within the Uchi Subprovince. Such studies include gravity surveys (Innes 1960, Barlow *et al.* 1976, Runnalls 1978, Gupta & Ramani 1980, Gupta *et al.* 1982, Gupta & Wadge 1978, 1980 & 1986), seismic work (Hall & Hajnal 1969), and magnetic anomaly, density, and electrical surveys (Szewczyk & West 1976, Gupta & Wadge 1980, Khan 1982, Hall & Brisbin 1982). The Western Superior Transect of Lithoprobe has completed parts of their ongoing seismic studies, acquiring seismic refraction and reflection data across several subprovinces, including the southern Uchi subprovince (Cruden & Hynes 1999, White *et al.* 1998, 1999).

The Birch-Uchi greenstone belt is characterized by supracrustal rocks, which are surrounded by oval-shaped granitoid plutons and batholiths (Gupta *et al.* 1982, Stott & Corfu 1991). This geological map pattern correlates well with existing residual bouguer anomaly map patterns. Higher-density greenstone and supracrustal rocks (mean density 2.75-2.94 g/cm3) are associated with distinct positive anomalies or gravity highs and the lower density granitoid bodies (mean density 2.63-2.65 g/cm3) are associated with negative anomalies or gravity lows (Thurston & Breaks 1978, Gupta *et al.* 1982, Gupta & Wadge 1986). The margin of the

measured gravity highs and their steep gravity gradients correspond well with the gradational granite-greenstone contacts (Gupta *et al.* 1982). In general, magnetic anomalies in granite-greenstone terranes reveal a broad "whirlpool" pattern (Condie 1981). Gupta & Wadge (1986) discovered that the magnetic anomalies also compare closely with the surficial geology where magnetic highs marked granitic terrane rocks while the lows matched greenstone rocks.

Gupta & Wadge (1986, Gupta *et al.* 1982) completed two-dimensional gravity modeling of several profiles taken across the Birch-Uchi greenstone belt. A second vertical derivative of bouguer gravity map was used in conjunction with the profiles to aid in the interpretation of the surface geology (Gupta & Wadge 1986). Profiles A & B (Figure 10a, b) represent two interpretive models for the geometry of the Birch-Uchi greenstone belt (Gupta *et al.* 1982, Gupta & Wadge 1986). Profile A (re-folded model; Figure 10a) suggests that the deformation of the belt began with folding of the supracrustal rocks about a north trending steeply plunging axis. The steep dips of strata mapped at the surface are thought to be the result of high frequency, tight isoclinal folding. This would allow the enveloping surface of the units to have a shallow dip while they appear to dip steeply at the surface (Gupta *et al.* 1982). Profile B ('rootless' greenstone model; Figure 10b) preserves the surface dips, location and synclinal structure of the strata observed at the surface in the belt. The steep dipping strata observed at the surface continues to the greenstone belt's vertical extent and is considered to be standing on end (Gupta *et al.* 1982). Gupta *et al.* (1982) use recognized geological mechanisms to explain the geometry and vertical extent of the Birch-Uchi greenstone belt interpreted from their measured profiles (e.g. Figure 10). Such processes include magmatic stoping during resurgent caldera activity of Confederation assemblage volcanism and production of felsic melts from amphibolite melting processes (Gupta *et al.* 1982). This agrees with the field observations of Thurston *et al.* (1978,

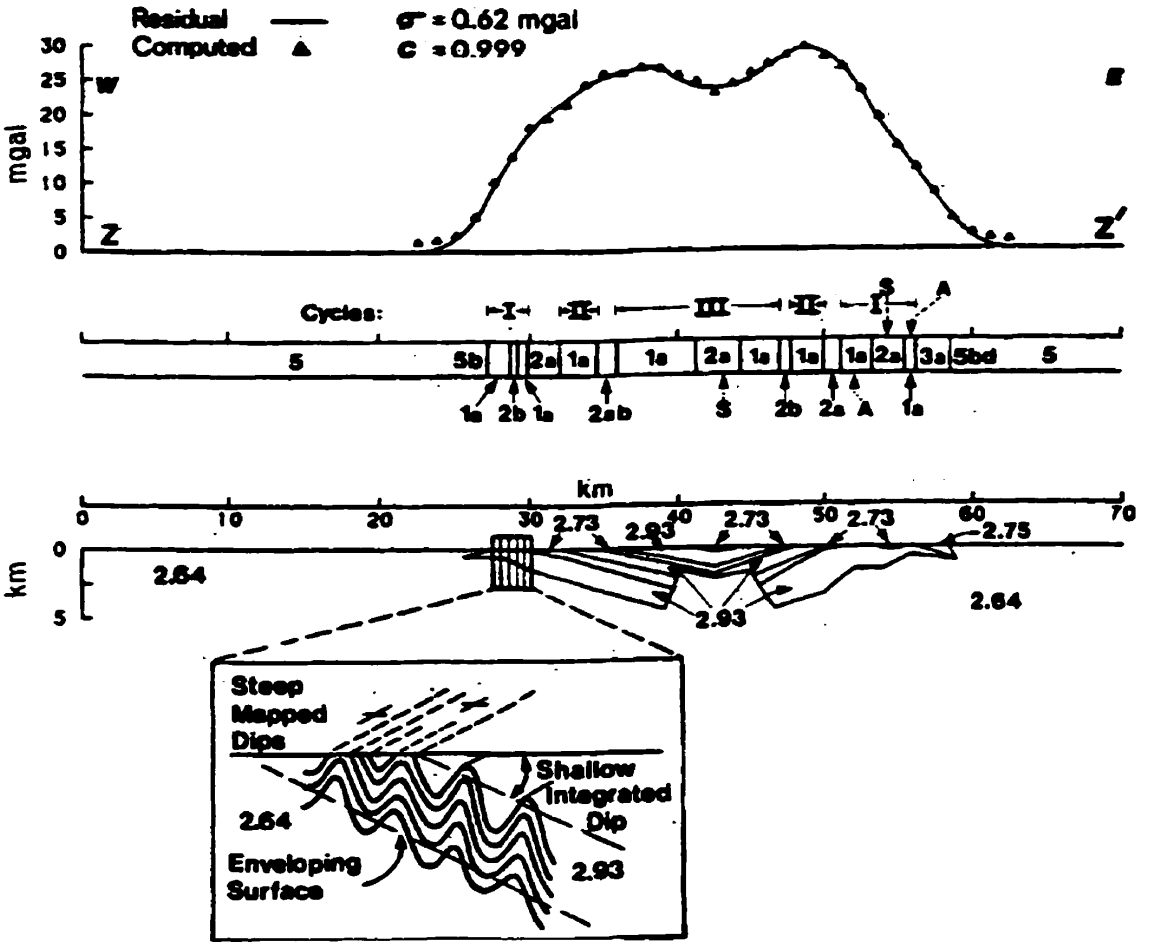

Profile A - re-folded model (after Gupta & Wadge 1986).

Figure 10a

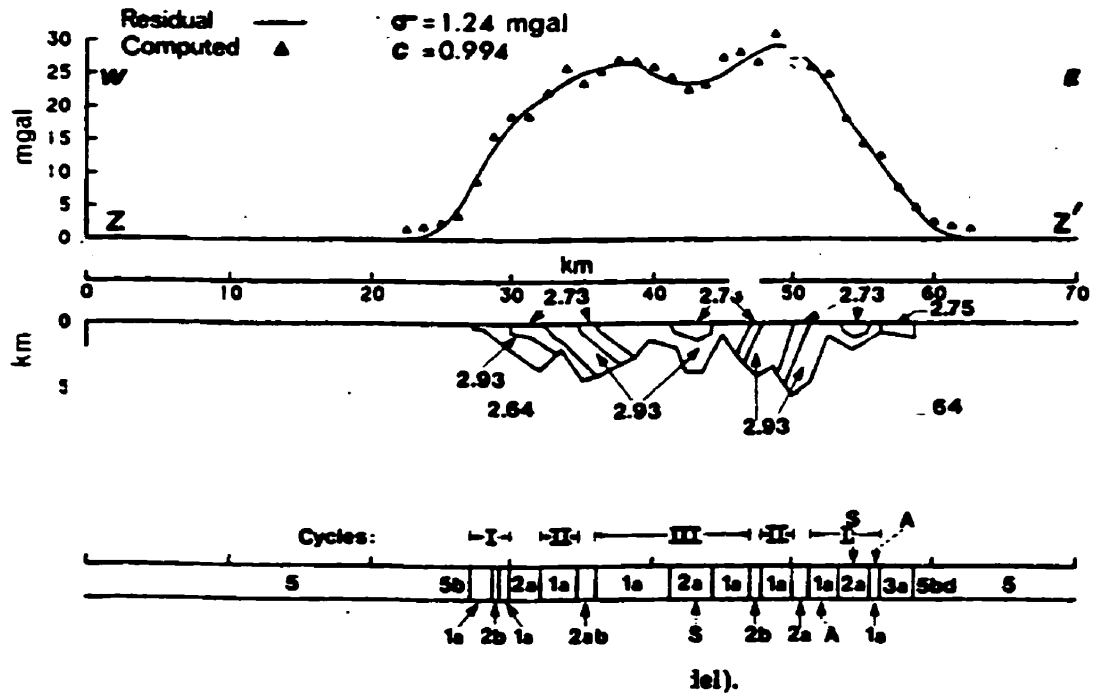

Profile B - 'rootless' greenstone model (after Gupta & Wadge 1986).

Figure 10b

Nunes & Thurston 1980), who deduced that the upper felsic portion of the Confederation assemblage was located within a fault-bounded block of a graben. They proposed that the graben be the result of cauldron subsidence followed by volcanic activity (Thurston *et al.* 1978, Stott & Corfu 1991). The bottom topography used in the profiles is governed by the surficial geology projected downward to depth (Gupta & Wadge 1986).

All profiles based on two-dimensional gravity modeling illustrate a broad basin-like geometry of greenstone masses and variable thickness for all greenstone belts (Figure 11, Condie 1981, Gupta *et al.* 1982, Gupta & Wadge 1986, Stettler *et al.* 1997). The vertical thickness of the Birch-Uchi greenstone belt is believed to be between 3.5 - 4 km. This differs by a factor of 2 from the stratigraphic thickness (10km) previously determined by Thurston (1978) and Pryslak (1979). The difference in thickness estimate is attributable to structural repetition of units on account of folding or thrust imbrication (Stott & Corfu 1991, Stettler *et al.* 1997, Stott 1998). Gravity modeling further reveals that the surrounding granitic batholiths are relatively thin or sheet-like and their lower contacts have a depth of 4-7 km and may form a cover over parts of the greenstone belt (Gupta & Wadge 1986, Stettler *et al.* 1997).

Independently, the geophysical data provide us with limited information. However, when used in combination with structural and geochronological and other studies, they can help elucidate the internal structure of greenstone belts and narrow down the possible geological models for Archean tectonics.

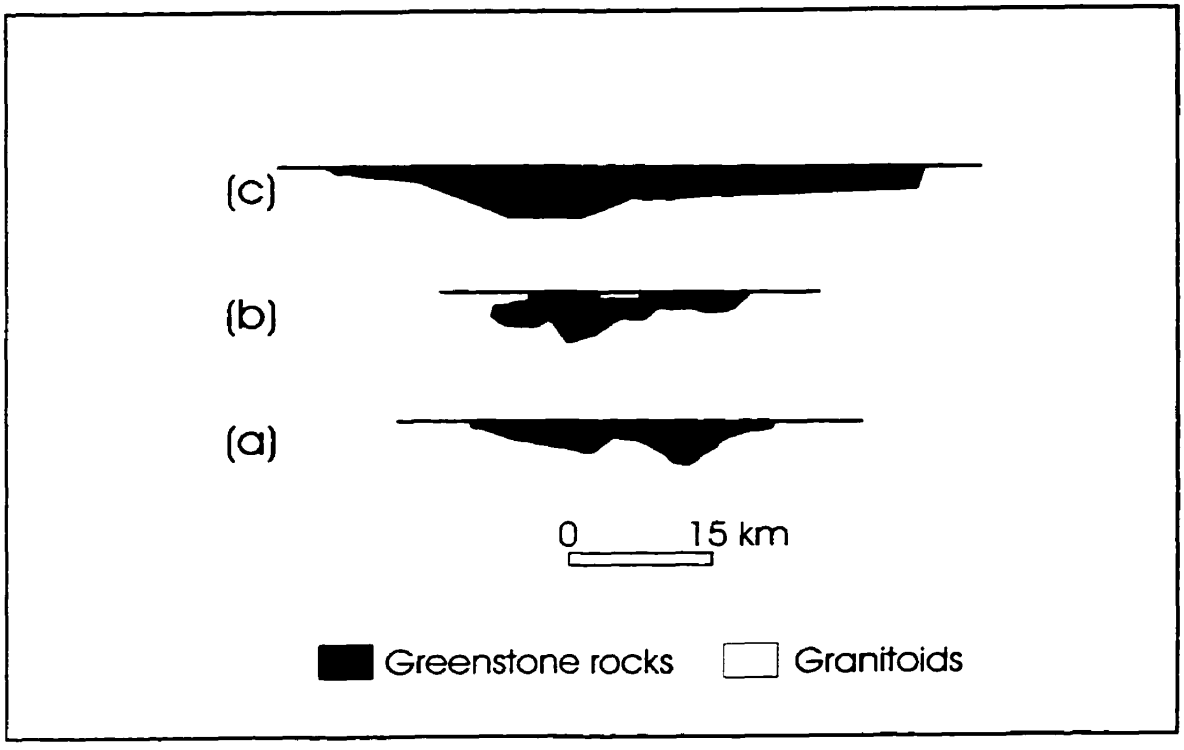

Three cross-sections of greenstone belts based on interpreted geophysical data displaying an overall shallow geometry (a) Birch-Uchi belt (b) Wawa belt (c) Seronera belt, Tanzania (modified from de Wit & Ashwal 1997).

Figure 11

CHAPTER III

STUDY OF ROCKS IN HAND SPECIMEN AND THIN SECTION

III. STUDY OF ROCKS IN HAND SPECIMEN AND THIN SECTION

3.1 Introduction

A detailed study of the foliation style was undertaken in the various rock types (cf. Chapter 2.2) discussed in the thesis. This is a summary of observations made at the scales of outcrops, hand specimens and thin sections, which were also used to determine the mineral assemblages and deformation style of different rock types.

3.2 Methods Used

Forty-five hand specimens, collected from various localities (Figure 4) were used to prepare 30 thin sections and 25 slabs usually oriented parallel, to the X-Z (and Y-Z) principal planes of the strain fabric for the purpose of both thin section and fabric analysis. The attitudes of the fabrics studied were measured at the outcrop (Figure 12, 13, 14; cf. Chapter 4). The mineralogy, modal percentages, textures and fabrics for the specimen studied are described in Appendix A. Sampling locations of the specimen studied are shown in figure 4.

The following sections briefly summarize the general mineralogy, mineral fabrics and structural relationships observed in the major rock types of the field area (Figure 3).

3.3 Results of Petrographic Study and Fabric Analysis

3.3.1 Ultramafic and mafic metavolcanic rocks

Mafic and ultramafic metavolcanic rocks occur at the stratigraphic base of each of the assemblages according to Stott & Corfu (1991) in the Birch-Uchi greenstone belt (Figure 3; cf. Chapter 2.2). The mafic metavolcanic rocks commonly consist of amphibole, plagioclase, carbonate, quartz, chlorite, sericite, epidote, biotite and opaques in varying amounts. In the case of the ultramafic rock studied (C8), the metamorphic mineral assemblage is dominantly

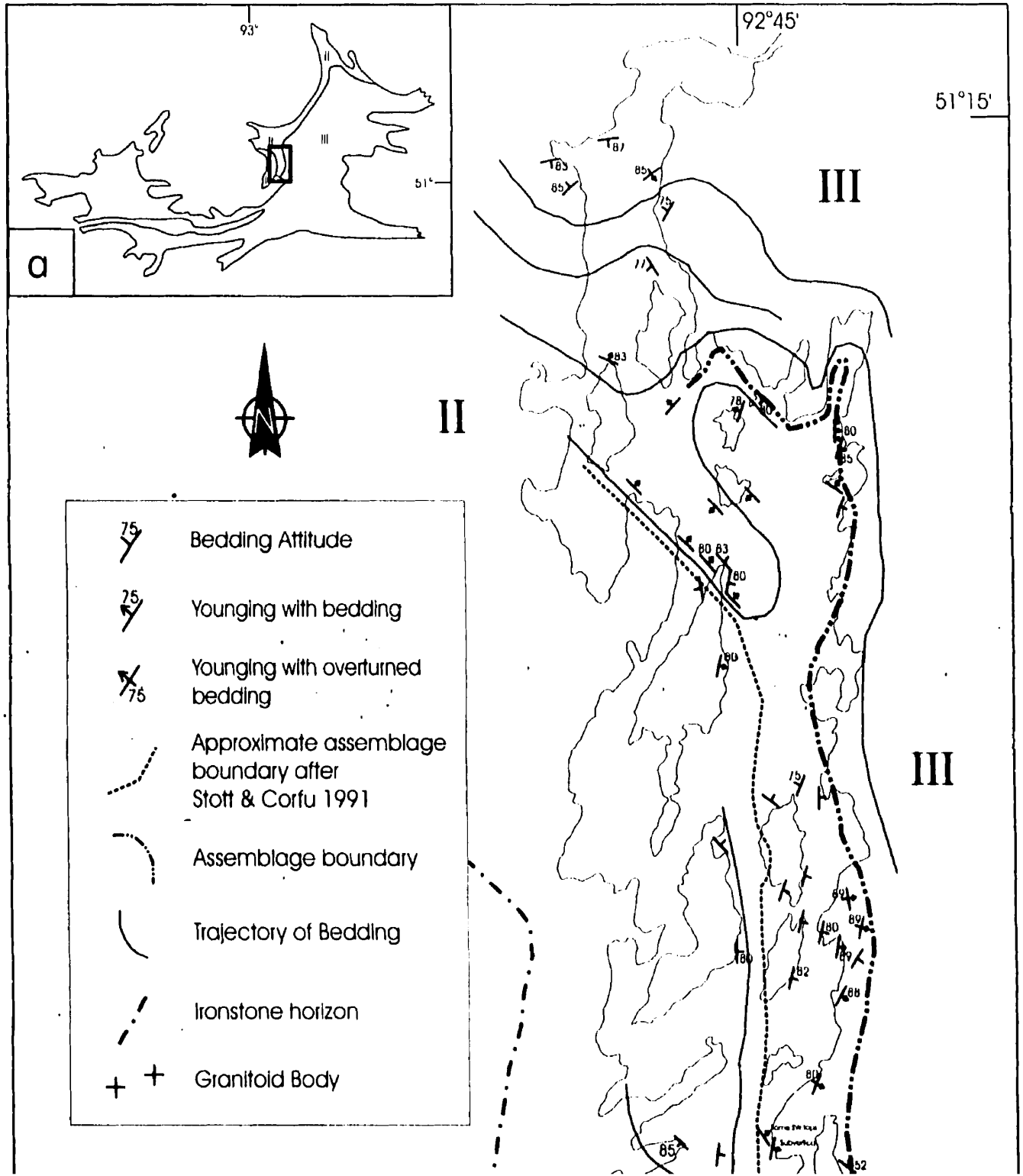
92°45'
51°15'
93°
51°
a
II
III
III
III
N
75
Bedding Attitude
75
Younging with bedding
75
Younging with overturned bedding
Approximate assemblage boundary after Stott & Corfu 1991
Assemblage boundary
Trajectory of Bedding
Ironstone horizon
Granitoid Body

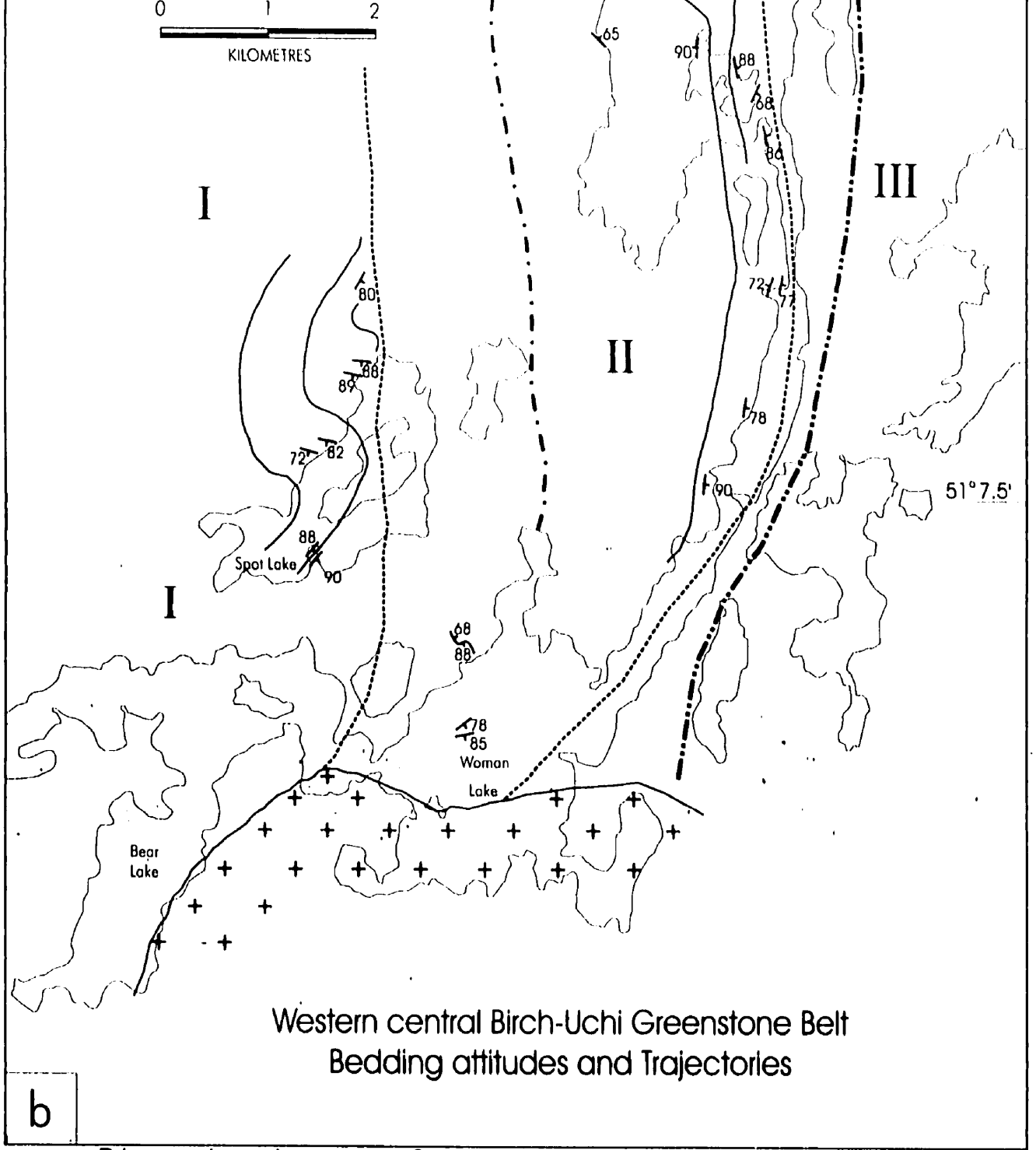

Primary layering map, Spot Lake-southern Woman Lake area

Figure 12

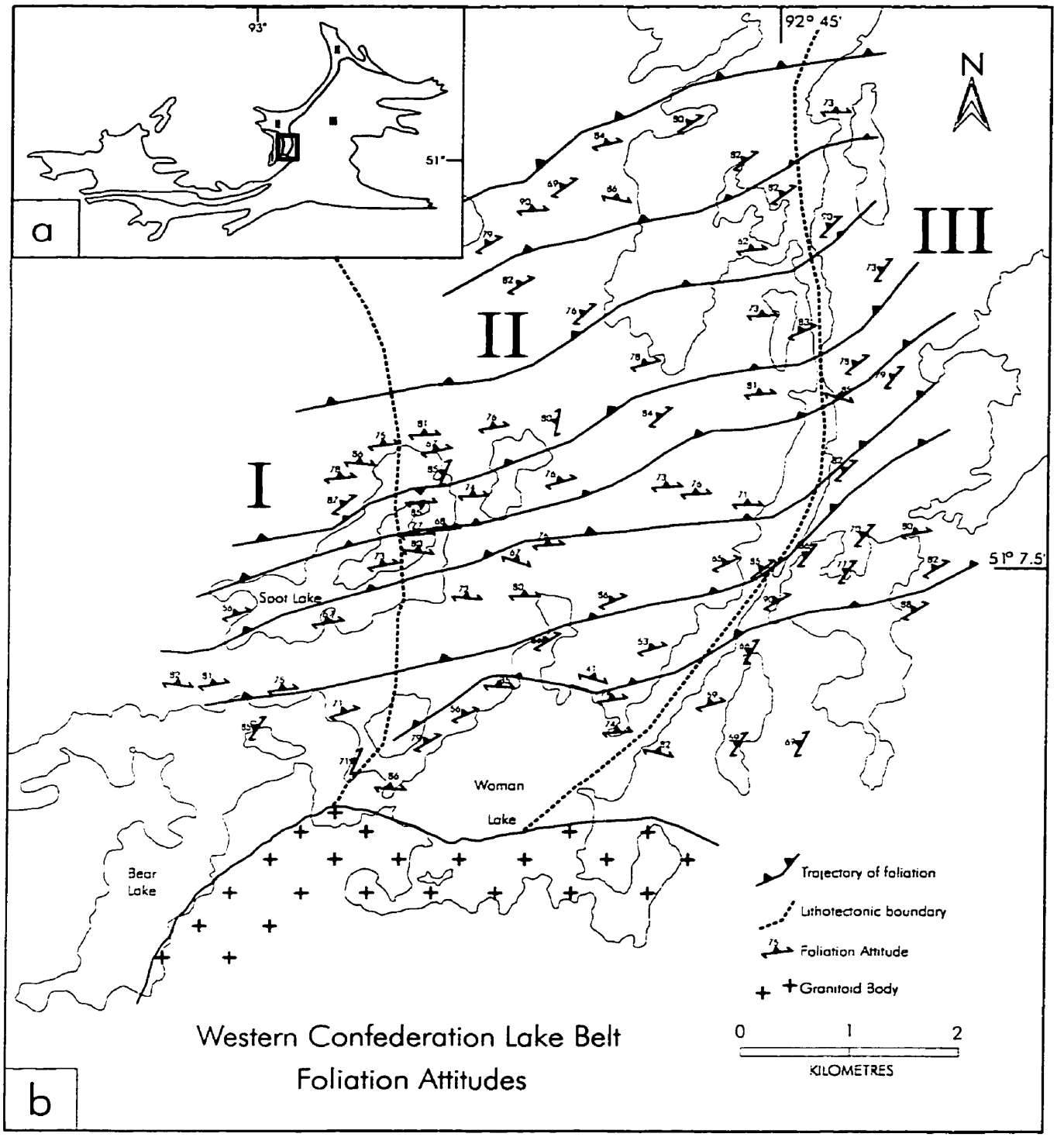

Foliation map, Spot Lake-southern Woman Lake area

Figure 13

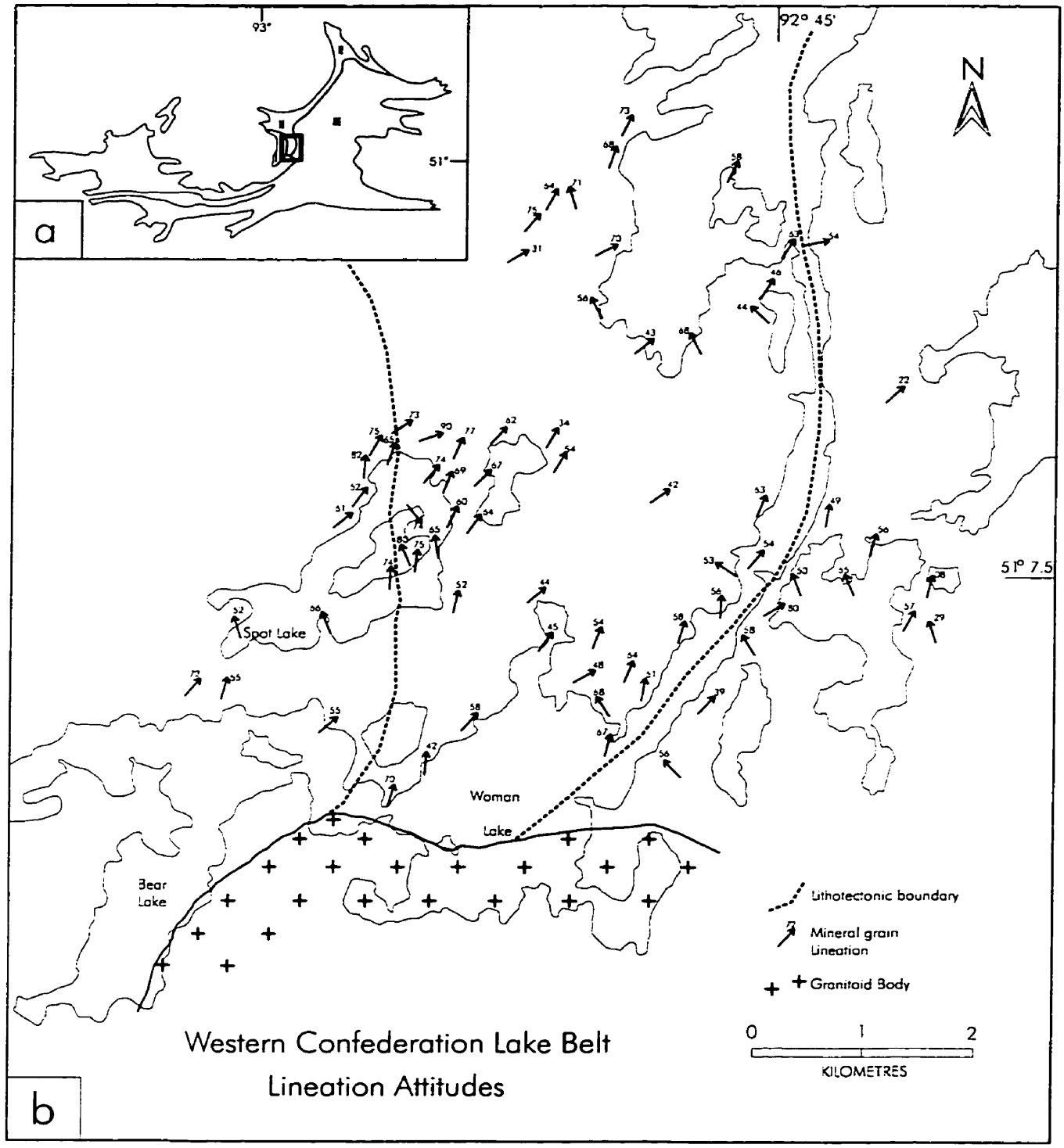

Mineral lineation map, Spot Lake-southern Woman Lake area

Figure 14

carbonate, talc, magnetite and chlorite. Both rock types are dark grey-green in hand specimen with or without dark amphibole (phenocrysts) and chlorite blebs. At some localities, the mafic metavolcanic units contain varioles whose shape depends on the local strain state (Plate 2). Varioles, in mafic metavolcanic rocks, are typically whitish grey with a blue-grey core and consist largely of quartz and albite, which form an interlocking mosaic (Gelinas *et al.* 1976). Sample A35 (Figure 3, 4) is a mafic metavolcanic rock displaying brecciated fragments (Plate 3f). The outcrops of mafic metavolcanics near this locality contain pillows (e.g. site A32; Plate 1b). Alternating dark (amphibole, chlorite, & opaques) and lighter (plagioclase, sericite, talc) regions define both a linear and planar fabric (A15 & C3; Plates 3, 4). Schistosity is dominantly defined by individual elongated chlorite, carbonate, amphibole and opaque mineral grains (Plates 3, 4). Sericite contained within plagioclase grains and alternating aggregates of chlorite, carbonate and quartz parallel the schistosity trace in some instances (eg. D12 & A15l Plate 4). The schistosity in the ultramafic (sample C3) is defined by elongate magnetite (& magnetite pseudomorphs), carbonate, and acicular talc grains (Plate 3). Talc and coarse grained carbonate grains (parallel to foliation) fill fractures that are perpendicular to the foliation trace. This feature can be observed in both hand specimen and thin section (Plate 3a-d). Similar extension fractures, also perpendicular to the foliation trace, are evident in phenocrysts of amphibole and are filled with carbonate or opaques (i.e. D12; Plate 3e).

3.3.2 Metagabbros

Metagabbroic rocks are found throughout the study area in all assemblages (Figure 3). Although these rocks typically appear unstrained in outcrop and hand specimen (Plate 5; except in local shear zones), the mineralogy was studied to determine which minerals might control the magnetic fabric in the rock (i.e. AMS study , Chapter 5).

Plate 2

Deformed and undeformed variolites.

Deformed variolite slab cut parallel with:

(a) the X/Y plane and (b) the Y/Z plane of the strain ellipsoid at site C-4,

(c) & (d) undeformed samples of variolites.

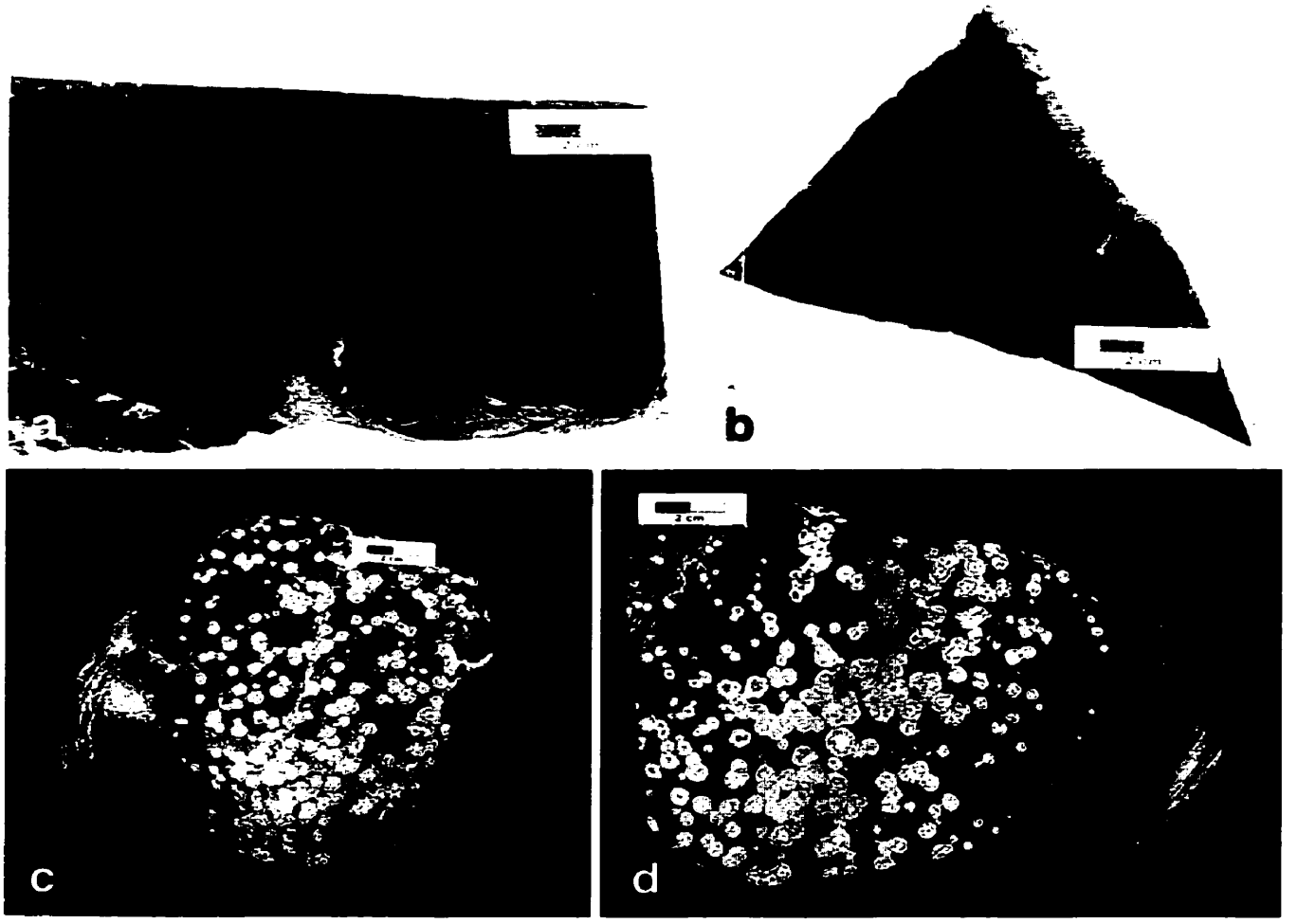

Plate 2

Plate 3

Mafic and ultramafic metavolcanics.

(a) & (b) Schistosity (horizontal) in this ultramafic rock is defined by elongate magnetite, carbonate and talc. Fractures normal to schistosity are filled with talc and carbonate

(c) & (d) Fractures may be tension gashes (NX & PPL respectively).

(e) Amphibole grains show possible extensional fractures normal to schistosity and are filled with carbonate (and opaques).

(f) a mafic metavolcanic pillow breccia.

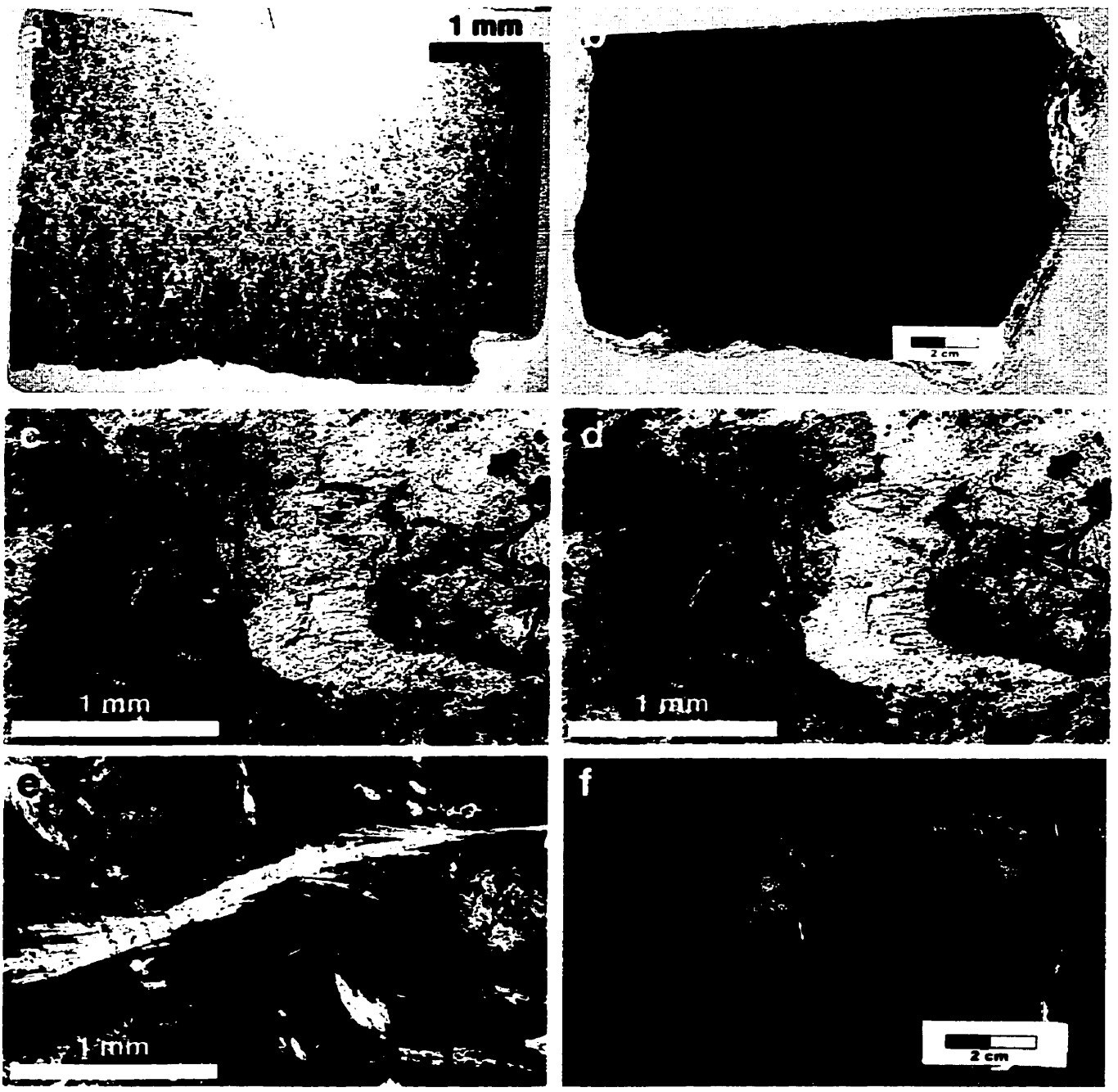

Plate 3

Plate 4

(a) Thin section of a strained mafic metavolcanic rock where mineral schistosity and lineation are defined by:

(b), (c) & (d) elongate grains of carbonate, chlorite, amphibole and opaque grains.

(c) The Y/Z plane reveals a weak schistosity suggesting the rock is dominantly lineated.

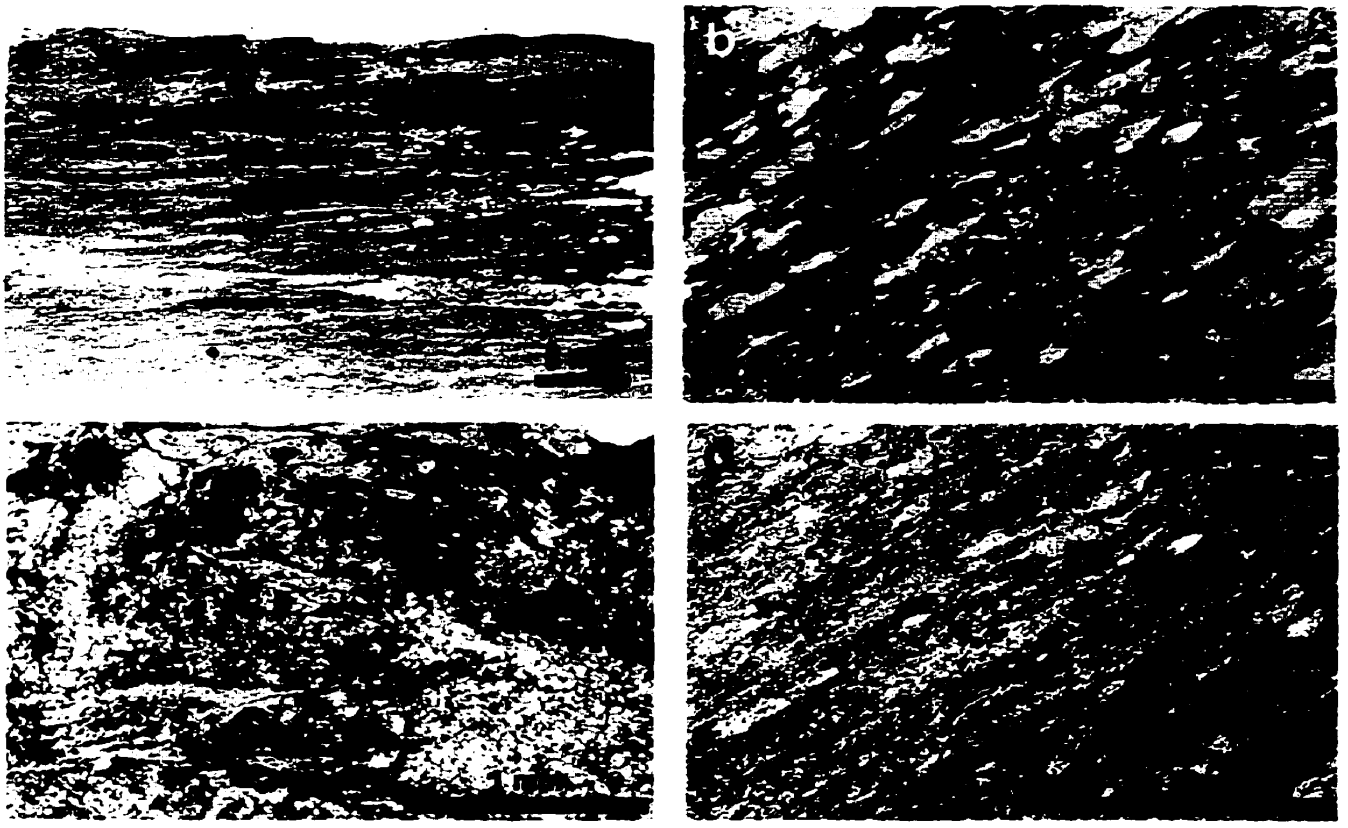

Plate 4

Plate 5

Metagabbro have a relict igneous texture and look relatively undeformed in both hand specimen (a) and thin section (b) & (c).

The mineralogy of the gabbro specimen was analysed to determine the contributing minerals to the magnetic fabric (cf. Chapter 5).

(d)-(h) Opaques found within the gabbro specimen studied.

(d) Ilmenite pseudomorphed by sphene

(e) Chalcopyrite with intergrowths of pyrrhotite

(f), (h) Sphalerite grains in reflected light and transmitted light, respectively.

(g) localized disseminated pyrrhotite.

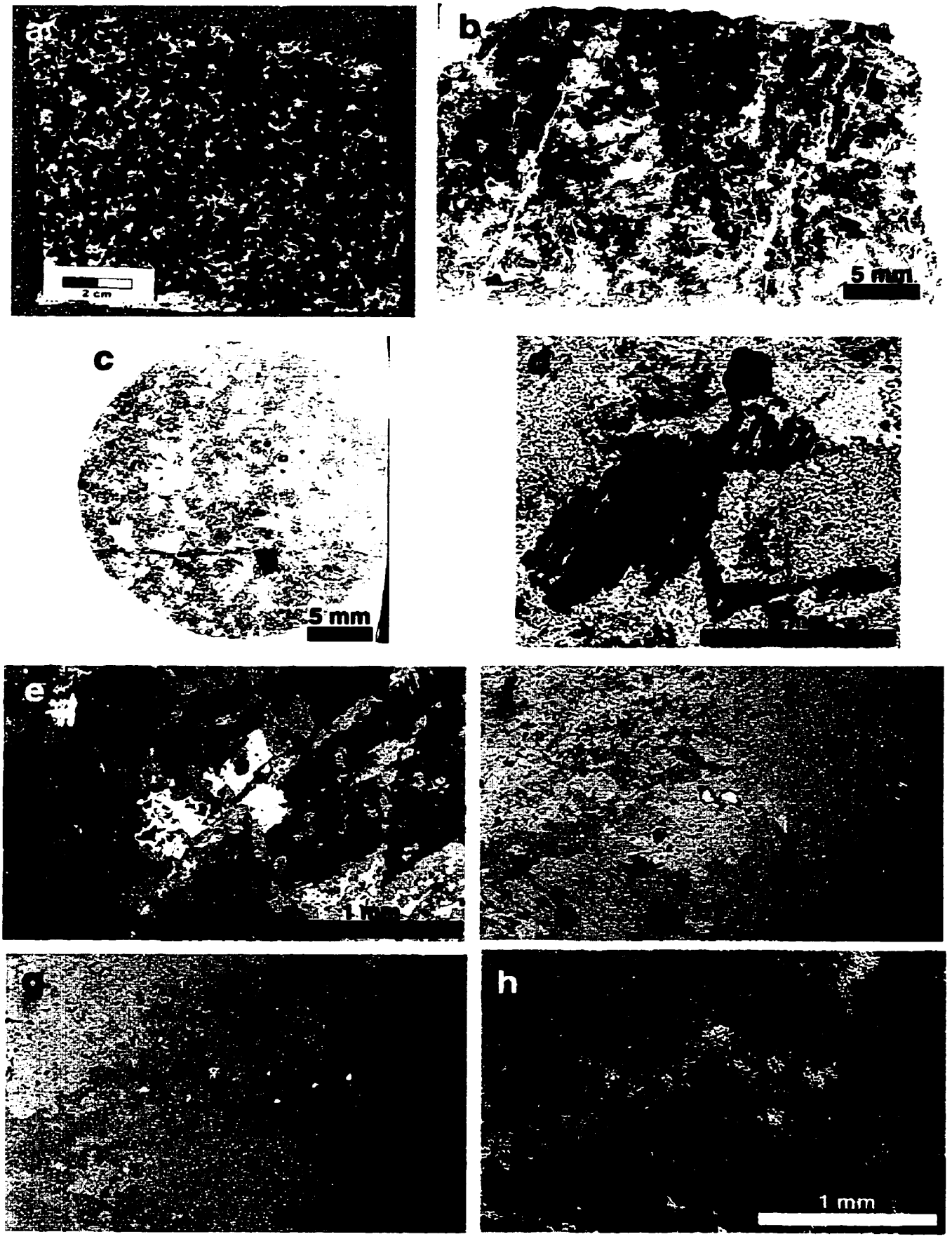

Plate 5

The metagabbro rocks studied consist dominantly of amphibole, clinozoisite, plagioclase, clinopyroxene, carbonate, chlorite, quartz, and opaques minerals. The amphibole is typically altered to chlorite, especially at the margins and along mineral cleavages while the plagioclase grains have almost been completely replaced by clinozoisite. The clinozoisite has in turn been slightly garnetized. Although these gabbros have been metamorphosed, they still exhibit a relic igneous texture whose constituents have a random orientation (Plate 5a-c). At outcrop and in hand specimen the metagabbros appear greenish-black and have a "spotty" massive texture consisting of mafic and felsic minerals. The opaque minerals tend to occur near and inside amphibole grains except for larger ilmenite grains that are located interstitially to other grains (Plate 5). The opaques consist mainly of ilmenite (pseudomorphed by sphene), pyrite, leucoxene, chalcopyrite, sphalerite and pyrrhotite (Plate 5). Sphene typically pseudomorphs ilmenite with only relic ilmenite lamellae remaining (Plate 5). Chalcopyrite, pyrite and the ilmenite-sphene pseudomorphs represent at least 85% of the opaques present in the metagabbros studied. However, pyrrhotite is observed as intergrowths with chalcopyrite and as fine-disseminated grains scattered locally in two specimen, A6 & A1 respectively (Plate 5).

3.3.3 Intermediate metavolcanic and pyroclastic rocks

The intermediate igneous rocks that display the best strain fabric are typically pyroclastic and metavolcanic units that contain phenocrysts and amygdules (Plate 6). However, even pyroclastic units may appear relatively unstrained at the outcrop (i.e. Plate 1a). They are generally light grey to light olive green in hand specimen containing both dark grey and white/green-grey phenocrysts and lapilli (Plate 1, 6). The minerals commonly observed in the intermediate metavolcanics are quartz, chlorite, carbonate, plagioclase (feldspars), sericite, sphene and opaques. In hand specimen the lapilli, phenocrysts and amygdules define a linear

Plate 6

Intermediate metavolcanics/pyroclastics appear to be dominantly lineated (a-f) however, the strained primary features (lapilli, phenocrysts, amygdules[h]) are slightly oblate and define a schistosity. (g) A schistosity defined by sericite passing through both phenocrysts and groundmass.

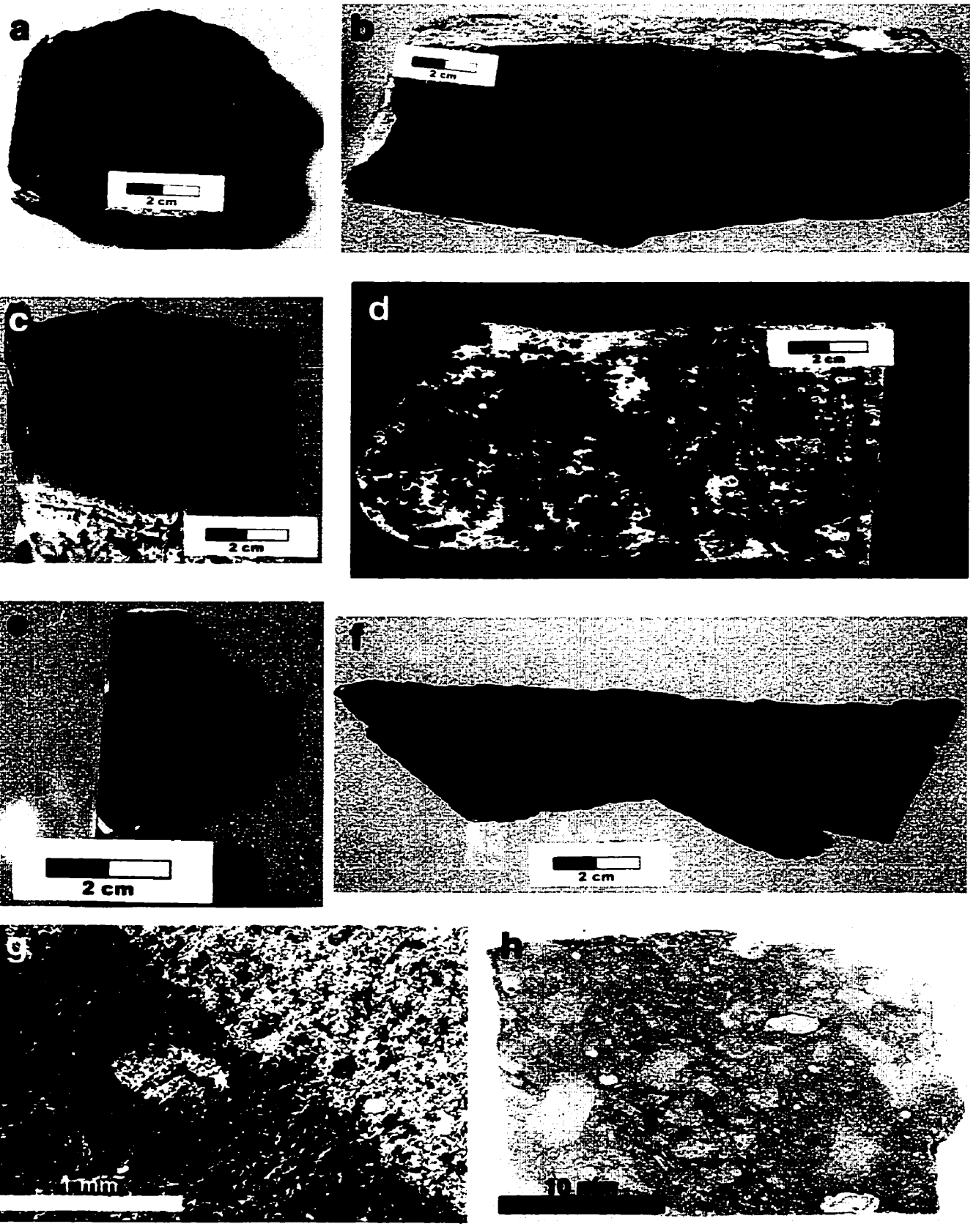

Plate 6

fabric, however, in most samples studied the "clasts" are slightly to moderately oblate and also contain a foliation (Plate 6a-f). Sericite grains define a pervasive mineral schistosity, which is seen passing through both phenocrysts and groundmass (Plate 6g). Intermediate metavolcanics lacking any prominent features like phenocrysts, lapilli etc., exhibit a weak mineral schistosity consisting of sericite and chlorite.

3.3.4 Felsic metavolcanic and pyroclastic rocks

The felsic metavolcanic and pyroclastic rocks studied throughout the field area consist mainly of quartz, plagioclase (feldspars), sericite, epidote, carbonate, muscovite and opaques. In hand specimen they are blue-grey and have a cherty appearance (Plate 7a, b). Several outcrops contain layers that vary from blue-grey to dark grey. In thin section the lighter areas are primarily quartz and the darker areas sericitized feldspars. These layers have been identified as a banded rhyolitic flow. No tectonic foliation was observed in these outcrops, however, the rocks may still have experienced some strain. Plate 7e & f shows the primary layering from sample F7 that has been enhanced by the presence of dark laminae between fine grain quartz (possibly sericite?). In the same specimen, dark seams have developed parallel to the primary layering and appear to bend around large euhedral quartz grains. These may represent pressure solution seams (Ramsay 1967, pg. 196, 197). Another example of strained primary layering is at site R1 where the bedding of a felsic tuff has been deformed into a disharmonic S-fold (Plate 1c; cf. Chapter 4.2). At several outcrops (e.g. F5, F8, F14, & F15) there are numerous quartz filled veins that strike (310-335°) sub-perpendicular to the average foliation attitudes (225-250°) measured in the area.

Hand specimens that do not contain primary layering appear relatively unstrained except for a few fractures (Plate 7a, b). However, in thin section a weak mineral schistosity is observed where recrystallized quartz phenocrysts are weakly aligned (Plate 7g). Amygdules containing

Plate 7

Felsic metavolcanics/pyroclastics. (a) & (b) Typical hand specimen with a possible cleavage expressed by several microfractures filled with quartz (a).

(c) Primary layering at F-7 enhanced by dark laminae between fine grained quartz (e).

(d) Amygdules define a weak schistosity (filled with amphibole and opaques).

(f) Possible pressure solution seams bending around competent quartz grains.

(g) Weakly aligned phenocrysts parallel schistosity.

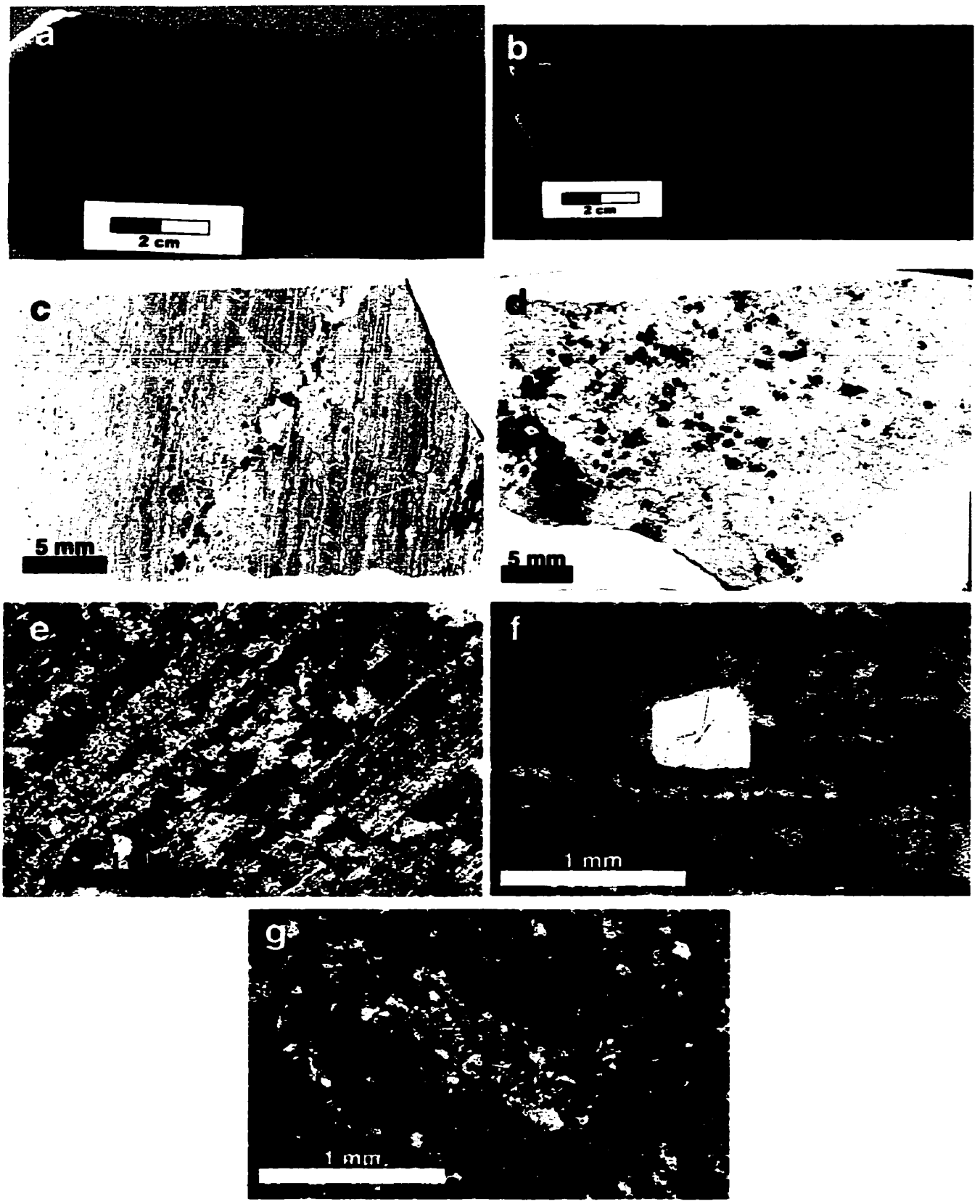

Plate 7

quartz, amphibole and opaque minerals are slightly elongate and further enhance the weak foliation observed (Plate 7d). In sample F3 several microfractures filled with quartz define a discontinuous foliation which may represent a fracture cleavage (Plate 7a).

3.3.5 Metasedimentary rocks

A ~100 metre thick unit of mylonitic stromatolitic marble (Hofmann *et al.* 1985, van Staal 1998, Rogers *et al.* 1999) and an outcrop of a metasedimentary unit are located along Woman Narrows (Figure 3). The marble unit mainly contains carbonate, quartz, and a few mica grains. In hand specimen bedding is evident by alternating dark grey and white/light grey layers (Plate 8a). Elsewhere resistant, siliceous stratiform and small mound structures are observed, which parallel bedding and are considered to be stromatolitic features (Hofmann *et al.* 1985, p.130). Contrasting primary beds are also evident in thin section (Plate 8b). The lighter layers consist of coarse-grained sparry carbonate and areas of quartz aggregates, while the darker layers are composed of an altered fine-grained granoblastic carbonate (Plate 8a-f). Bedding parallel dark laminae that are concentrated between the sparry coarse grain carbonate and areas with quartz aggregates (Plate 8c-f) further enhance bedding. These dark laminae may be pressure solution seams, which behave similarly to the pressure solution effects described by Ramsay (1967, p.196). The sparry coarse carbonate grains tend to have mechanical twins while the finer carbonate grains lack twins (Plate 8c, d). Also common in most specimens are carbonate veins sub-perpendicular to the dark laminae and bedding (Plate 8d-f). The veins appear to emerge from areas containing higher concentrations of the dark laminae (Plate 8d-f).

A sericitic-epidote-chlorite metasedimentary outcrop (E7) at the northern end of Woman Narrows was previously mapped as a stromatolitic marble unit (Figure 3). The outcrop appears very similar to the marble outcrops elsewhere, with contrasting dark grey and light grey-green

Plate 8

(a) Slabs of marble and metasediment specimen collected from outcrops at Woman Narrows. (b) & (g) Contrasting primary bedding layers of coarse grained carbonate, quartz layers and fine grained carbonate (b) or alternating layers of sericite that are either epidote-rich or poor (g).

(c)-(f) Primary layering in marble specimen is enhanced by bedding parallel pressure solution seams.

(c-d) Pressure solution seams are concentrated between sparry carbonate grains and quartz aggregates.

(d)-(f) Carbonate veins are perpendicular to bedding that appear to emerge from areas containing higher concentrations of the pressure solution seams.

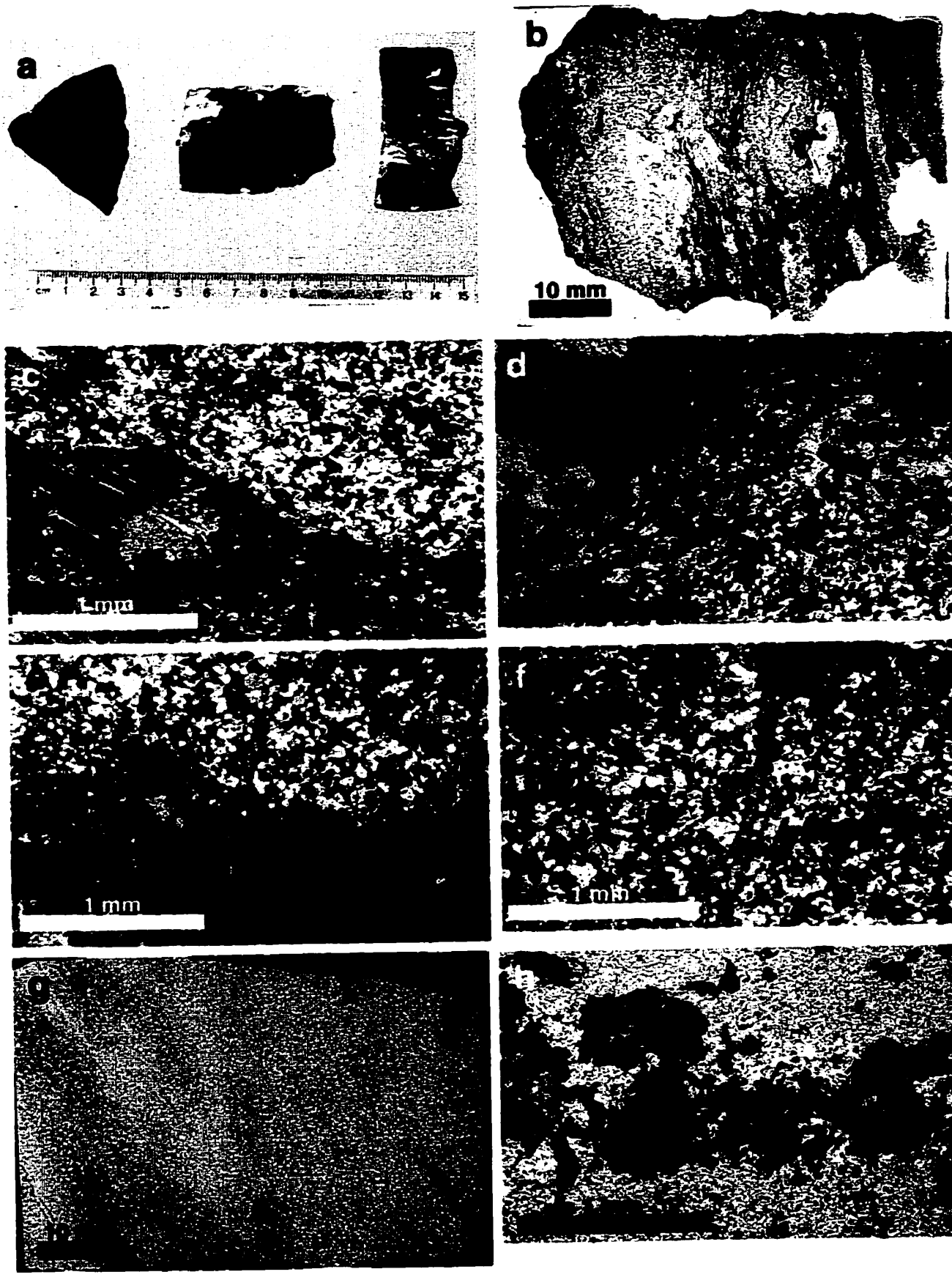

Plate 8

layers. In thin section the lighter layers consist of epidote with interstitial sericite and chlorite while the darker layers are comprised dominantly of sericite. It is these alternating layers of dominantly epidote and dominantly sericite that define the bedding observed.

3.4 Discussion

Mineral strain fabrics (schistosity and lineation) are more prominent and penetrative in mafic metavolcanics and intermediate rocks containing lapilli, abundant phenocrysts or amygdules. One reason for this may be that these rocks contain (1) minerals that grew during deformation according to the strain experienced (e.g. sericite, chlorite or amphibole) or (2) features that better record the total strain (e.g. varioles, lapilli; Plates 2, 3, 4, 6). In rocks that were more competent (e.g. felsic metavolcanics), strain fabrics are not as prevalent, however, numerous quartz veins strike sub-perpendicular to the regional schistosity. The veins may represent extensional fractures that formed as a result of a regional NNW-SSE compression (discussed later). Similar carbonate and talc filled extensional fractures were observed in mafic rocks (i.e. C3, Plate 3a-d). The fractures have been interpreted as tension gashes, which formed normal to the schistosity and other flattening fabrics.

A strain fabric is not discernible in the metagabbros studied (Plate 5a-c). The metagabbro from which the specimens were collected transects the Balmer-Woman assemblage boundary and appears unstrained in outcrop. Therefore, AMS of this unit was measured in order to determine whether or not a slight strain gradient exists across the assemblage boundary (cf. Chapter 5).

It was found that the opaque constituents of a metagabbro consist dominantly of pyrite, chalcopyrite, and sphene (pseudomorphs of ilmenite) with lesser amounts of pyrrhotite in the form of disseminated grains and as intergrowths with chalcopyrite (Plate 5d-h). Since the

opaques are composed of weakly magnetic minerals and typically represent <1% of the rock the magnetic fabric is controlled mainly by the paramagnetic minerals (cf. Chapter 5).

Intermediate pyroclastic rocks have a strong linear fabric and a weak schistosity which are defined by lapilli that are dominantly prolate with a flattening component (Plate 6a-f). This may be the result of a tendency to visually overestimate the linear fabric of a rock while underestimating the planar fabric (Schwerdtner 1977).

In the marble specimen studied, bedding-parallel dark laminae are interpreted to be pressure solution seams (Plate 8). This is based on 3 observations: (i) laminae are concentrated between the more competent constituents of the rock (quartz aggregates and coarse grained carbonates; Plate 8c-e), (ii) carbonate veins are found to be at high angles to the laminae and may represent dilational extensional fractures which formed in response to compression and provided space for carbonate to move into from areas of higher pressure, leaving the fine dark material behind (Plate 8d-f), and (iii) only the coarse carbonate grains appear to be mechanically twinned. This indicates that the competence of carbonate grains decrease with size, during pressure solution.

Van Staal (1998) and Rogers *et al.* (1999) report that the marble unit is mylonitic. However, the marble specimen studied contains carbonate grains of various size that are either primary or diagenetic in origin. Relict structures (i.e. bedding) are preserved and enhanced by bedding-parallel pressure solution, which further indicates that the marble has escaped pervasive recrystallization.

CHAPTER IV

RESULTS OF FIELD-BASED STRUCTURAL MAPPING

IV. RESULTS OF FIELD-BASED STRUCTURAL MAPPING

4.1 Introduction

The structure of various rock masses located near two assemblage boundaries in the southwestern portion of the Birch-Uchi greenstone belt was studied in detail. Attitudes of bedding, foliations (S), mineral and shape lineations (L) were obtained in the field, from available outcrops, and utilized in analyzing the total shear strain (Chapter 7). Together with estimates of principal-strain ratios (Chapter 6), lineation and schistosity trajectories form the basis for approximating the relative upward and northward displacement of the Woman and Confederation assemblage masses. As stated in the Introduction, however, the structural behaviour of the assemblage boundaries resembled more closely that of stretching faults, than that of shallow-crustal dislocations. This will be considered in detail in section 4.8 and other parts of the present thesis.

The following sections describe the areal pattern of structures observed in southwestern Birch-Uchi greenstone belt and provide stereoplots and structural maps summarizing the structural data collected in the field.

4.2 Attitude of Primary Layering

Local bedding attitude and trajectories of bedding are indicated on figure 12. Bedding (primary layering in igneous units) was observed and measured typically in metasediments, fragmental volcanic rocks and banded ironstone (e.g. E1, F5, F16; Figures 3, 4, 12). Where observed, bedding attitudes vary with position and dip at angles of 65° - 90° (Figure 15). In a fragmental volcanic unit (Plate 1a) west of the Balmer-Woman assemblage boundary, on Spot Lake, the strike of bedding changes from northeasterly on the south shore to east-southeasterly on the west-central shore, but returns to a northeasterly strike north of the lake (Figure 12).

Bedding Attitude Normals For The Field Area

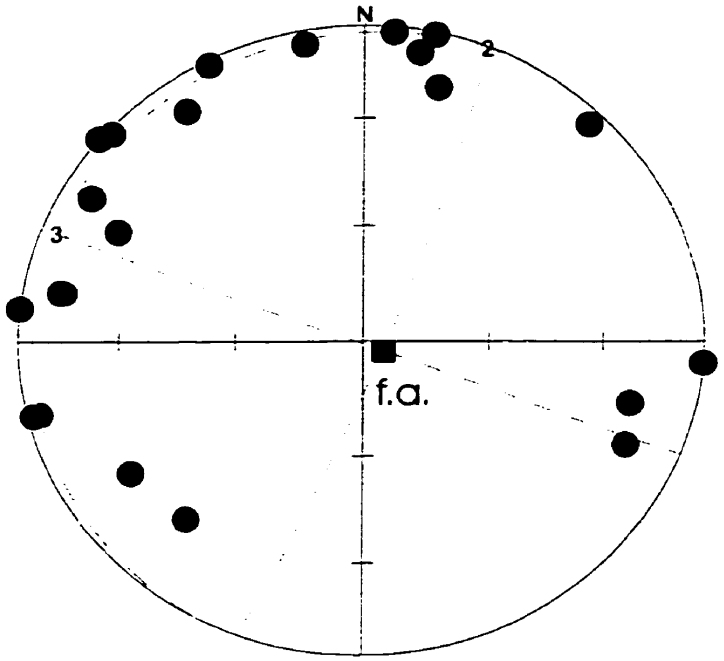

N =22

Equal Area (Schmidt)

f.a. = fold axis (119/85)

Eigenvectors
1 119/85
2 021/01
3 291/05

Figure 15

An S-fold is evident in the bedding trajectories north of Spot Lake (Figure 12). Here the map pattern suggests that the Balmer-Woman assemblage boundary coincide with an enveloping surface to the fold, which may itself be folded. The strike values of bedding in the Woman Lake area range from north-northeast in the south to northwest just above Woman Narrows. However, the bedding trajectories appear to parallel closely the Woman-Confederation assemblage boundary (Figure 12). From Woman Narrows to the top of Woman Lake, bedding trajectories oscillate between northwest and north-northeast (Figures 12, 16). Most bedding measurements were taken in a metaconglomerate unit located near the north-end of Woman Lake (Figure 12). The curvature of the trajectories points to gentle S-folding on the kilometre-scale. Further evidence is provided by figures 15, 16, & 17, which indicate open folds about a sub-vertical axis. A unit of banded ironstone in the Woman assemblage follows the general S-fold geometry of the folded Woman-Confederation assemblage boundary (Figure 12).

South of Woman Narrows, the bedding of a felsic tuff (sample location R1; Figure 12) has been deformed or redeformed into a disharmonic S-fold on the metre-scale. The fold axis, as determined from the intersection line between the two bedding limbs, plunges 67° and trends to the northeast. At sample location M144, the strike of bedding in a banded ironstone unit varies from 055° to 080° east of north (Figure 12). Therefore, the unit may also be folded on a scale of 20 metres.

4.2.1 Bedding π-Pole of S-folds

Two S-folds, delineated from available bedding attitude readings, are located at the Balmer-Woman and Woman-Confederation assemblage boundaries (Figure 12). The bedding normals for each fold were plotted on a stereonet using Spheristat 2.0 (Figures 16, 17). Density distribution contours and eigenvectors were also determined.

Bedding Attitude Normals For S-fold on Woman Lake

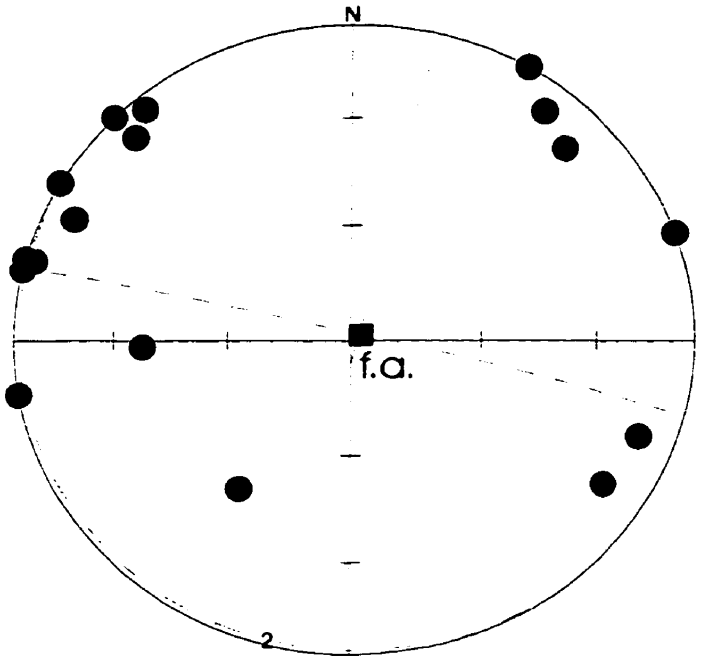

N = 17

Equal Area (Schmidt)

f.a. = fold axis (059/86)

Eigenvectors
1 059/86
2 194/02
3 284/02

Figure 16

Bedding Attitude Normals from Spot Lake Area

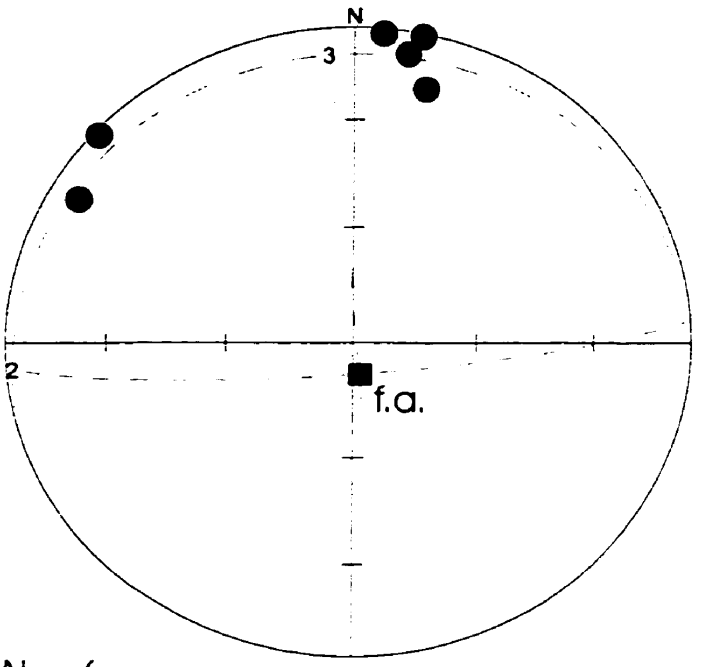

N = 6

Equal Area (Schmidt)

f.a. = fold axis (168/82)

Eigenvectors
1 168/82
2 265/01
3 356/08

Figure 17

Figure 17 plots the bedding normals observed in a fragmental volcanic unit at Spot Lake, west of the Balmer-Woman assemblage boundary (Figure 12). Although few measurements were available, a crudely cylindrical fold form can be discerned (Figure 17). Provided that this fold is indeed cylindrical, the fold axis determined by means of eigenvectors, plunges steeply and trends to the south-southeast (Figure 17).

Available bedding normals in a metasedimentary unit that defines a large S-fold on northern Woman Lake also point to a quasi-cylindrical fold geometry (Figure 16). Accordingly, the eigenvectors reveal a subvertical fold axis that trends to the northeast. However, there is an observational bias of field measurements.

4.3 Local Attitude and Trajectories of Schistosity

Figure 13 summarizes the schistosity attitudes obtained and presents their associated trajectories. Figure 18 plots the foliation normals measured in the field area. A Common type of schistosity is defined principally by chlorite and mica grains (cf. Chapter 3). At one or several localities (e.g. Station D2), stretched feldspar grains are preferably oriented in the schistosity (S). Dips of schistosity are moderate to subvertical throughout the field area. Schistosity is generally discordant to bedding and best developed in mafic-intermediate flows and fragmental metavolcanics.

Mineral schistosity in the field area is locally concordant to the planar shape fabric defined by primary strained features (lapilli and pillows) in mafic rocks of the Balmer assemblage (Figure 2, 13; Crews & Schwerdtner 1997, Crews *et al.* 1998). Also parallel to this schistosity are relatively undeformed metagabbroic dykes, which are thought to have been feeders for the Woman-assemblage basalts (Pryslak 1969, 1971, Crews & Schwerdtner 1997, van Staal 1998, Crews *et al.* 1999). Metagabbroic bodies transecting the Balmer-Woman assemblage

Schistosity Normal Attitude For The Field Area

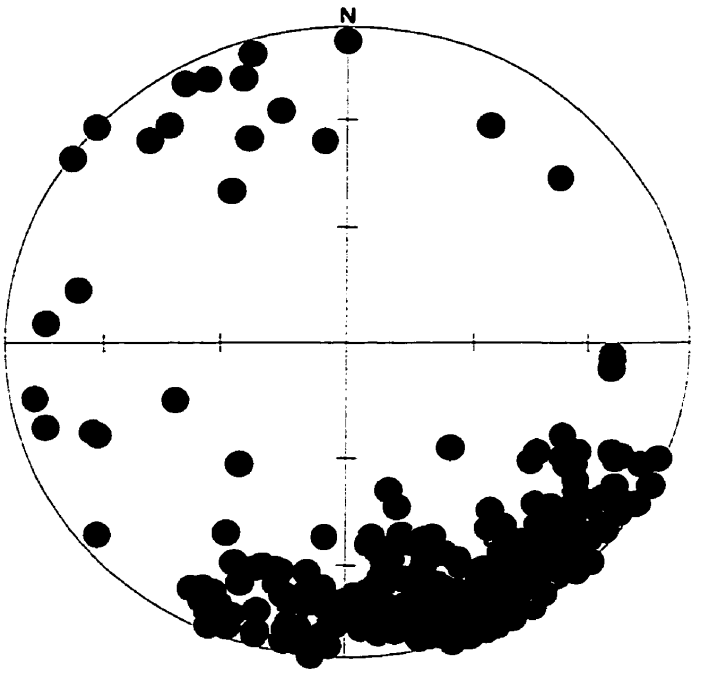

Equal Area (Schmidt)

N = 277

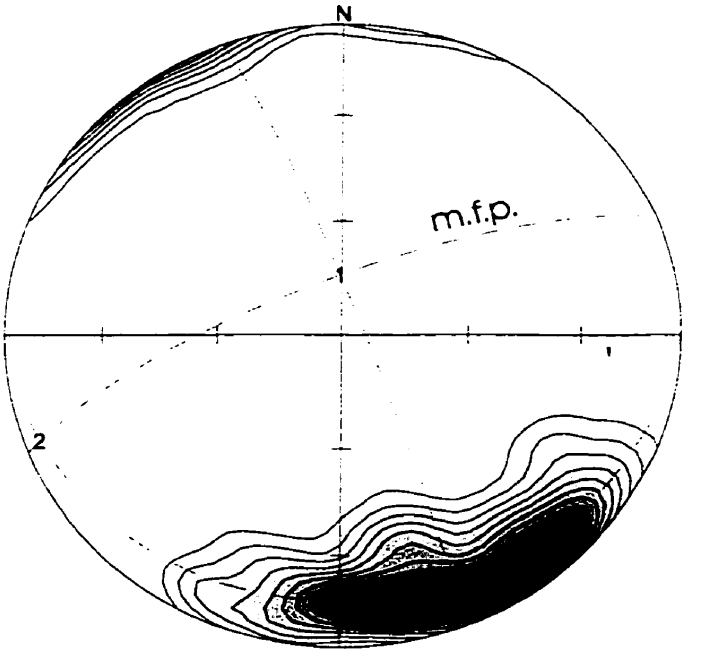

■ mean foliation normal (158/15)

m.f.p. = mean foliation plane

Figure 18

boundary and occurring throughout the Woman assemblage mass have mineral fabrics that range from being highly schistose, in metre-scale shear zones, to being undeformed or massive-looking. This range in mineral fabric is observed also in other rock units such as rhyolitic tuff, consisting of alternating "panels" with and without foliation (sample location D2; Figures 4, 13).

At a few localities (e.g. A22, A47, D18) there are two or three generations of foliation crosscutting each other. The first foliation is generally the schistosity , the second foliation is a closely spaced fracture/cleavage, seen at many outcrops throughout the area (Plate 9; Crews *et al.* 1999). Crews *et al.* (1999) attribute two fracture cleavages to the products of successive stresses, since the cleavages make various acute angles with the mineral schistosity. Schistosity is generally unaffected by narrow shear zones. An exception was found at station A22 where the schistosity is deflected.

Schistosity trajectories are constructed on the km-scale by connecting the strikes of foliation attitudes. Trajectory maps delineated the structural (strain) pattern in the field area (Figures 8, 13). Note that most trajectories pass through the greenstone assemblage boundaries without refraction (Figures 1, 8; Crews & Schwerdtner 1997, Crews *et al.* 1998, Borowik *et al.* 1999). On the other hand, trajectories appear to curve or deflect away at the Trout Lake Batholith (Figure 8). There is a slight local deflection of schistosity trajectories near the Woman-Confederation assemblage boundary at the lower end of Woman Narrows. Elsewhere at the boundary, there is no systematic deflection of schistosity. Similarly, no transverse strain gradient is discernible in rocks at the Balmer-Woman assemblage boundary. At Spot and northern Woman Lakes, the schistosity is approximately axial planar to both S-folds mentioned above (Figures 8, 12, 13). In Woman-assemblage rocks, the schistosity diminishes at a triple junction where the strain fabric is dominantly linear (Figure 8; Schwerdtner *et al.* 1999).

Plate 9

Oblique cleavages in schistose mafic metavolcanics of Woman Assemblage, eastern Quartz Lake, near west end of portage from Woman Lake.

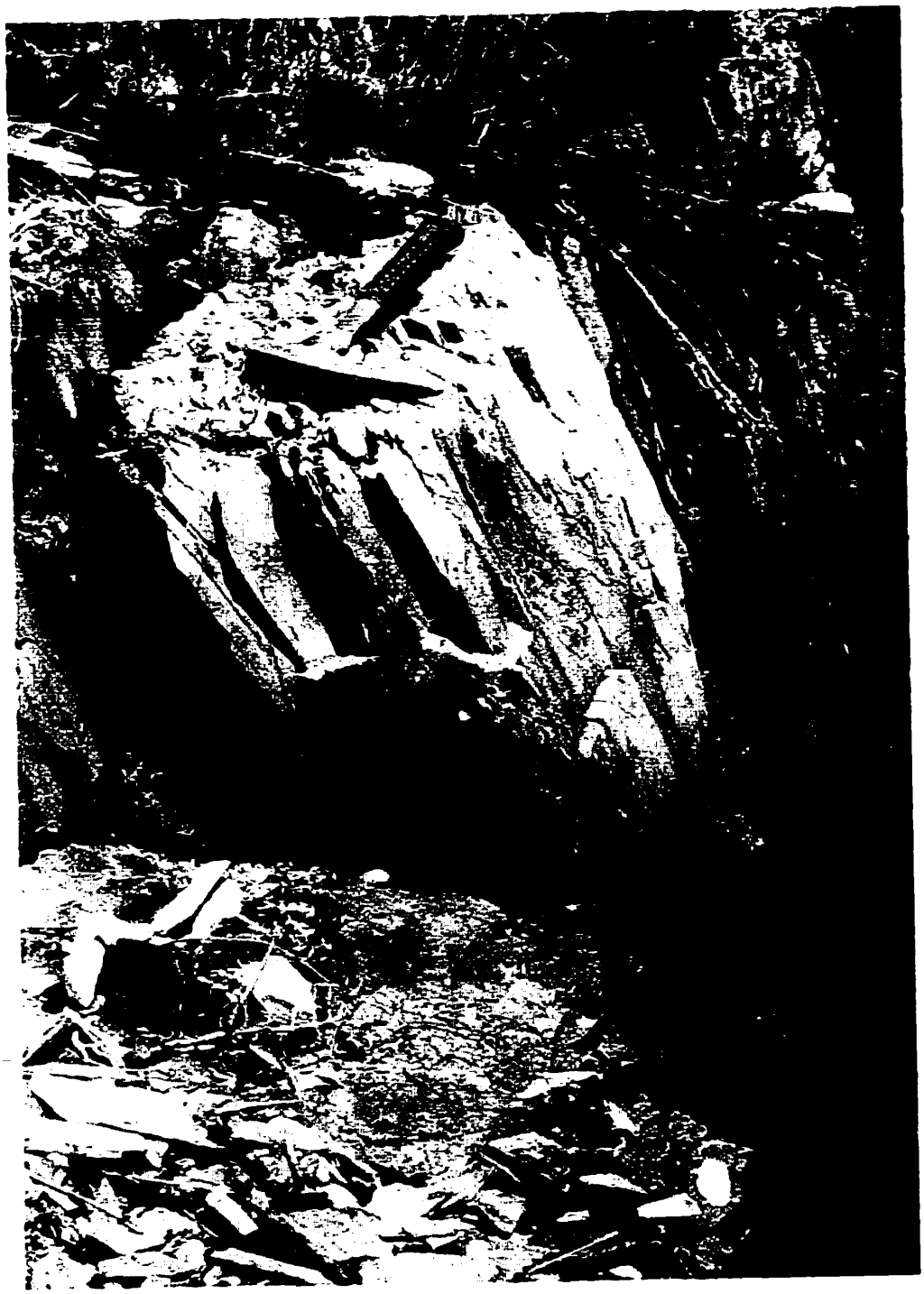

Plate 9

Figure 18 plots all the schistosity normals for the main study area, density distribution contours. The normals are effectively parallel to the short axis of strained primary features (varioles/spherules, lapilli) wherever seen in the field area (Figures 18, 19). However, there is considerable scatter in normal values across the field area (close to 90°, Figure 18). Eigenvectors for the foliation normals were calculated using Spheristat 2.0, and plotted on stereonets (Figure 18)

4.4 Attitudes of Mineral and Shape Lineations

Mineral and shape lineations were measured wherever possible (Figure 14). Metamorphic minerals such as mica, chlorite and stretched mineral aggregates, which define the mineral schistosity, also define the mineral lineation. By contrast, various strained primary features like lapilli and varioles/spherules define the shape lineations. Invariably, the shape lineation is effectively parallel to the mineral-grain lineation; therefore all linear features related to ductile deformation were denoted by L.

Lineation trends north-northeast in most of the study area, but, at northern Woman Lake, the trend values vary between 00° and 90° (Figure 14). Plunge values of L range from moderately steep to steep although there are a few shallow occurrences to the south of the field area (Figure 14). Steeper and well-developed lineations were observed more frequently in mafic and intermediate rocks. Conversely, lineations measured in felsic units are poorly developed and typically have shallower plunge values (Figure 3, 14). As a result, most lineation measurements were made on outcrops of mafic-intermediate rock.

At a triple point in the strain pattern (Figure 8; cf. section 4.3), the rock fabrics are dominantly linear. However, elsewhere, mineral lineation coexists with schistosity to form an L-

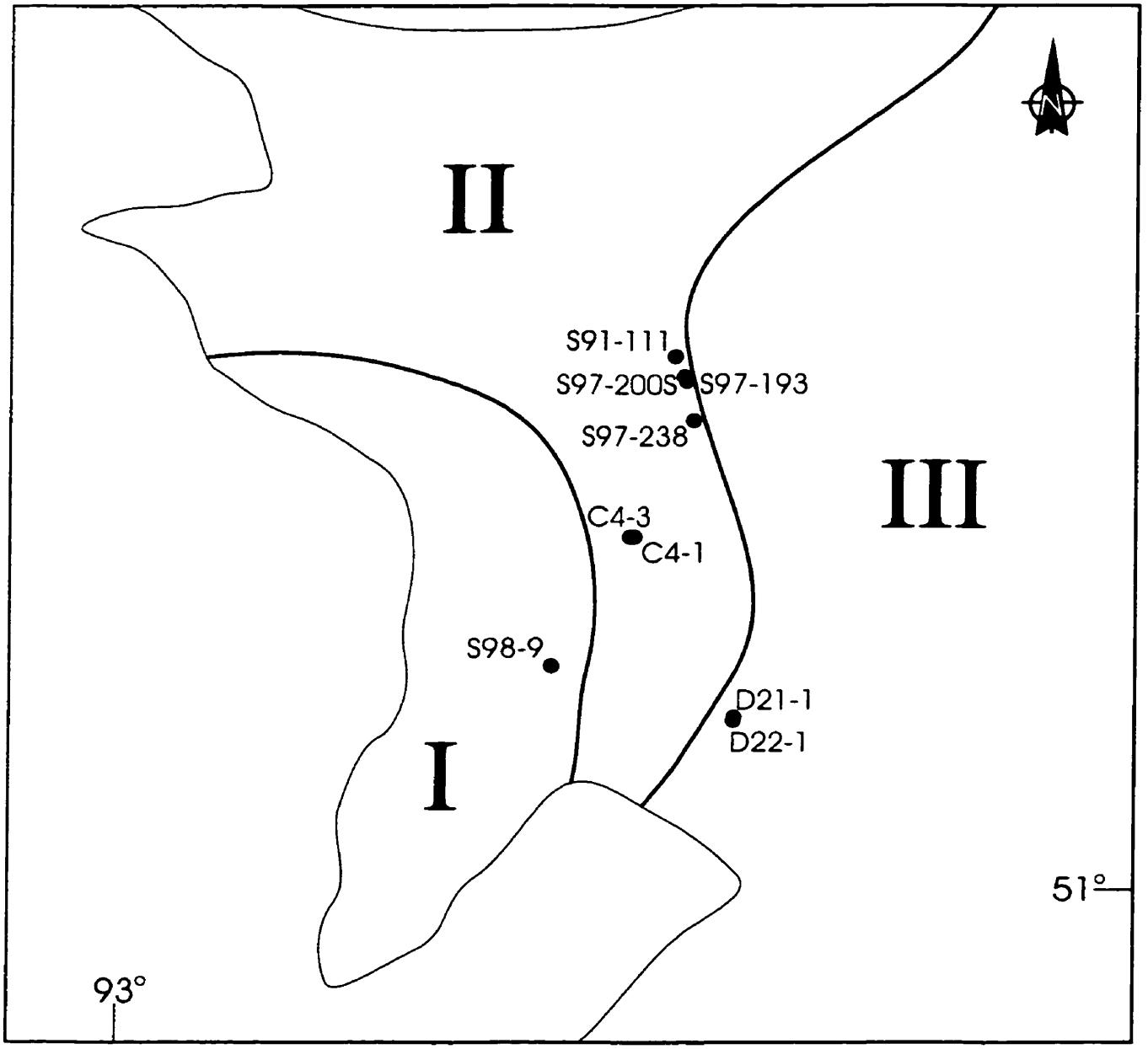
II
III
I
S91-111
S97-200S
S97-193
S97-238
C4-3
C4-1
S98-9
D21-1
D22-1
51°
93°
I Balmer assemblage
II Woman assemblage
III Confederation assemblage
greenstone
granitoids
station locations
assemblage boundaries
0
5
10 km

Figure 19

S mineral fabric (Figure 8; Flinn 1965). Lineation appears to be crudely parallel with the horizontal trace of the axial plane of the S-folds at the assemblage boundaries (Figure 12, 14).

Trend and plunge values of all lineation measurements were plotted on a stereonet using Spheristat 2.0 (Figure 20). Density distribution contours and eigenvectors were also calculated (Figure 20). Figure 20 confirms that the mineral lineation observed is parallel with the long axis of the strained primary features that define the shape lineation. The eigenvectors show an average lineation of 022/65 for the study area, which is sub-parallel to the maximum elongation direction, determined previously (cf. Figure 18).

4.5 Sampling Bias of Structural Field Data and Dip Angle of Assemblage Boundaries

The available data point to steeply plunging, quasi-cylindrical folds in stereoplots of bedding normals (Figures 15, 16, 17). However, the actual S-folds may be non-cylindrical and/or plunge less steeply than the stereoplot would suggest.

The bedding attitudes of the S-folds that were obtained at both assemblage boundaries are predominantly steep (Figure 12). As explained in the following paragraph, this is a result of a structural/geometric bias in favour of steep attitudes (Figure 21). The bias contributes to the difficulty in correctly estimating the plunge angle of these large-scale folds from the scattered bedding attitudes obtained in the field (Figure 12).

In common S-Z folds bedding in the long limb is steeper and tends to be better preserved than bedding in the short limbs (Figure 21). Measurements in narrow hinge zones of buckles are critical, but strategic outcrop may not exist in an area of <10% exposure. In ductilely deformed lithologic complexes, parasitic buckle folds are commonly tight giving the bedding in the limbs a steep attitude (Figure 21). The bedding measurements collected on Woman Lake may have been

Lineation Attitudes and Eigenvectors For The Field Area

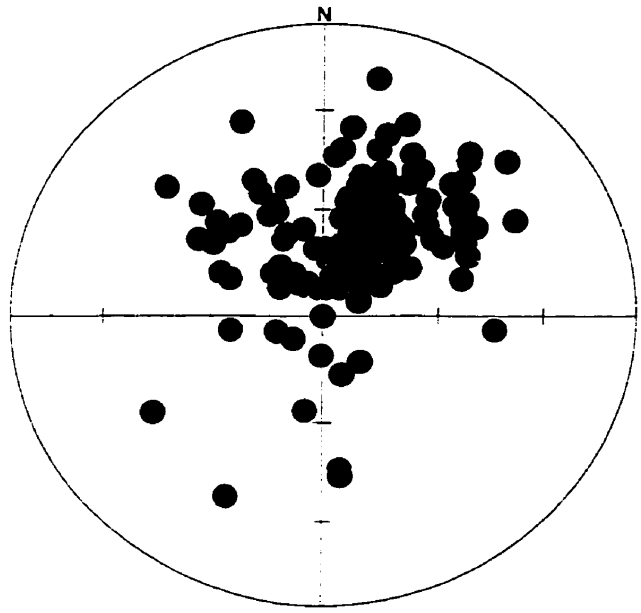

N = 156

Equal Area (Schmidt)

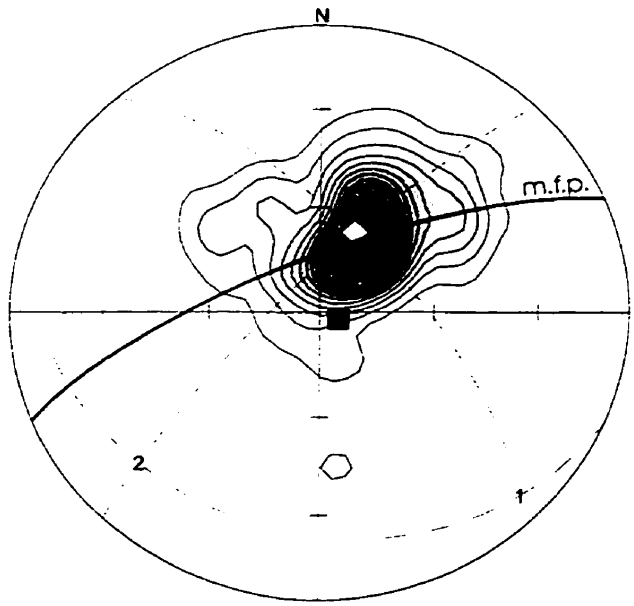

◇ mean lineation attitude (022/65)

■ fold axis (119/85)

m.f.p. = mean foliation plane

Figure 20

Schematic section perpendicular to sub-horizontal fold axis

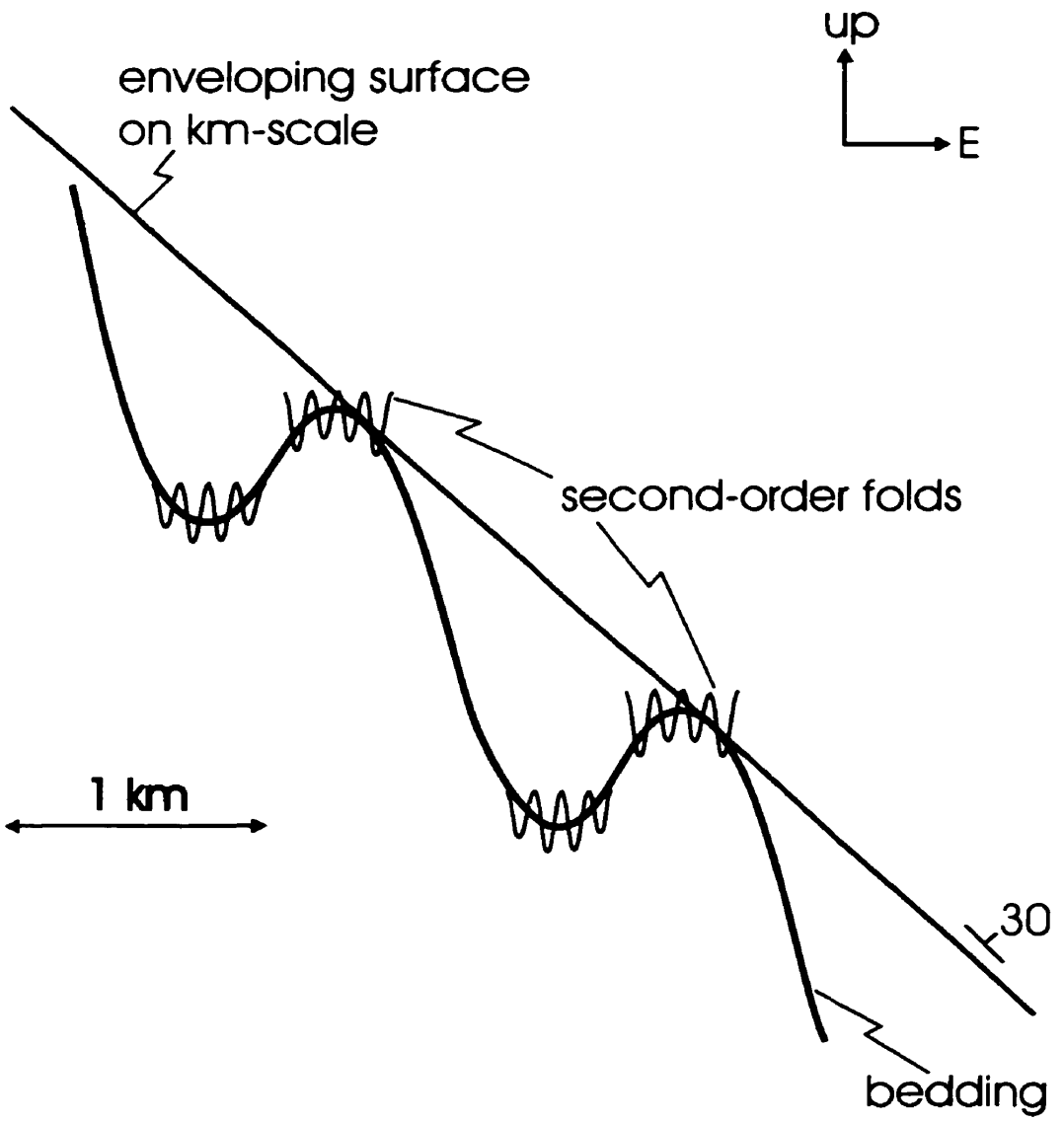

Structural bias against finding low dip values of bedding on small outcrops (<20m across).

Figure 21a

Simple map of northerly plunging structure similar to large S-fold on Woman Lake

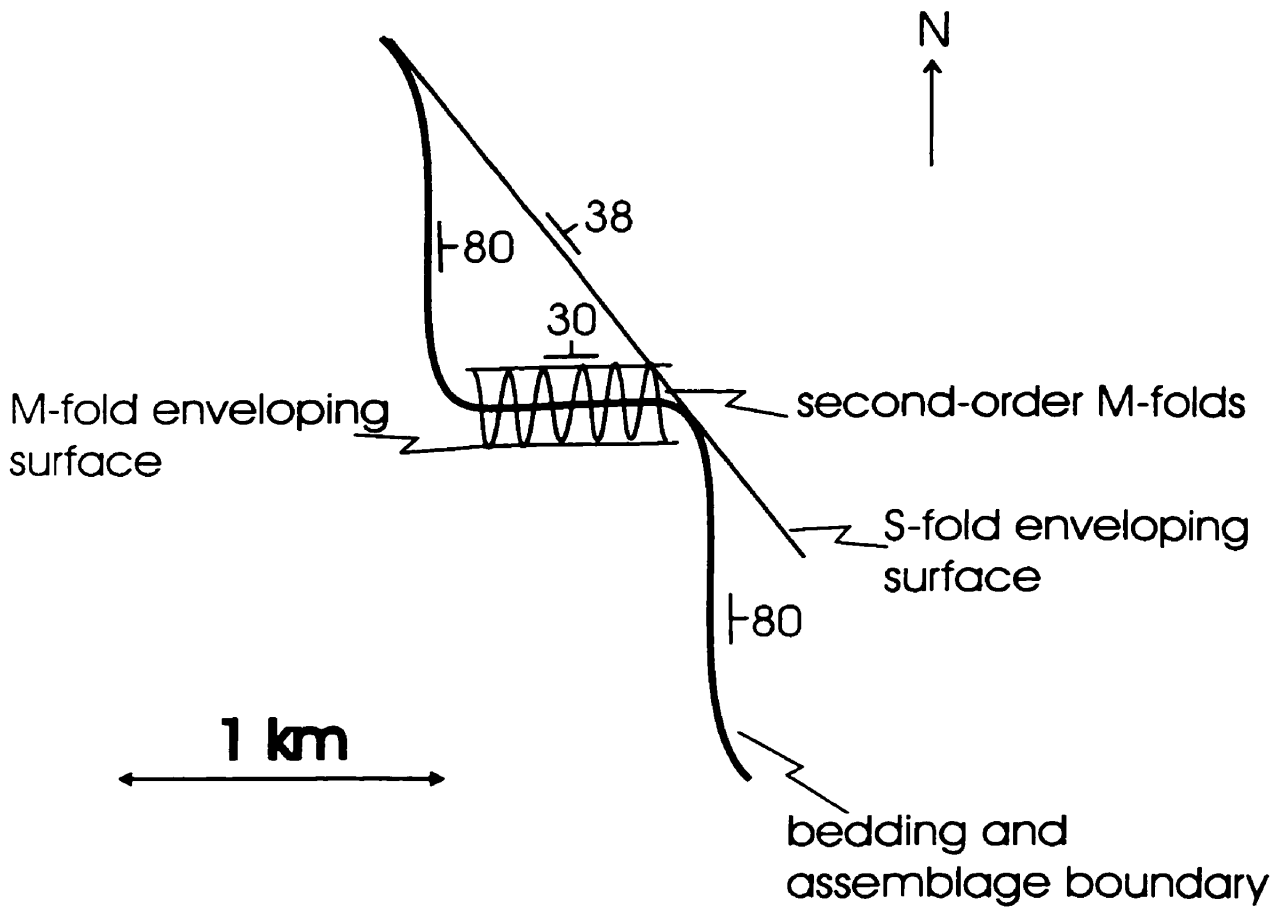

Structural bias against finding low dip values of bedding in the short limb.

Figure 21a

obtained on limbs of the S-structure or even of the second-order buckles (Figure 21). As a result, the large S-fold on Woman Lake appears to be cylindrical and have a steeply plunging fold axis.

The smaller a parasitic fold, the smaller its hinge zone. This decreases the chance of obtaining bedding measurements that are critical for the construction of fold enveloping surfaces to the short limb of any first-order S-fold exposed on the Precambrian peneplain. Without the envelope to parasitic folds of the short limb, the axis of the plunge of the first-order fold can not be determined (Figure 21). This in turn, prevents a dip estimate for the first-order, fold enveloping surfaces (Figure 21).

At the kilometre-scale, the attitude of both assemblage boundaries in the western central Birch-Uchi belt may correspond to the enveloping surfaces of the two folds observed (Figure 12). It is very important to know the dip of the assemblage boundaries for strain analysis purposes (cf. Chapter 7). If the S-folds could be properly delineated the true attitude of the fold-enveloping surface (LTB) can be obtained (Figure 21). (The enveloping surfaces do not need to be straight or planar.)

The fold axis of the metre-scale S-fold at sample location R1 furnishes the maximum dip angle of the local segment of the Woman-Confederation assemblage boundary (Figure 12), provided that the structure is a first-generation fold. However, if it s a second-generation fold, it lies within the foliation and does not permit an estimate of the boundary dip on the kilometre-scale. If the fold is assumed to be first generation and cylindrical and have a fold axis of 068/67 (calculated using bedding measurements, figure 22), the southern end of the Woman-Confederation assemblage boundary can be fixed with a minimum dip angle of 79° at the metre-scale (Figure 21, 22). Further estimation of the dip-angle variation with scale requires better knowledge of the geometric style of folding in assemblage boundaries and lithologic contacts.

Determination Of Woman-Confederation Assemblage Boundary Dip Using Fold Axis Of Fold At Location R-1

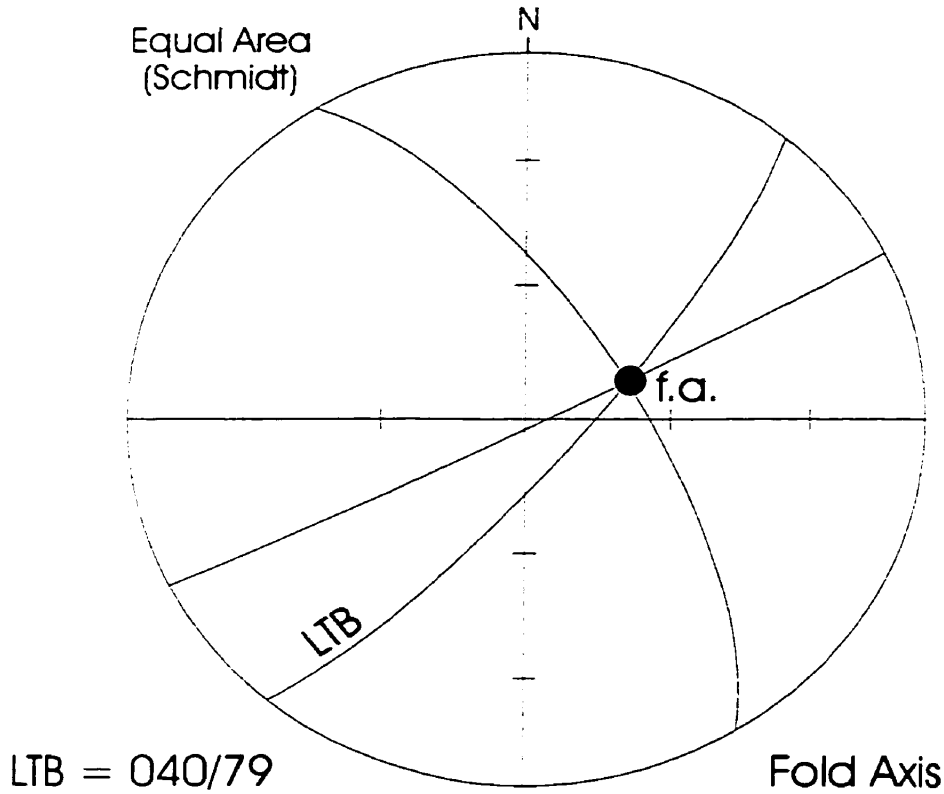

LTB = 040/79

Fold Axis = 068/67

Figure 22

4.6 Discussion and Summary

The geologic map patterns of all stratigraphic units in the walls of both assemblage boundaries affirm the presence of several large S-folds (Figure 12). A prominent ironstone horizon west of the Woman-Confederation assemblage boundary further confirms this S-shaped geometry. Plots of available bedding normals are not incompatible with a steep fold axis and suggest that both folds may have cylindrical geometries (Figures 12, 16, 17). However, since structural bias can not be avoided in the glaciated terrain of NW Ontario, it is uncertain whether the fold axis actually plunges steeply (Figure 21). A magnetic anomaly at the Balmer-Woman assemblage boundary supports the idea that, on the kilometre-scale, the boundary is a fold-enveloping surface (Figure 12, van Staal 1997). The large S-fold, at the Woman-Confederation assemblage boundary, points to a sinistral component of north-south shear strain, distributed across rocks of both assemblages (Schwerdtner *et al.* 1997). However, the shear strain component parallel to the hinge lines can not be judged from the folding.

The metre-scale fold at R1 (Figure 4, 12) is probably part of a larger-scale fold limb and should perhaps not be used to estimate the boundary dip on the kilometre scale. However, if it is indeed a first-generation fold and the structural bias is ignored the Woman-Confederation assemblage boundary has a maximum dip angle of 079°E.

Mineral schistosity (S) and associated mineral lineation (L) pervade the meta-volcanic-metasedimentary rocks mapped in the field area (Figure 2, 13, 14). Strained primary features (varioles/spherules, lapilli; Table 1, Plate 1a, 2) are seen at many localities. The long axis of these features parallels the mineral lineation and their short axis is everywhere normal to mineral schistosity. This clearly demonstrates that the schistosity is effectively normal to the local direction of maximum shortening and that the mineral-grain lineation is effectively parallel to the

Specimen Number	Greenstone assemblage/ rock type	$\frac{X}{Y}$	$\frac{Y}{Z}$	X*	Y*	Z*	Prolateness Factor ν	Strain Intensity γ_o
S97-111	Metacong.	1.997	2.392	2.121	1.062	0.444	0.116	1.281
S97-193	Frag. Volc.	1.458	2.069	1.638	1.124	0.543	0.317	0.916
S97-200S	Metacong.	1.396	1.466	1.419	1.016	0.693	0.068	0.585
S97-238	Frag. Volc.	1.33	2.39	1.617	1.216	0.509	0.507	0.983
S98-9	Balmer	1.5	1.2	1.392	0.928	0.774	-0.379	0.491
C4-1	Woman	1.92	1.51	1.772	0.923	0.611	-0.227	0.875
C4-3	Woman	2.46	1.48	2.077	0.844	0.570	-0.390	1.090
D21-1	Confederation	2.79	2.47	2.679	0.960	0.389	-0.063	1.580
D22-1	Confederation	5	1.3	3.191	0.638	0.491	-0.720	1.655

Table 1: Principal strain ratios in mafic variolites/spherulites, metaconglomerates and fragmental volcanics using the diameter ratio method of Robin (1977) and Peach & Lisle (1979). The mean long axes of the varioles is effectively parallel to the mineral grain lineation in the matrix and the mean short axes of the varioles is approximately parallel to the foliation normal.

$X > Y > Z$ = Principal radii of strain ellipsoid. X*, Y*, Z* = principal components of distortion. Parameters ν and γ_o are defined in Hossack (1968).

local direction of maximum extension (Figures 18, 20). The mineral schistosity thus pertains to total strain since it conforms everywhere to the planar shape fabric defined by the primary strain features. The scatter of schistosity normals (Figure 18) may be regarded as evidence of repeated folding or perhaps a result of heterogeneous strain.

Locally, strain is strongly heterogeneous on the metre-scale, as indicated by gabbroic mineral fabrics that range from being apparently undeformed to highly schistose. However, on the kilometre scale and especially near the assemblage boundaries, the strain is virtually homogeneous. This is shown by the lack of deflection of schistosity trajectories across both assemblage boundaries (Figure 13). This lack of trajectory refraction attests to mechanically passive behaviour of the assemblage boundaries during ductile deformation (Crews & Schwerdtner 1997, Crews *et al.* 1998). However, schistosity relates to the total strain and it is conceivable that the assemblage boundaries were incoherent for short periods of time. Nonetheless, the schistosity trajectory pattern indicates that the apparent age gaps between the greenstone assemblages predate the ductile regional deformation (Borowik *et al.* 1999).

In western parts of field area metagabbro dykes appear to be parallel to schistosity. Two tectonic scenarios may be envisaged to explain the parallelism. In the first scenario, the dykes were emplaced before schistosity and governed further ductile deformation of the host rocks. In the second scenario, a prominent schistosity and associated shape fabrics existed before and acted as an effective plane of weakness during concordant dyke emplacement. Using current and available geologic evidence, it is difficult to discriminate between the two explanations.

Two deformation episodes (D_1, D_2) have been proposed for the Birch-Uchi greenstone belt (Fyon & Lane 1985, Stott & Corfu 1991). The first episode involved northwest-southeast transpression that produced the pervasive schistosity. The Trout Lake batholith acted like a rigid

block during schistosity development causing the bedding to bend around it. Other possible effects of D_1 are being debated (Fyon & Lane 1986, van Staal 1998, Rogers *et al.* 1999).

D_2 led to north-south directed compression that buckled the assemblage boundaries and created the S-folds and associated strain (Figure 12). However, this does not prove that schistosity (a feature related to the total strain) is axial planar to the large S-fold.

On the kilometre scale, the dip of the assemblage boundaries is uncertain. Not knowing the boundary attitude makes it difficult to study the sense of tangential shear along the assemblage boundaries as well as determining the magnitude and direction of total shear strain. The true dip of both assemblage boundaries will eventually be determined by a combination of extensive geological and geophysical work. Until such work is done, the structural bias favouring steep bedding attitudes (Figure 21) poses a difficult problem for structural geologists.

4.7 Tectonic Evaluation of the Areal Strain Pattern

With the possible exception of a high pressure aureole around the Trout Lake batholith (Figure 2), evidence for steep horizontal gradients of vertical displacement components is lacking in western central parts of the Birch-Uchi belt. This seems to rule out the possibility of large-scale tilting and other types of solid-body rotation about horizontal axes.

The pattern of total strain in the wall rocks differs between the two boundaries (Figures 13, 14). In the vicinity of Spot Lake and the Balmer-Woman assemblage boundary, the mean attitude of schistosity is nearly vertical so that the minimum radius of the overall-strain ellipsoid is approximately horizontal. Schistosity trajectories are nearly perpendicular to the horizontal trace of the assemblage boundary, which parallels the minimum radius. The other principal radii are inclined so that the material surface now coincident with the erosion level reached the horizontal plane by strain-induced rotation about the boundary trace. The rotation angle will be

modest because the total-strain intensity is small to moderately large at most localities in the wall rocks (cf. Chapter 6).

Strain-induced rotation about the horizontal boundary trace implies that the direction of mean tangential-shear strain parallels the dip line of the assemblage boundary. (This disregards the special case in which the dip line is fortuitously parallel to the mean mineral lineation so that the resultant tangential shear strain is zero.) Therefore, the geometric effects of mean tangential shear, particularly the transverse gradient of point displacement, need to be shown in a vertical section (cf. the example illustrated in Figure 23).

The situation is very different at the Woman-Confederation assemblage boundary, where schistosity is subvertical but its trajectories are markedly oblique to the horizontal boundary trace (Figure 13). This amounts to a large horizontal component of the tangential shear strain, together with a significant dip-parallel component. Because of the counter-clockwise sense of obliquity between schistosity trajectories and the boundary trace, horizontal components of transverse displacement gradients are sinistral. Rigorous graphic evaluation of the local conditions of the tangential shear strain shows (Chapter 8) that the γ-vector generally has a northerly plunge and an inclination of 10-40°. Therefore, the transverse gradient of tangential point-displacement components can be shown in the map plane (Figures 24, 25), and used in structural tests of the northward transportation hypothesis (Stott & Corfu 1991).

The southern part of the Woman-Confederation assemblage boundary of Roger's *et al.* (1999) is marked by a brittle-ductile shear zone, which may have been partially incoherent. No evidence has been found for mechanical incoherence of the Woman-Confederation assemblage boundary of Stott & Corfu (Figure 8). In either case, the total tangential displacement was mostly distributed across the boundary walls, instead of being confined to a surface of

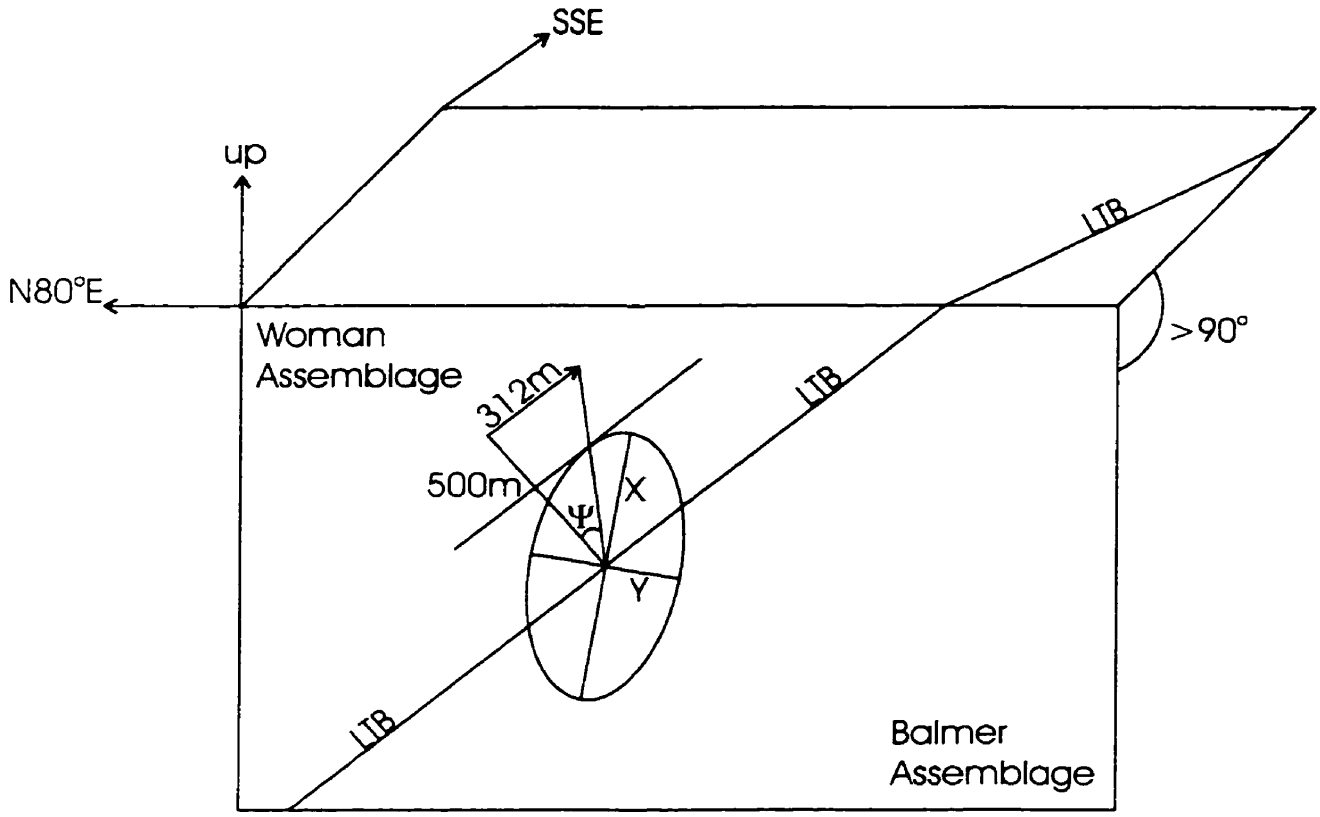

Upward displacement of interior of Woman-assemblage mass. LTB attitude: N002E/40E. LTB = assemblage boundary. Principal-strain ratios for rock specimen C4-1 (Woman assemblage).

Figure 23

Balmer-Woman assemblage boundary (vertical section)

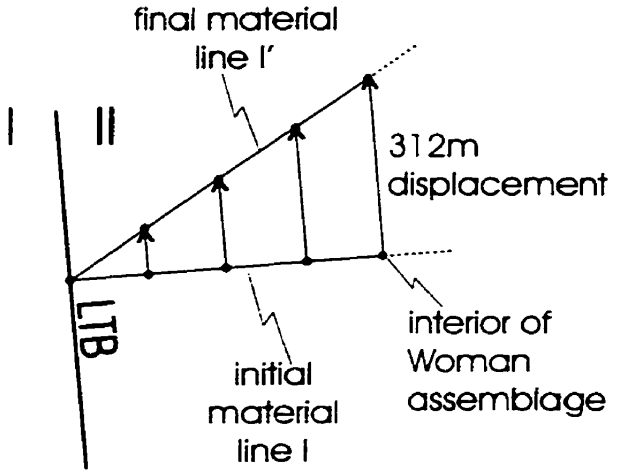

Woman-Confederation assemblage boundary (map view)

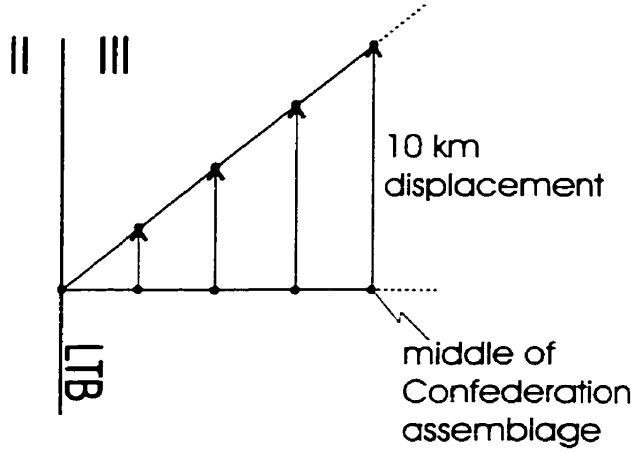

Gradients of tangential DDV components may be parallel and/or transverse to the assemblage boundaries. Shown are actual transverse gradients, which are responsible for tangential shear strain. Not shown are tangential gradients of tangential DDV components leading to contraction/extension of the LTB trace (cf. Figure AL).

Figure 24

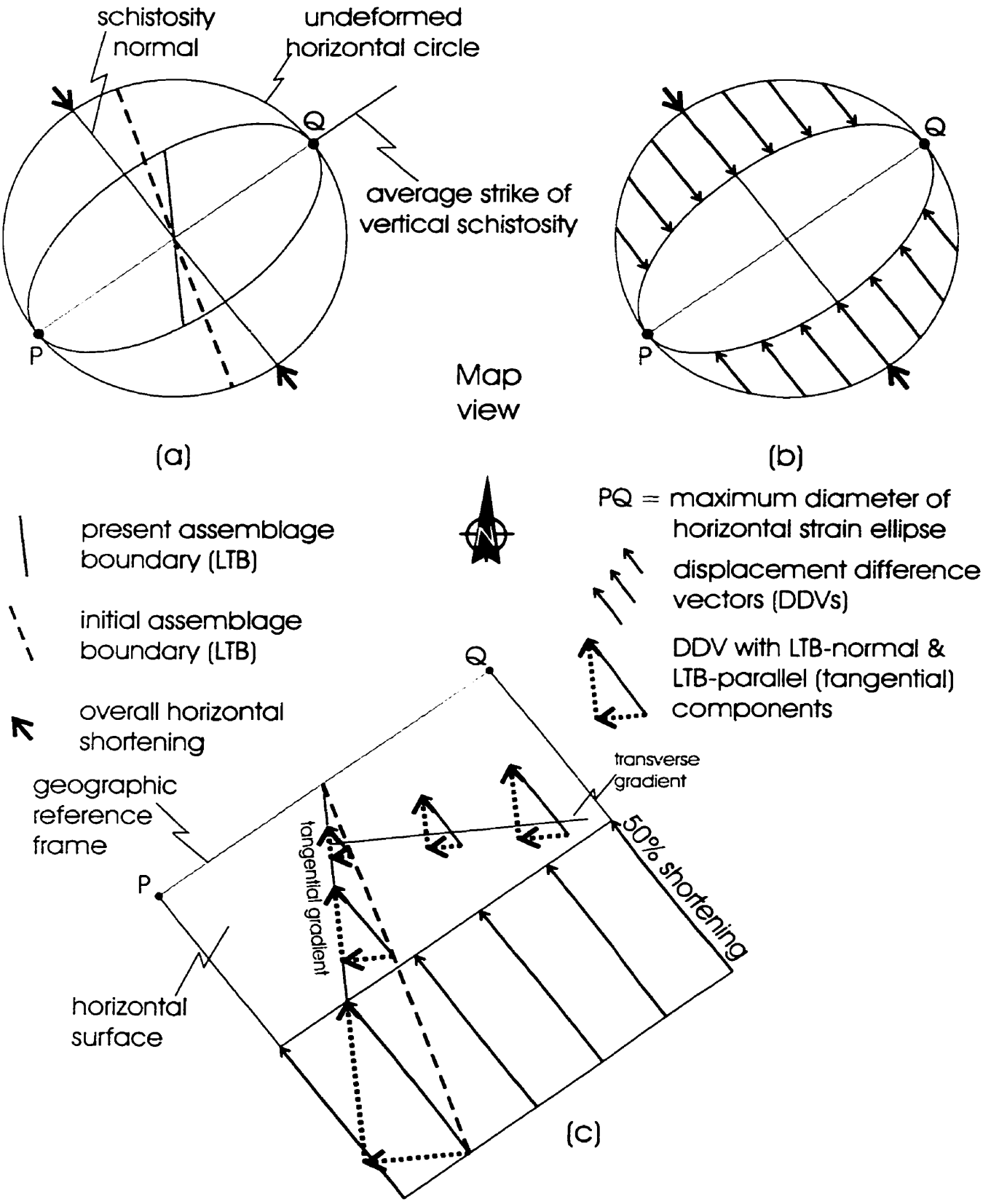
schistosity normal
undeformed horizontal circle
Q
average strike of vertical schistosity
P
Map view
(a)
(b)
present assemblage boundary (LTB)
initial assemblage boundary (LTB)
overall horizontal shortening
PQ = maximum diameter of horizontal strain ellipse
displacement difference vectors (DDVs)
DDV with LTB-normal & LTB-parallel (tangential) components
geographic reference frame
transverse gradient
tangential gradient
50% shortening
horizontal surface
(c)

Figure 25

translational faulting. Of particular interest are differences in horizontal displacement components parallel to the boundary trace (Figure 24), which rotated clockwise during ductile deformation of the wall rocks (Figure 25). Because the boundary trace was shortened while rotating toward the schistosity trace, the boundary surface qualifies as a negative stretching fault on which the slip magnitude is close to zero (Means 1989). The horizontal component of tangential displacement distributed in the boundary walls is sinistral, as explained above. This is compatible with the requirements of the northward transportation hypothesis (Stott & Corfu 1991), but the situation becomes more complicated if one analyses the tangential shear strain in three dimensions (cf. Chapter 8). The sinistral horizontal displacement documented at the N-S striking trace of the Woman-Confederation assemblage boundary results from areal NW-SE compression rather than translational faulting. This satisfies the conditions for the development of stretching faults, as originally formulated by Means (1989) and quoted in the Introduction (Chapter 1). However, NW-SE compression does not suffice to explain the fist-like map pattern recognized by Stott & Corfu (1991, cf. Chapter 1.2 above). In particular, the advance of a "fist" requires dextral shear strain on the eastern side, which is far beyond the present field area.

CHAPTER V

ANISOTROPY OF MAGNETIC SUSCEPTIBILITY (AMS) STUDY

V. ANISOTROPY OF MAGNETIC SUSCEPTIBILITY (AMS) STUDY

5.1 Introduction

Several studies have revealed that the magnetic properties of rocks can be useful in determining their degree of deformation and structural evolution (Hirt et al. 1988). Anisotropy of magnetic susceptibility (AMS) has been used as a way of quantifying the fabric of deformed rocks in structural studies (Hrouda 1982, Borradaile 1988, Sun et al. 1995).

The purpose of this study was to determine, with the aid of AMS, whether a strain gradient exists within an apparently unstrained gabbro sheet that "stitches" an assemblage boundary. Information about the nature of the AMS may provide valuable insight into the mechanical behaviour of the assemblage boundary during ductile deformation of the wall rocks.

5.2 AMS and Magnetic Fabrics

Study of the anisotropy of magnetic susceptibility (AMS) has many uses in geology. The AMS may be described by a symmetric second-rank tensor, partly represented by a triaxial magnetic susceptibility ellipsoid (Borradaile 1988, Hrouda 1982). The eigenvectors are principal directions and the eigenvalues ($k_{max} \geq k_{int} \geq k_{min}$) principal radii whose length may be given in dimensionless SI units/volume (Borradaile and Stupavsky 1995). The AMS tensor expresses the linear relationship between induced magnetization (M) and applied field (H, Borradaile 1988, Tarling & Hrouda 1993).

Rock-forming minerals fall into one of three groups: paramagnetic, diamagnetic, or ferrimagnetic. According to grouping, the minerals are the causative factors in the magnetic anisotropy of rocks and control their bulk susceptibility (Kmean; Hrouda 1982). The bulk susceptibility is the "summation of the susceptibilities of all the mineral species that are present in a sample" (Tarling & Hrouda 1993). The causes of AMS are thought to be the shape

alignment of ferrimagnetic grains (largely the shape preferred orientation, SPO) and/or the lattice alignments of crystals with magnetic crystalline anisotropy, i.e. the crystallographic orientations of the diamagnetic and paramagnetic minerals (Richter et al. 1994). Other kinds of influence include the alignment of magnetic domains and the linking of magnetic grains so that they act as one, also called "distribution anisotropy" (Canon-Tapia 1996). In rock forming minerals, the bulk susceptibility (Kmean) is generally small, typically -10^{-5} SI units/unit volume for diamagnetic minerals (e.g. calcite, Rochette 1987), and for paramagnetic minerals (e.g. plagioclase, feldspars, amphiboles) the susceptibilities are positive and approximately 10^{-4} SI units/volume (Tarling & Hrouda 1993). The susceptibility of ferrimagnetic minerals (e.g. magnetite) is several orders of magnitude larger than either para- or diamagnetic minerals, with typical values ranging from 5 SI units/volume for magnetite to $6x10^{-3}$ SI units/volume for hematite (Borradaile 1988). This vast difference between susceptibility values demonstrates the need to establish what the controlling magnetic mineralogy is prior to the analysis of AMS fabrics (Borradaile 1991).

AMS fabrics consist of two parts, the magnetic foliation containing k_{max} & k_{int} and the magnetic lineation, which parallels the k_{max} axis (Jelinek 1981). The magnetic foliation and lineation are defined, respectively, by the scalar parameters $F=k_{max}/k_{int}$ and $L=k_{int}/k_{min}$. These are considered to be two of the most useful parameters used in AMS studies (Hrouda 1982). However, Jelinek, (1981), suggests the use of two parameters depending on all three principal components. These parameters are called P' and T. The shape factor (T) resembles Flinn's (1962) k-value, and best illustrates the shape of the AMS ellipsoid (Borradaile et al. 1993). $T=[2(\ln k_{int} - \ln k_{min})/(\ln k_{max} - \ln k_{min})] - 1$ varies from a perfect prolate (rod shaped) ellipsoid with a value -1 to +1 for a perfect oblate (disk shaped) ellipsoid. A value of 0 corresponds to a plane-

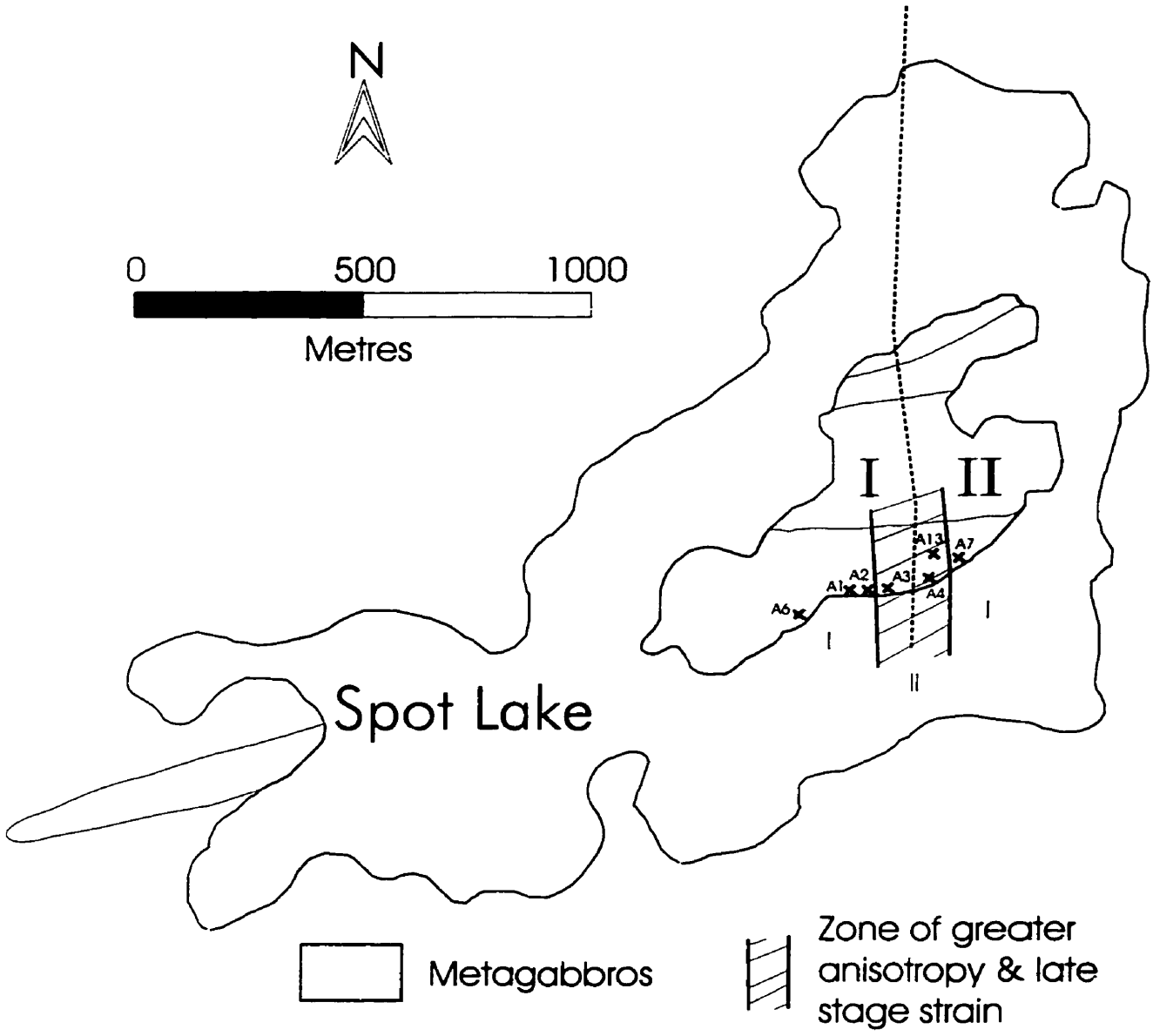

Map of Spot Lake showing the zone of greater anisotropy and later stage strain of the metagabbro samples studied. I & II mark the two groups of samples.

Figure 26

strain or neutral ellipsoid. P' is the intensity or degree of anisotropy (Jelinek 1981), and is defined by $P'=\exp[2(A_{max}^2 + A_{int}^2 + A_{min}^2)]^{1/2}$, where $Amax=\ln(k_{max}/kb)$, etc., and $kb=(k_{max} + k_{int} + k_{min})/3$.

5.3 Method

Ten rock specimens were collected from a metaleucogabbro sheet that transects the Balmer-Woman assemblage boundary (Figure 26). A total of 141 core samples (2.2cm x 2.54cm diameter) from 59 drill holes were prepared in the laboratory. The anisotropy of low-field magnetic susceptibility (AMS) was determined using Sapphire Instruments SI-2B AC bridge. Anisotropy was determined using 7 orientations (including both cube edge and body diagonals) for each specimen. The eigenvectors and eigenvalues (k_{max}, k_{int}, k_{min}) and other AMS parameters (e.g. P', T, & kmean) were calculated, along with the mean values of the AMS data, using the APLOTWIN program of Dehls (1997). Several plots were constructed including T vs. P', P vs. kmean, L vs. F (with natural logarithms) and k_{max}, k_{int} & k_{min}. Plots for the mean values of AMS parameters were also prepared. A petrographic analysis of the samples studied was also undertaken to determine which minerals contribute to the magnetic fabric measured (cf. Subsection 3.3.2; Plate 6).

5.4 Results and Analysis

Bulk susceptibility (Kmean) ranges from a low of 4.49×10^{-4} (A3-4) to a high of 8.88×10^{-4} (A13-1) (Figure 27). The range here indicates that the paramagnetic minerals probably control susceptibility (cf. Chapter 3.3.2). The Kmean of A13-1 (& partly A13-4) is slightly higher than the entire group. This may be caused by a greater contribution of the ferrimagnetic minerals in these samples (i.e. pyrrhotite; cf. Chapter 3.3.2). Location does not appear to influence the bulk

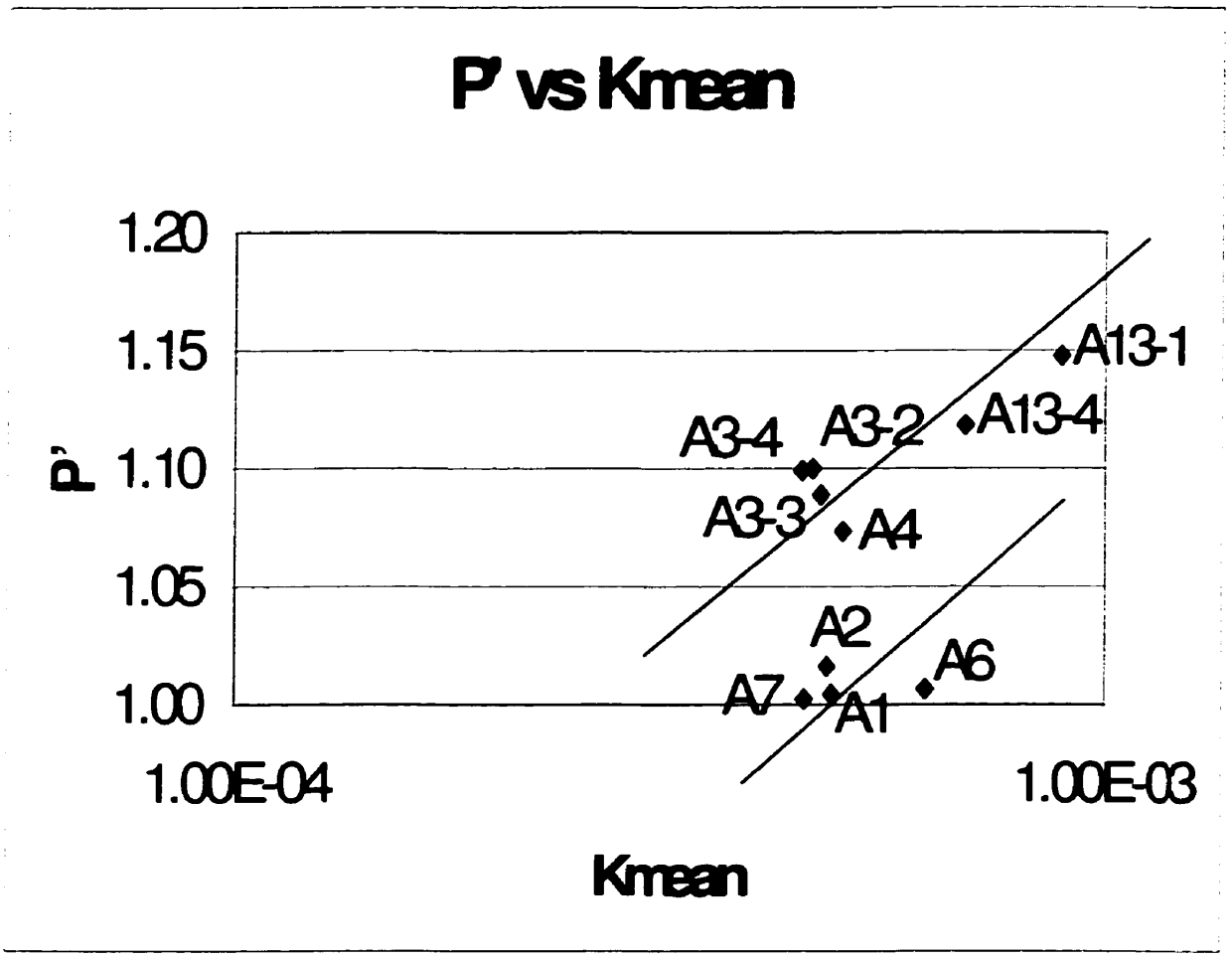

Plot expressing the relationships between P' and Kmean, where P' is the anisotropy intensity and kmean the bulk susceptibility. There is a slight positive correlation between P' and kmean suggesting that P' is related to composition (i.e. mineralogy).

Figure 27

susceptibility. Moving from west (A-6) through to east (A7), across the assemblage boundary, kmean remains almost constant at ~5.0×10^{-4} (Figures 27, 28). The degree of anisotropy (P') changes with virtually constant bulk susceptibility across the boundary (Figure 27).

The degree of anisotropy (P') varies from 1.0022 (0.2%) for A7 to 1.1478 (15%) for A13-1 (Figures 27, 29). Location with respect to assemblage boundary does appear to play a role in values of P'. Lower values of P'(<1.02) were obtained in the samples furthest away from the boundary (Figures 26, 30) (Group I in figure 27 consisting of A6, A1, A2 & A7). Group II, those samples located near the boundary (A4, A3, & A13), have a markedly higher degree of anisotropy (>1.07) (Figure 27).

An oblate to plane-strain fabric dominates most of the samples studied (Figures 29, 31). Three samples hold a subtle to strong prolate fabric, A7, A2 & A1 respectively. The oblate examples (A3, A4, & A13) have low to moderate values of T (0.0821 to 0.4027) and imply a moderately strong L-S fabric (Figure 29). Note that the oblate fabrics were obtained in samples nearest the tectonic assemblage boundary (i.e. Group II; Figure 26). Conversely, samples further away from the boundary in both west and east directions (Group I) have a strongly prolate fabric (especially A1 with T=-0.8399), and L fabric (Figures 26, 31, 32). As the intensity of anisotropy increases (from 0%) the shape factor (T) also increases from -0.8399 to 0.4027 for a 15% increase in P'(Figure 29).

Both figures 29 and 31 attest to a relationship between intensity and fabric. The prolate (L-fabric) samples are clustered near the origin of the plot indicating a very low intensity. Figures 29 and 31 also reveal that the samples from sites closer to the boundary have a higher intensity and magnitude ellipsoids with oblate geometry (L-S fabric; Figure 32).

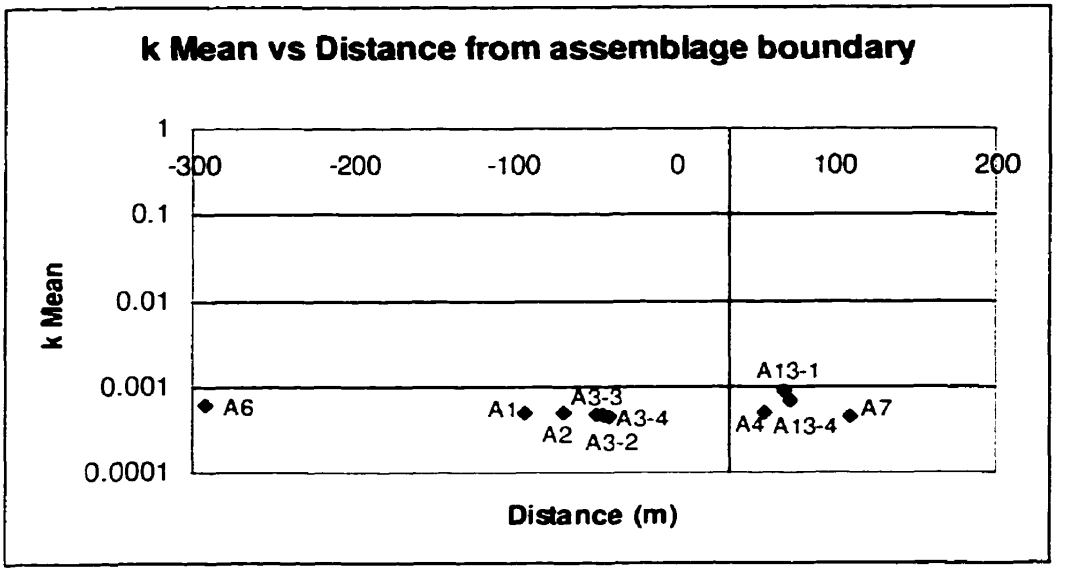
k Mean vs Distance from assemblage boundary
1
0.1
0.01
0.001
0.0001
k Mean
-300
-200
-100
0
100
200
Distance (m)
A6
A1
A2
A3-3
A3-4
A3-2
A13-1
A4
A13-4
A7

Figure 28

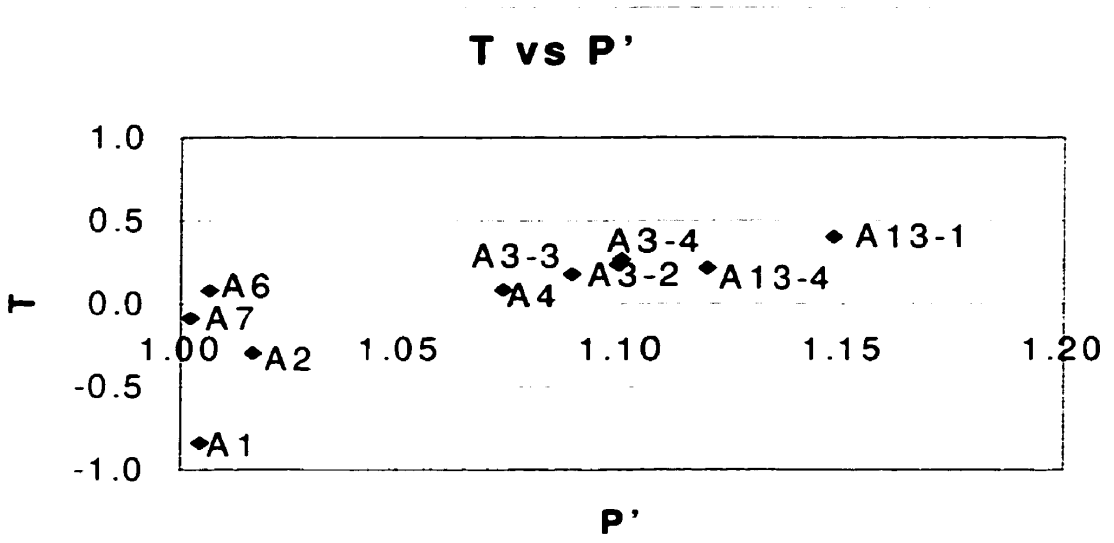

T vs P' plot illustrating the anisotropy shape (T) and intensity (P') for the magnetic fabric ellipsoids defined by AMS.

Figure 29

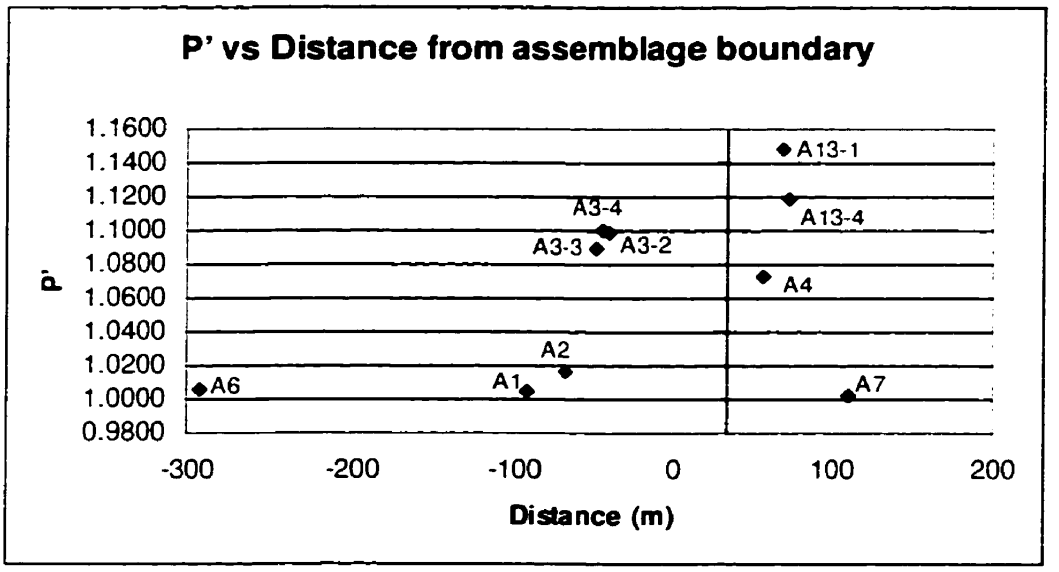
P' vs Distance from assemblage boundary
1.1600
1.1400
1.1200
1.1000
1.0800
1.0600
1.0400
1.0200
1.0000
0.9800
P'
A13-1
A13-4
A3-4
A3-3
A3-2
A4
A2
A6
A1
A7
-300
-200
-100
0
100
200
Distance (m)

Figure 30

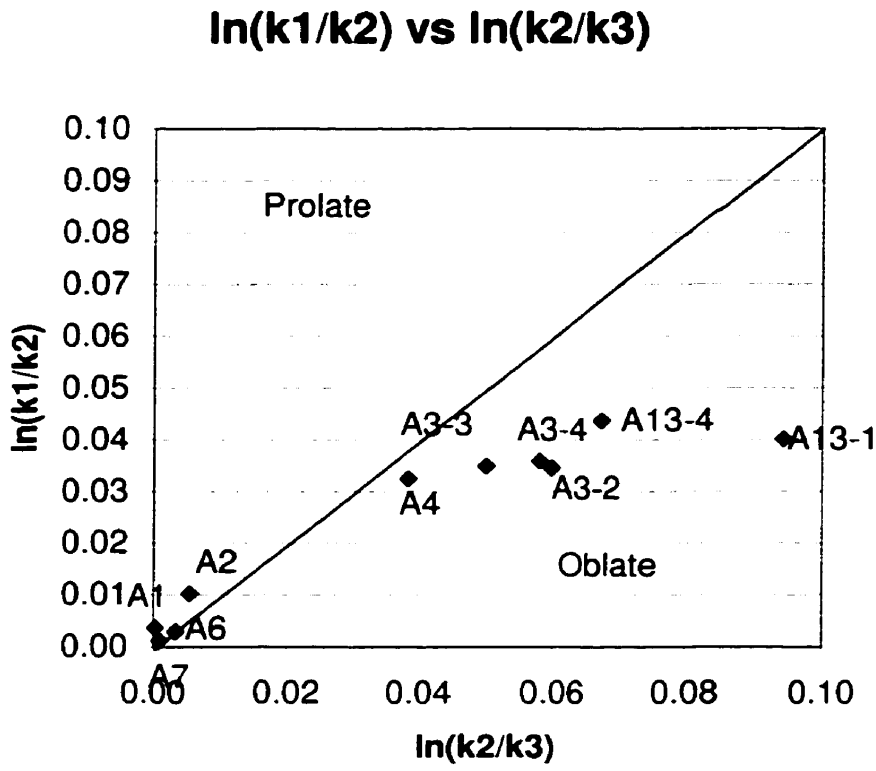

Logarithmic plot of the magnetic fabric (lineation and foliation).

Figure 31

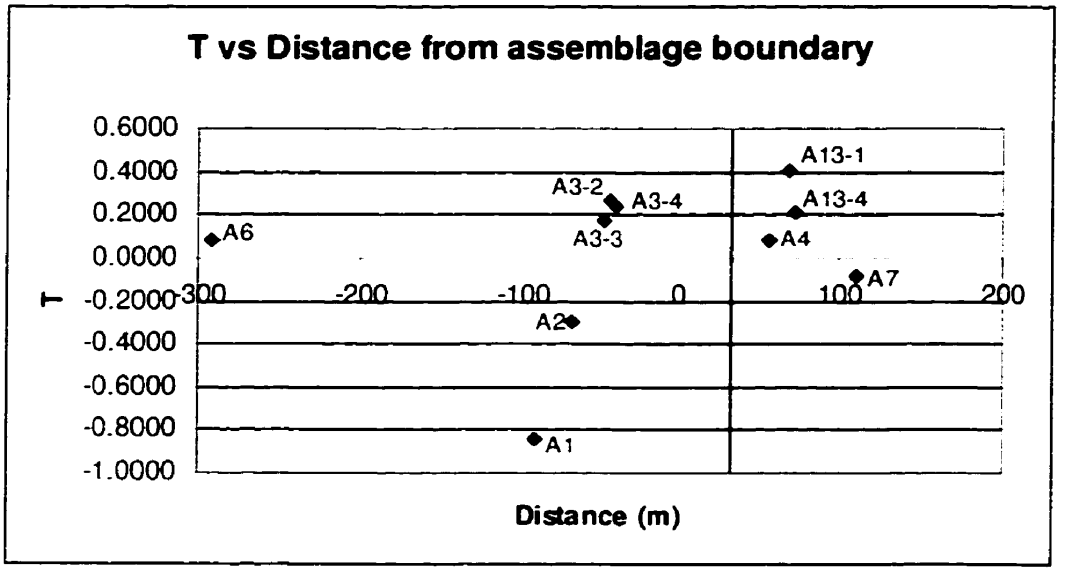
T vs Distance from assemblage boundary
0.6000
0.4000
0.2000
0.0000
-0.2000
-0.4000
-0.6000
-0.8000
-1.0000
T
-300
-200
-100
0
100
200
Distance (m)
A13-1
A3-2
A3-4
A13-4
A6
A3-3
A4
A7
A2
A1

Figure 32

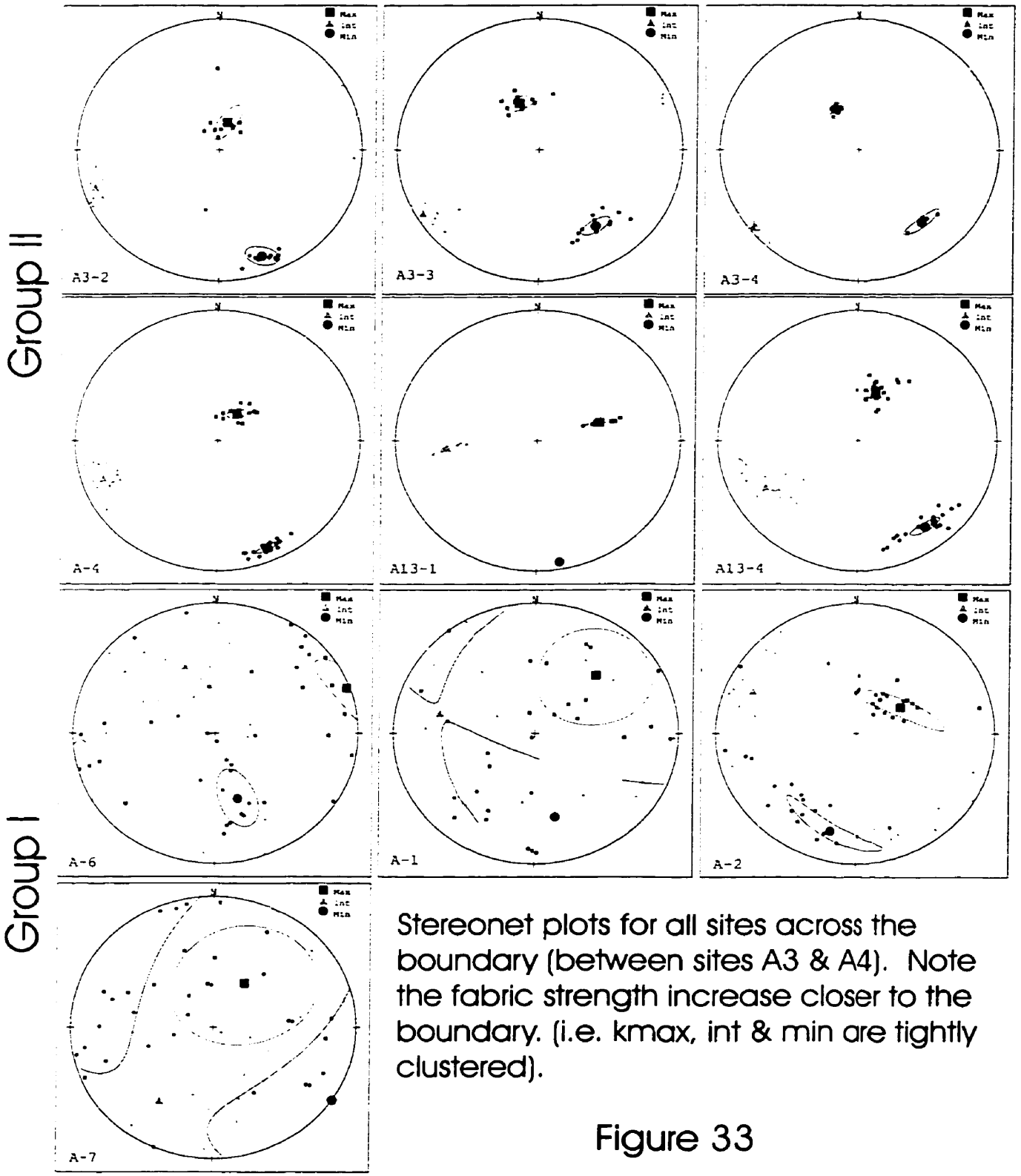

Stereonet plots for all sites across the boundary (between sites A3 & A4). Note the fabric strength increase closer to the boundary. (i.e. kmax, int & min are tightly clustered).

Figure 33

The principal susceptibility directions (k_{max}, k_{int}, & k_{min}) were plotted on stereonets (Figure 33). The fabric strength increases towards the assemblage boundary, as revealed by the tighter clusters of the susceptibilities for A3-2, 3,4; A4; A13-1, 4. A13-1 has a stronger foliation than the rest since both the k_{max} and k_{int} clusters are spread out towards each other on the same plane (great circle) while its k_{min} is very tightly clustered (highest P' values). This is demonstrated in figure 29 where A13-1 has the highest T value (oblate) and thus the strongest foliation.

Samples of Group II (A3, A4, A13) exhibit a very consistent foliation and lineation with values for k_{max}, k_{int} and k_{min} clustered tightly (Figure 33). By contrast, principal susceptibility directions in group I are scattered and do not define strong maxima of lineation or foliation as seen in Group II samples (Figures 26, 33). The magnetic fabrics of group II (Figure 33) compare closely with the regional petrofabric data (Table 2; e.g. site A4: Foliation 246/79 --> 261/69; Lineation 034/70 --> 025/60) while Group I magnetic fabrics are nearly orthogonal to the regional strain fabric (Table 2; e.g. A6: magnetic foliation 252/44 --> mineral schistosity 183/64).

5.5 Discussion

Additional samples should be studied to obtain a more accurate interpretation of the relationships between the AMS parameters. With the exception of A2, the data from samples in Group I are so scattered that their data may be meaningless. Nonetheless, my study revealed that the degree of anisotropy (P') increased with constant bulk susceptibility, although the range of P' is limited (1-1.16) (Figure 27). The degree of magnetic anisotropy increases towards the assemblage boundary (Figures 27, 29, 30). There is an apparent transition from a prolate magnetic fabric to an oblate fabric towards the boundary (Figures 29, 31, 32). The magnetic

Site	# of Specimen	k Max	Dec	Inc	k Int	Dec	Inc	k Min	Dec	Inc	k Mean	P'	T	Max/Int	Int/Min	Max/Min	ln(k2/k3)	ln(k1/k2)	Foliation		Lineation	
A6	20	1.0031	69	3	1.0002	337	44	0.9967	162	46	0.00062	1.0064	0.0786	1.00295	1.00345	1.00641	0.003446	0.002944	252	44	69	3
A4	15	1.0346	34	70	1.0015	250	17	0.9639	156	11	0.000502	1.0734	0.0821	1.03303	1.03904	1.07336	0.038301	0.032492	246	79	34	70
A13-4	20	1.0519	20	58	1.0069	242	25	0.9412	143	19	0.000688	1.1186	0.2145	1.04464	1.06987	1.11763	0.067533	0.043675	233	71	20	58
A13-1	8	1.0582	72	53	1.0166	265	37	0.9252	170	6	0.000888	1.1478	0.4027	1.04090	1.09872	1.14366	0.094148	0.040090	260	84	72	53
A2	20	1.0087	59	58	0.9984	293	20	0.9929	194	24	0.000481	1.0162	-0.2984	1.01032	1.00556	1.01594	0.005547	0.010266	284	66	59	58
A1	14	1.0025	43	39	0.9989	283	32	0.9986	167	35	0.000487	1.0044	-0.8399	1.00363	1.00032	1.00395	0.000315	0.003625	257	55	43	39
A7	15	1.0011	34	57	0.9999	214	33	0.9989	124	0	0.000453	1.0022	-0.0872	1.00119	1.00100	1.00220	0.001002	0.001194	214	90	34	57
A3-2	11	1.0431	15	72	1.0077	252	10	0.9493	159	15	0.000463	1.1000	0.2678	1.03510	1.06155	1.09881	0.059731	0.034495	249	75	15	72
A3-3	12	1.0401	339	59	1.0044	239	6	0.9555	146	30	0.000473	1.0890	0.1772	1.03549	1.05117	1.08847	0.049900	0.034875	236	60	339	59
A3-4	6	1.0434	329	61	1.0066	233	4	0.9500	140	29	0.000449	1.0993	0.2351	1.03652	1.05962	1.09831	0.057909	0.035867	230	61	329	61

Table 2

fabric strength also increases towards the boundary (Figures 26, 33). The magnetic foliation is strongest at the boundary and gives way to a moderately defined lineation away from the boundary. This may be seen as evidence for a slight strain gradient toward the assemblage boundary.

The directions of k_{max} & k_{min} in samples with strong AMS are respectively subparallel to the lineation direction and the schistosity normal, as measured in the field. The obliquity between field data and principal directions of AMS in A6 & A7, especially the large difference between the magnetic foliation and schistosity may be the result of (i) a strong contribution from the crystal lattice orientations of paramagnetic minerals or (ii) an overprinting effect of multiple deformation events (cf. Chapters 4, 8). Alternatively, the mineral assemblage or mineral composition in leucogabbro at the assemblage boundary may be different, and this may explain the high degree of AMS. The leucogabbro may have been homogeneous before deformation created a zone of weakness that permitted fluids to penetrate the rocks near the assemblage boundary. This may have resulted in a structurally induced, compositional change of the leucogabbro. Such compositional effects would support the notion that the assemblage boundary was incoherent, at least for short tectonic intervals.

CHAPTER VI

ESTIMATE OF PRINCIPAL STRAIN RATIOS

VI. ESTIMATE OF PRINCIPAL STRAIN RATIOS

Principal strain ratios provide information that is essential to solving structural problems. For example, Lisle's method (1998, cf. chapter 8) requires principal strain ratios to determine the precise direction of shear strain (γ) parallel to a given structural surface. This method is readily applicable to the present assemblage boundaries.

Strained primary features, such as varioles, lapilli and pebbles, occur throughout the study area. The principal directions of these deformed primary objects are effectively parallel to those of the L-S mineral fabric (Figures 18, 20; cf. Chapter 4). The present geometry of primary features pertains to the total strain or the entire ductile deformation experienced by the rocks (Hudleston & Schwerdtner 1997). Principal-strain ratios, regardless of volume change, allow calculation of principal components of total or incremental distortion (Schwerdtner 1977, Themistocleous & Schwerdtner 1977).

To estimate the strain ratios, principal diameter ratios of deformed natural objects are determined by making geometric measurement on object sections normal to the directions of principal strain (Robin 1977, Peach & Lisle 1979). Of all the available natural objects, varioles/spherules provide the best gauges of total distortional strain due to their initial sphericity and mechanically passive behaviour (Plate 2, 4; de Wit & Ashwal 1997). Volcanic fragments and granite pebbles, by contrast, may have a markedly different ductility/viscosity than their respective rock matrix. Rocks with such objects commonly have an initial depositional fabric, which may compensate for the competency difference. For the purpose of this paper, all rheologic differences are assumed to have been compensated for by other factors. This implies that the principal directions of the shape fabric correspond and are geometrically similar to the directions of the total strain at all localities (Figure 19, Table 1).

It has been inferred many years ago that the total strain in the rocks of the Birch-Uchi greenstone belt may be a net result of multiple stages of deformation (Thurston & Breaks 1978, Fyon & Lane 1985, Thurston 1985, Beakhouse *et al.* 1989, Stott & Corfu 1991). The first stage of deformation (D_1) is thought to have created the first-order, north-south trending synclinorium whose axial surface is in the middle of the greenstone belt (Fyon & Lane 1985, Thurston 1985). However, no evidence of D_1 strain have been recognized in the field area suggesting that most rocks were effectively rigid during D_1 (van Staal 1997, Crews *et al.* 1997, Rogers *et al.* 1999, Crews *et al.* 1998). Therefore, the strain in the field area may have been caused entirely by the second deformation event (D2, Fyon & Lane 1985, Stott & Corfu 1991, Crews & Schwerdtner 1997).

The principal-strain ratios in nine specimens of mafic variolites, metaconglomerates and fragmental volcanics, from all three assemblages (Figure 19), were estimated using the analytical method of Robin (1977) or Peach & Lisle (1979) (Table 1). The variolite specimens (S98-9, C4-1, C4-3, D21-1, D22-1; Figure 19) have a weakly to moderately prolate fabric (Table 1, Moslehi 1998, Crews *et al.* 1998, Crews *et al.* 1999, Capes 1999). By contrast, the metaconglomerate and fragmental volcanic specimen (S97-111, S97-193, S97-200S, S97-238) have an oblate strain fabric (Table 1, Figure 19, Moslehi 1998, Crews *et al.* 1998, Crews *et al.* 1999, Capes 1999). The strain intensity (γ_o; Hossack 1968) for all samples studied varied from a low of 0.491 (S98-9, Figure 19), to a high of 1.655 (D22-1, Figure 19). For biaxial strain this corresponds to an elongation of 40 to 175%.

CHAPTER VII

COMPONENTS OF DISTORTIONAL STRAIN

VII. COMPONENTS OF DISTORTIONAL STRAIN

Distortion is that part of the deformation tensor which specifies the shape change (Turner & Weiss 1963, p.266; Schwerdtner 1977). Principal directions of strain and distortion in the study area are generally neither horizontal nor vertical (Table 1). This presents a problem if a component of horizontal longitudinal strain is needed to determine shear and relative displacement magnitudes on a horizontal or vertical plane. The maximum shortening direction (schistosity normal) in most of the field area deviates from horizontal by 10-20 degrees (Figures 18, 20). The principal-distortion value (Z) normal to schistosity would be, therefore, at some angle to the horizontal surface and may not provide a good approximation. This prompted calculation of horizontal components of distortional strain by using the total strain ratios (Table 1) and formulae for the reciprocal quadratic elongation of a line segment (λ'; Ramsay 1967, Jaeger 1969). The values of total-strain ratios determined from the principal ratios of shape fabrics may be considered as the minimum values on the kilometre scale. This is due to an exposure bias against highly sheared rocks in heterogeneously deformed strata (cf. Chapter 4.6). The reciprocal quadratic elongation of lines in any direction in the deformed state is:

$$\lambda' = \lambda_1' l'^2 + \lambda_2' m'^2 + \lambda_3' n'^2$$

where l', m', n' are the direction cosines of the deformed line (cosines of the angles between the principal directions and the line in question) and λ_1', λ_2', λ_3' are the reciprocal principal quadratic elongations. (λ_1 is calculated parallel to lineation, λ_3 is obtained normal to schistosity.)

$$\lambda_1' = \frac{1}{X^2}; \quad \lambda_2' = \frac{1}{Y^2}; \quad \lambda_3' = \frac{1}{Z^2},$$

where $X \geq Y \geq Z$ are the principal radii of the ellipsoid of total distortion (Table 1). Formulae for the quadratic elongation (λ) can not be used because the initial orientation of the line segment is not known (Ramsay 1967, p.65, 126).

Distortional strain values were computed for possible enveloping surfaces of the large S-fold and one foliation trajectory on Woman Lake (Figures 12, 13, 21, Table 3). On enveloping surfaces for buckle structures, 30% shortening is required (Ramsay 1967, p.386-388) to generate a fold that has a geometric style and interlimb angle similar to the S-fold at the Woman-Confederation assemblage boundary (Figure 12). Fold strain values were calculated for two possible fold axes to the S-fold (Figures 16, 21, Table 3). For a fold axis with steep plunge (N60E/80NE) a minimum shortening value of 26% is obtained, while for a moderately plunging fold axis (N60E/30NE) a shortening value of 43% is found. An intermediate percentage of shortening is expected for an intermediate plunge value.

Volume change was ignored above, but, at the metre-scale and less, the scale at which the principal-ratios were determined (Table 1), volume is probably lost by pressure solution (cf. Chapter 3). As a result, when calculating distortional strain components on the metre-scale and in the direction of the enveloping surface, the values determined will be minimal. Even if the distortion is larger on the kilometre-scale, the calculated strain components still represent minimum values.

Feature	Attitude	Shortening/ Elongation (%)	Miscellaneous Information
Normal to hinge lines of S-fold on enveloping surface	170/04	-26	Fold enveloping surface E171S/80E, Fold hinge lines N60E/80NE
	155/09	-43	Fold enveloping surface E171S/32E, Fold hinge lines N60E/30NE
Schistosity trajectory	040/00	23	Dip of schistosity 78SE, Attitude of mineral lineation 090/74E

Table 3: Shortening/elongation values for large S-fold and schistosity trajectories. Principal-strain ratios for S97-238 (*cf.* Table 1). Volume change disregarded.

The minimum folding strain values for both fold axes considered nearly meet or exceeds the requirement for the formation of this type of fold (Table 3). Since these are only minimum values, no other strain is needed for the fold as all strain is explicable by one deformation.

In a general study of mineral foliation, Schwerdtner (1973) found that a prominent schistosity and associated mineral lineation can be generated by moderate amounts of tectonic strain (10-20%). The horizontal distortional strain components for a trajectory of mineral schistosity on Woman Lake were determined from the principal-strain ratios (Figure 13, Table 3). These values indicate that the strike lines of the schistosity were elongated by 23% making the strain ellipsoid quasi-biaxial to moderately oblate. This is not the case at all locations, however (Figure 19, Table 1). Nonetheless, the strain more than meets the minimum amount required (Schwerdtner 1973) to form the foliation studied in the present field area.

The calculation of horizontal distortional strain also serves to test the relative error inherent in the assumption that the principal planes are either vertical or horizontal (e.g. in Figure 25). Since the maximum elongation (lineation - X) is actually subvertical, the strike line of schistosity must parallel Y in the horizontal plane. By comparing the horizontal distortion strain (1.23) with the principal distortion value of Y (1.22) it is apparent that there is only about 1% difference between the two values probably well within the error of shape fabric analysis. Therefore, we can ignore the departure of the Y/Z plane from the horizontal surface (Figure 34) at many localities. Furthermore, we can faithfully rely on the strain ratios obtained in the present study and, by association, use the assumption that the X/Y plane of the strain ellipsoid is subvertical (Figure 23).

Central Woman Lake
(S97-238)
Y/Z = 2.39
foliation = 028/77

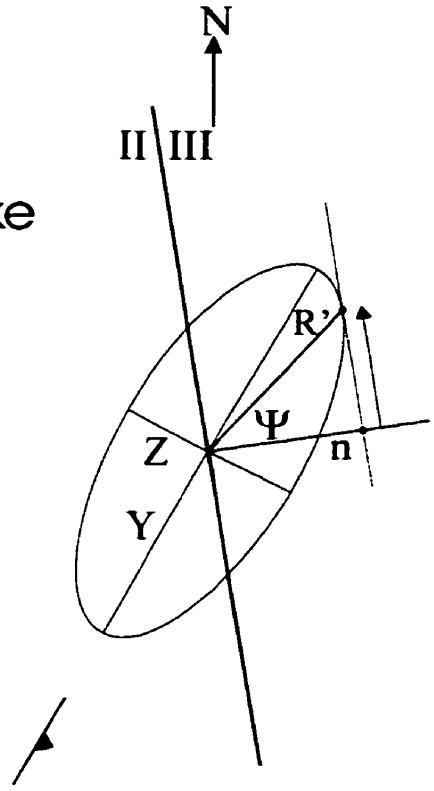

N transport
10.25 km

Rowe Lake
(D21-1)
Y/Z = 2.47
foliation = 219/74

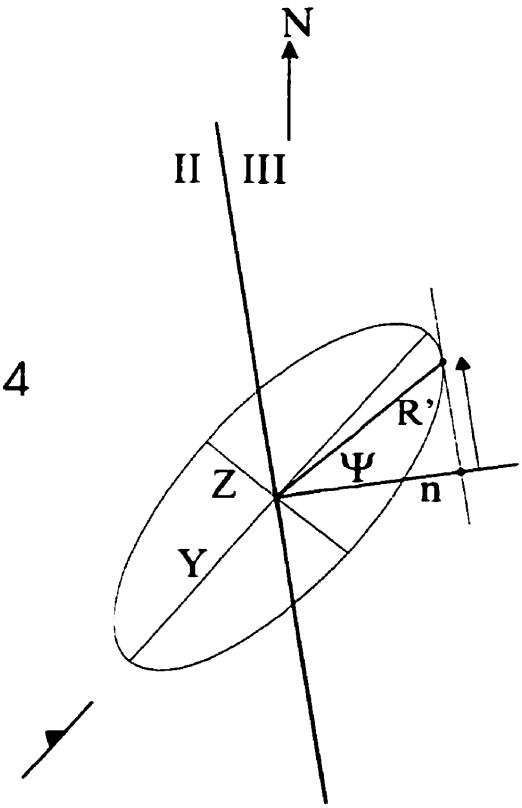

N transport
7.79 km

Figure 34

CHAPTER VIII

LOCAL SENSE OF TANGENTIAL SHEAR STRAIN IN WALLS OF THE ASSEMBLAGE BOUNDARIES (LTBS)

VIII. LOCAL SENSE OF TANGENTIAL SHEAR STRAIN IN WALLS OF THE ASSEMBLAGE BOUNDARIES (LTBS)

8.1 Introduction

Shear strain (γ) is a geometric property of a material line in a state of continuous finite deformation (Lisle 1998). More particularly, γ is defined as the tangent of the obliquity angle between a strained material line (M) and the material plane (LTB) to which M was initially normal (Figure 35, Ramsay 1967, p.125-129; Lisle 1998, Schwerdtner 1998). Shear strain may be treated as a vector quantity, whose magnitude $\gamma=\tan \psi$ (Figure 35). In the graphic derivations of γ (Lisle 1998, Schwerdtner 1998), the shear-strain vector is projected onto two, generally oblique cross-sections, and therefore has two non-orthogonal components, labeled γ_{xn} and γ_{zn}, respectively (Schwerdtner 1998).

A material line element, whose shear strain is being considered, may be represented by a nonprincipal radius of the finite strain ellipsoid. The initially perpendicular plane, which is now tangential to the strain ellipsoid (at the end point of the nonprincipal radius), is equivalent in structural geology to a shear-surface element or an LTB segment (Jaeger 1971, Borowik 1999). In 3D, the sense of shear strain varies with orientation of the line element/nonprincipal radius in the strain ellipse (Figure 36). If the line element is in either the top right or bottom left quadrant of figure 36 the shear strain is dextral. Conversely, the shear strain direction is sinistral in the remaining quadrants (Figure 36). However, if the line element parallels one of the principal directions of the strain ellipse, there is no finite shear strain since $\psi = 0$ (Figure 36). It is vital in the analysis of tangential shear strain that one knows the current attitude of the material plane that was pegged to an LTB throughout ductile deformation. However, the LTB dip is uncertain in the study area, where vibroseismic images of the assemblage boundaries are unavailable

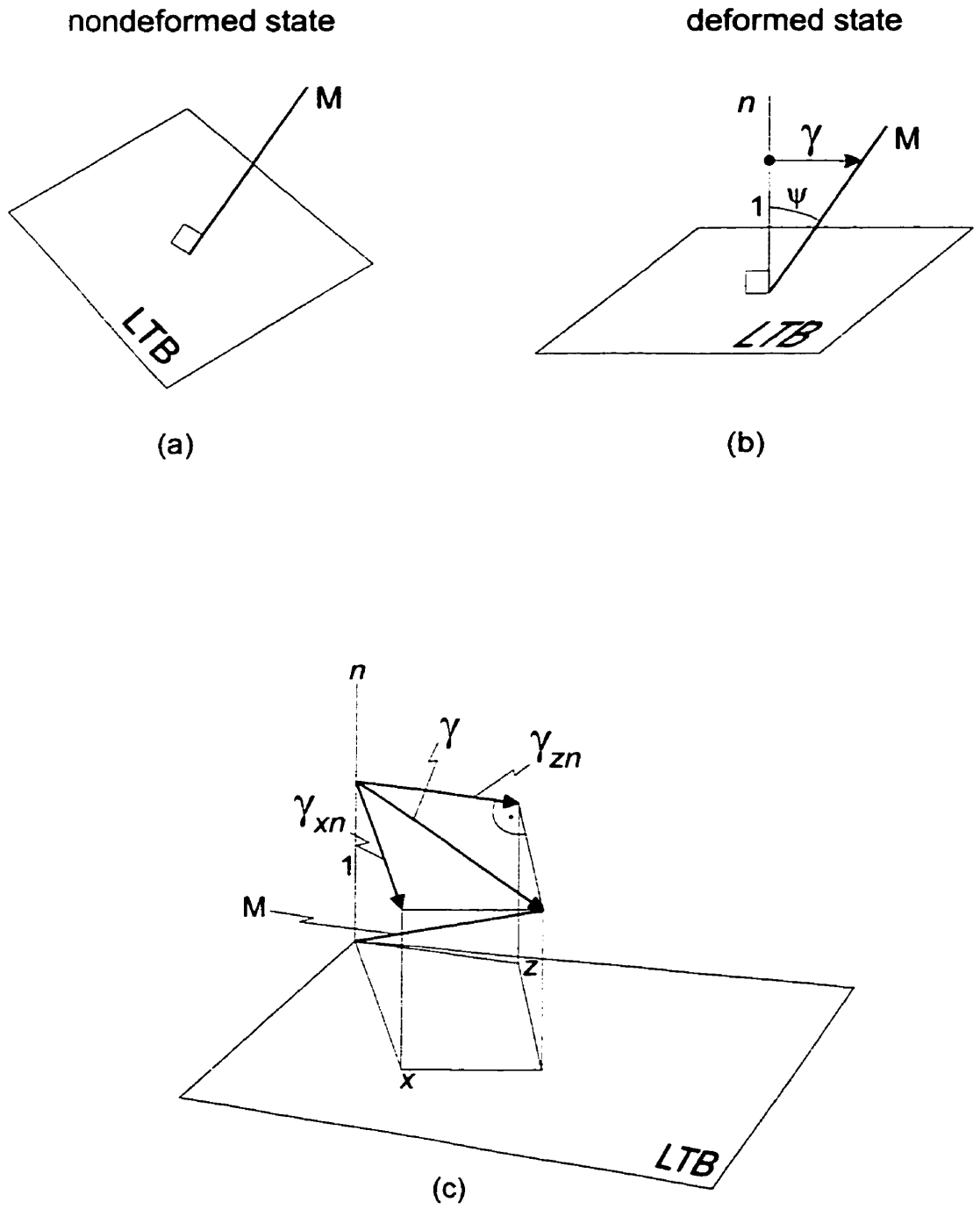

Figure 35
(from Schwerdtner 1998)

Sample Strain Ellipses

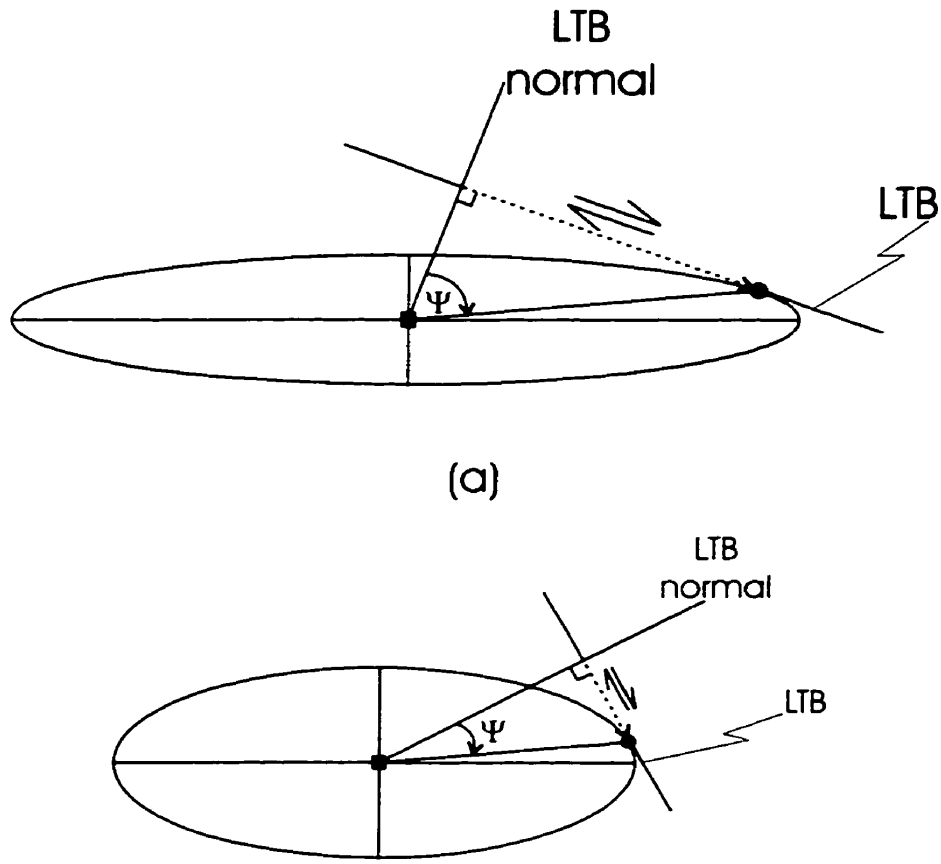

(a) The sense and amount of shear strain varies depending on where the material line is in the strain ellipse. If the LTB is perpendicular to the principal strain directions the shear-strain (γ) will be zero. (b) If the strain ellipse ratio is smaller then the amount of shear strain (γ) will be less, while the shear sense remains the same.

Figure 36

(Schwerdtner *et al.* 1997). The Balmer-Woman and Woman-Confederation assemblage boundaries represent apparent gaps in the stratigraphic record (Nunes & Thurston 1980, Wallace *et al.* 1986). Such gaps suggest that the assemblage boundaries are either disconformities and/or dislocation surfaces (Thurston 1985, Stott & Corfu 1991). Because of macroscopic folding on the km-scale both boundaries now correspond to fold enveloping surfaces whose true dip is uncertain because of a structural bias in favour of steep attitudes (Figures 12, 21; cf. Chapter 4.6). As discussed in Chapter 4, the local boundary dip is needed to determine the contribution of lineation and foliation to the tangential shear strain (Figures 21, 36). Although the dip of both assemblage boundaries is unknown, at present, it will hopefully be determined from future drilling, vibroseismic profiling or other geophysical work (Crews *et al.* 1997, Schwerdtner 1998, Borowik *et al.* 1999).

In this chapter, two recent techniques of shear-sense derivation will be applied at various localities in the walls of the assemblage boundaries in the Birch-Uchi greenstone belt.

8.2 Schwerdtner's Graphic Derivation of Tangential Shear Strain

8.2.1 Introduction

Schwerdtner's (1998) graphic technique uses L-S fabrics to obtain the local sense of tangential shear strain components (γ_{xn} & γ_{zn}) in stretched or shortened walls of lithotectonic boundaries (LTBs). For the general case of an arbitrarily oriented boundary surface, none of the principal strain directions lies on the LTB plane (Figure 37). In this technique, two LTB cross-sections are used, (i) the cross-section through the lineation direction (forming plane Xn) and (ii) the cross-section through the foliation normal (plane Zn) (Figure 37, Schwerdtner 1998). Moreover, the technique does not require knowledge of the section ellipse shape to determine the sense of shear components and range angle of the shear-strain (γ) (Figure 37, Schwerdtner 1998).

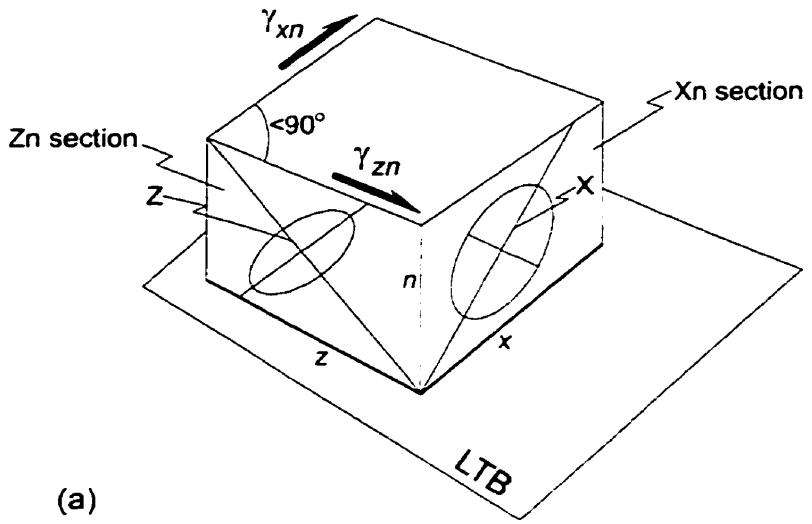

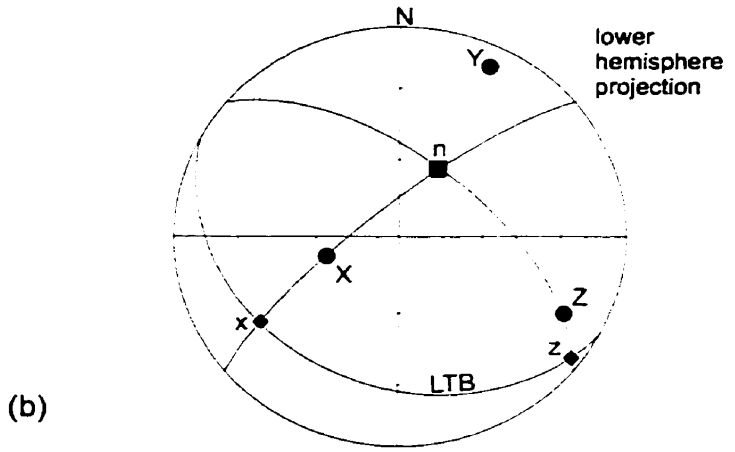

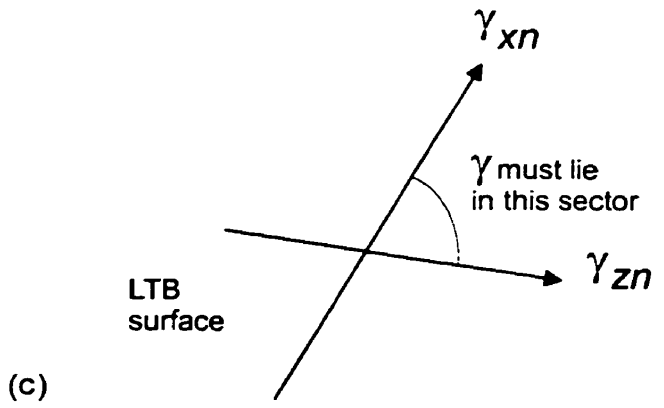

Figure 37
(from Schwerdtner 1998)

The traces of the cross-sections (X, Z) on the LTB surface are the directions of tangential shear components (<90°, Figure 37). Since the magnitude of the components is unknown, the γ direction may lie anywhere within the acute angle between x and z on the LTB surface (Figure 37). In a special case, the shear strain direction can be determined from the above if the strain ellipsoid of the wall rock segment studied degenerates into a prolate or oblate spheroid. In wall rocks that have a strongly prolate strain ellipsoid (L-tectonite), the γ direction will be subparallel to the intersection line between the lineation direction and the LTB surface (γ_{xn}, Figure 37). Conversely, if the strain ellipsoid is strongly oblate (S-tectonite) the γ direction will be subparallel with γ_{zn}, which is the intersection line between the LTB surface and the foliation normal (Figure 37, Schwerdtner 1998). In general, the strain fabric contains both a prominent foliation and lineation so that the γ direction lies with the range angle between the components of tangential shear strain. The components in figure 37 have the sense of a sinistral thrust (reverse) fault and sinistral normal fault, for γ_{xn} & γ_{zn}, respectively. In general, the componental shear-strain sense depends on the position of the principal directions, X & Z with respect to the LTB surface (Figure 38).

Attitudes of L-S fabrics were obtained, in the field area, to analyze the local sense of tangential shear strain in the walls of both assemblage boundaries (Figures 13, 14). Since Schwerdtner's (1998) graphic technique does not require knowledge of the shape of the section ellipse to assess the local sense of tangential shear strain, the L-S fabric of sites was used wherever principal strain ratio data were unavailable (Figure 39; Schwerdtner 1998). Sample sites at which principal ratio data are available will be used with Lisle's method (1998, Figure 19, cf. Chapter 8.3).

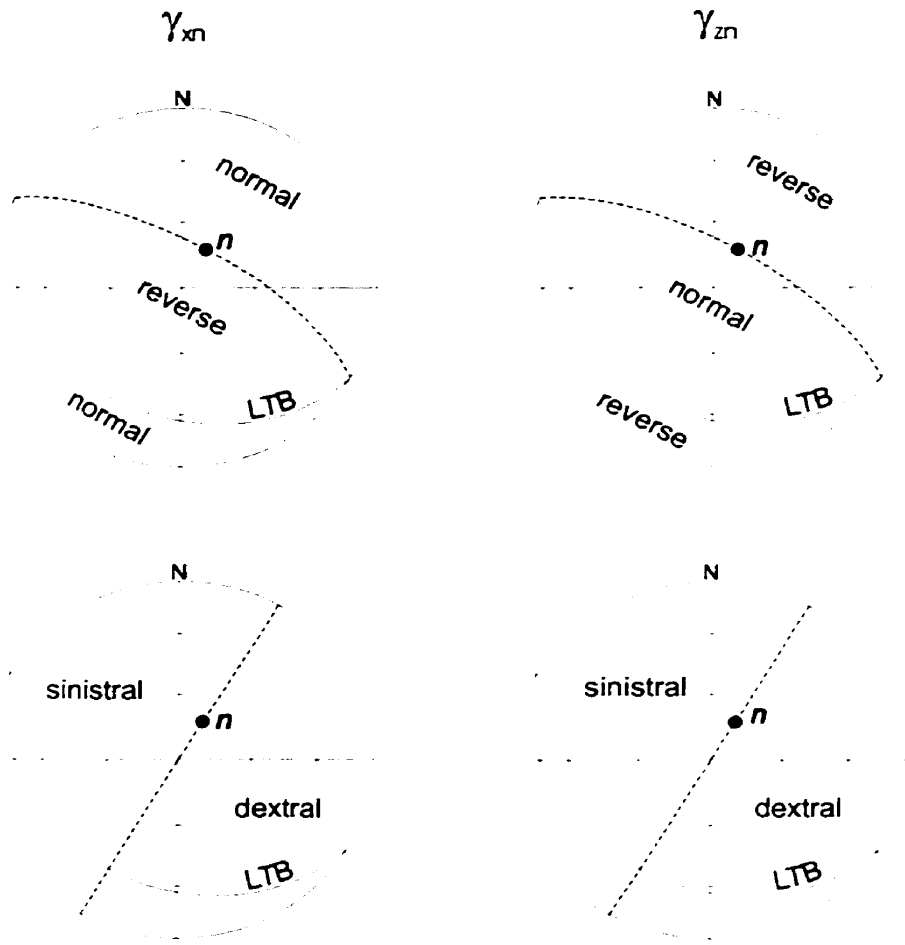

Fields of different shear-strain sense for principal directions in lower hemisphere stereographic projection (modified from Schwerdtner 1998).

Figure 38

Station Locations Used In Schwerdtner's Method

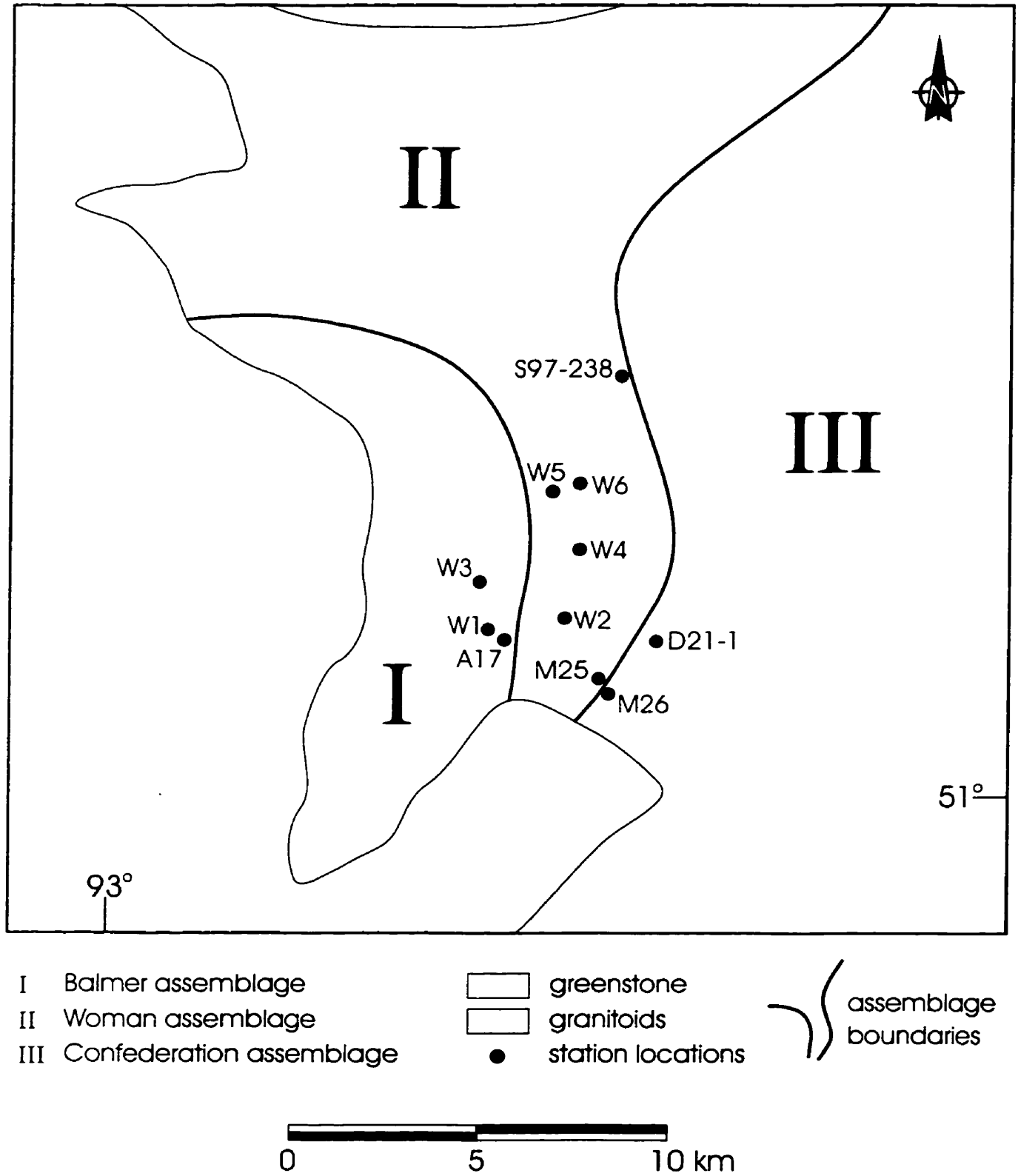

Figure 39

8.2.2 Balmer-Woman Assemblage Boundary

An assessment of the sense of tangential shear-strain was made at 7 localities in the walls of the Balmer-Woman assemblage mass (Figure 39). Since the inclination of the assemblage boundary is presently unknown three possible dip options were used (80, 60 & 40°E). Consideration of these options is tantamount to analyzing the shear strain on three different tangent planes of the same strain ellipsoid. Therefore, the results of the options are mutually compatible at any locality. Figures 40 & 41 show, respectively, the results of the tangential shear-strain analysis in the footwall and hanging wall of the Balmer-Woman assemblage boundary (Figure 39).

The stereoplots of Figures 40 & 41 display the Balmer-Woman assemblage boundary attitude (one of the three dip values), foliation attitude and their respective normals, mineral lineation, long axis of section ellipses perpendicular to the foliation normal and the components of tangential shear strain (γ_{xn} & γ_{zn}). The attitude of corresponding sectional strain ellipses on the Xn & Zn planes (Figure 37) reveal the sense of γ_{xn} & γ_{zn}. The directions of γ_{xn} & γ_{zn} are plotted as points on the great circle representing the hanging wall of the assemblage boundary, and the angle between these points contains the tangential shear strain direction.

At the localities represented by Figures 40 & 41 (Figure 39), the shear strain is reverse, with a small sinistral or dextral component. The sense of strike shear is unknown because the LTB dip lies in the acute angle between γ_{xn} & γ_{zn} (Figures 40, 41). However, in the footwall at A-17 (LTB dip = 60°), and in the hanging wall at W-2 & W-4 (LTB dip = 40°), the value of γ_{zn} must be zero (Figure 39). This follows from the fact that γ_{zn} is parallel to the foliation normal and the strain level is not very high (Figures 40, 41). The γ_{xn} component is therefore equal to γ, which has dextral normal sense at W-1 for an LTB dip of 80° (Figures 39, 40).

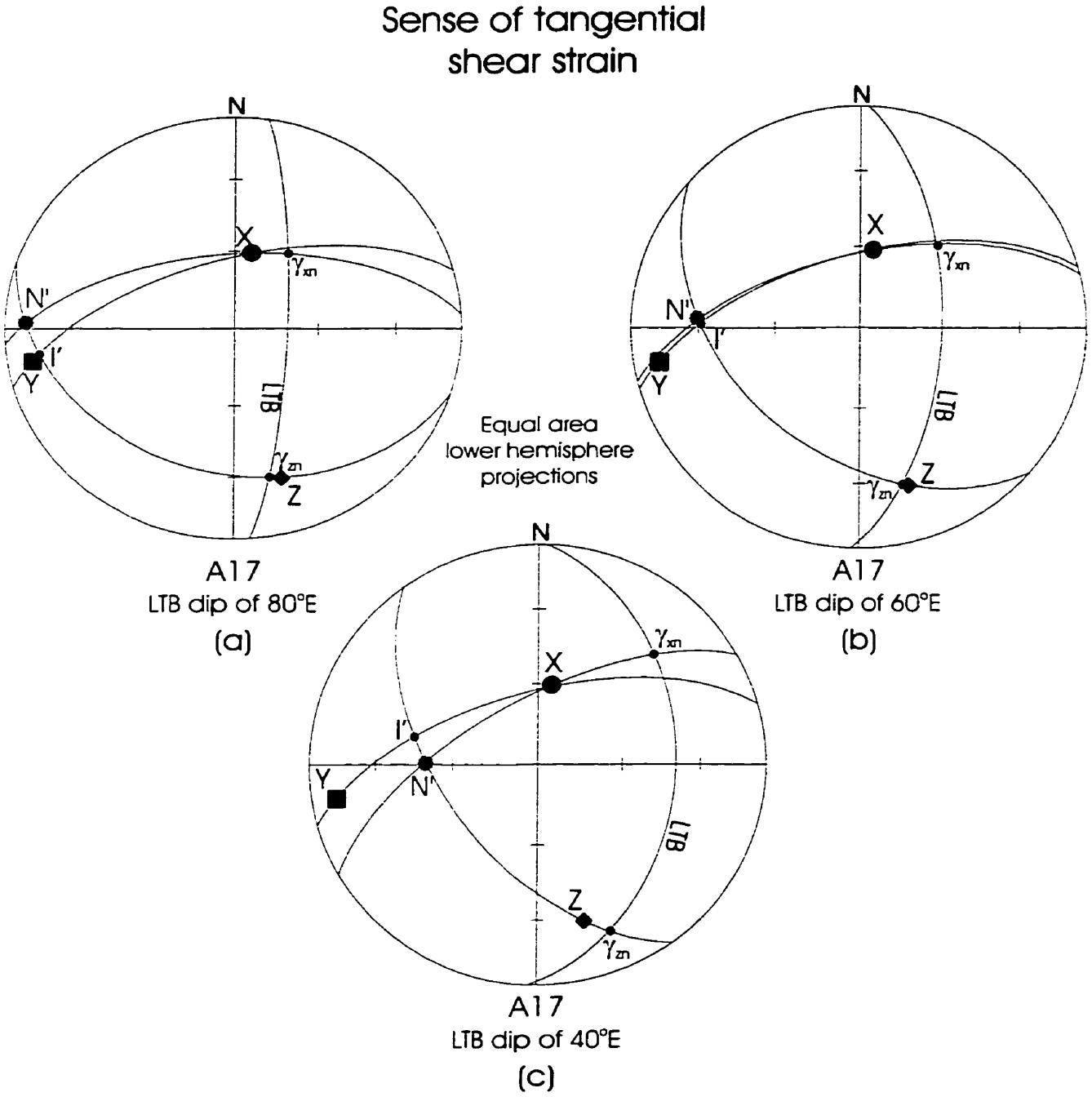

Foot wall of Balmer-Woman assemblage boundary (LTB).
X, Y, Z= principal directions of total strain. N' = LTB normal,
γ_{xn} and γ_{zn} = directions of shear-strain components.
I' = long axis of section ellipse.

Figure 40 (a, b, c)

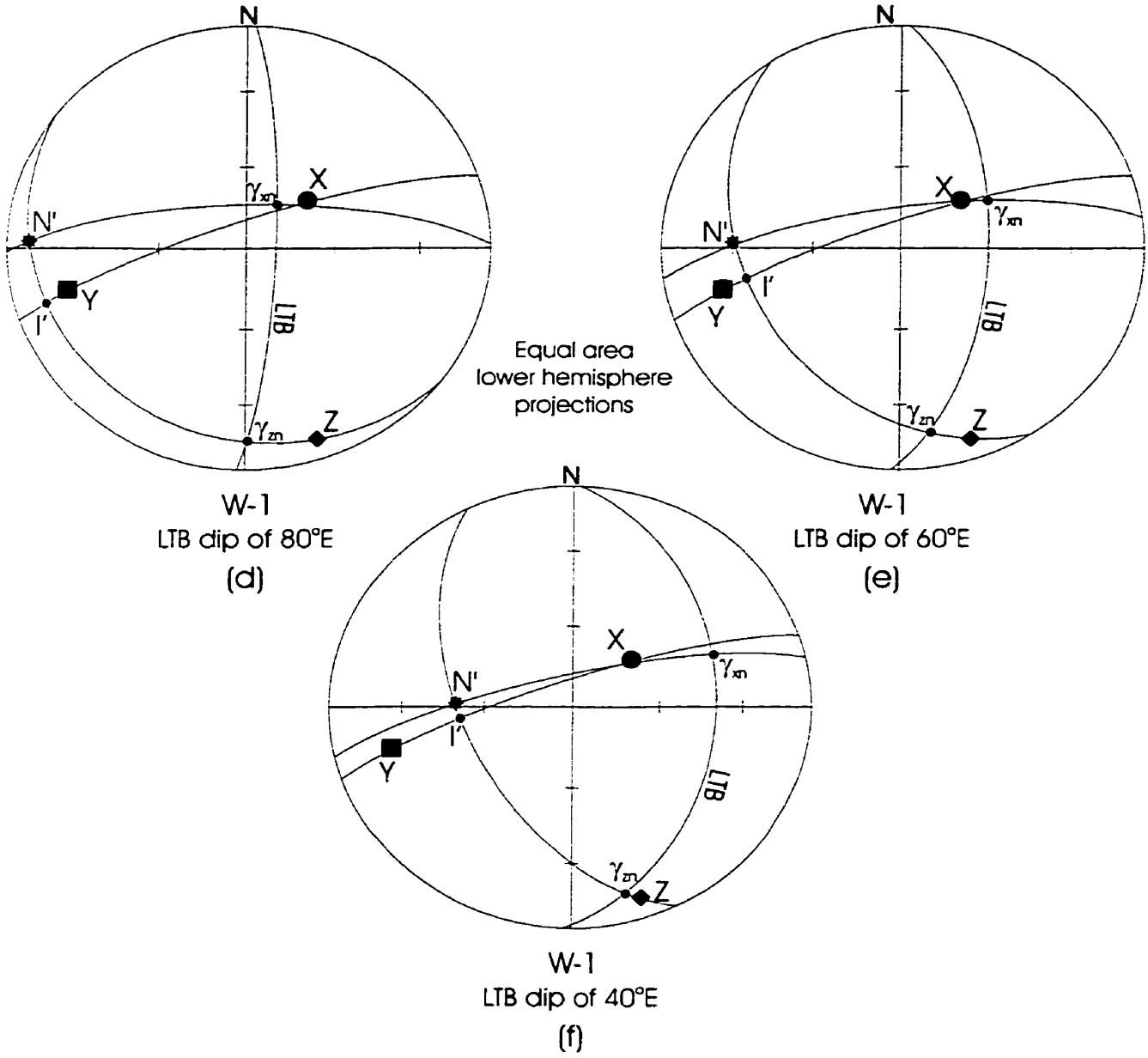

Foot wall of Balmer-Woman assemblage boundary (LTB).
X, Y, Z= principal directions of total strain. N' = LTB normal,
γ_{xn} and γ_{zn} = directions of shear-strain components.
I' = long axis of section ellipse.

Figure 40 (d, e, f)

Sense of tangential shear strain

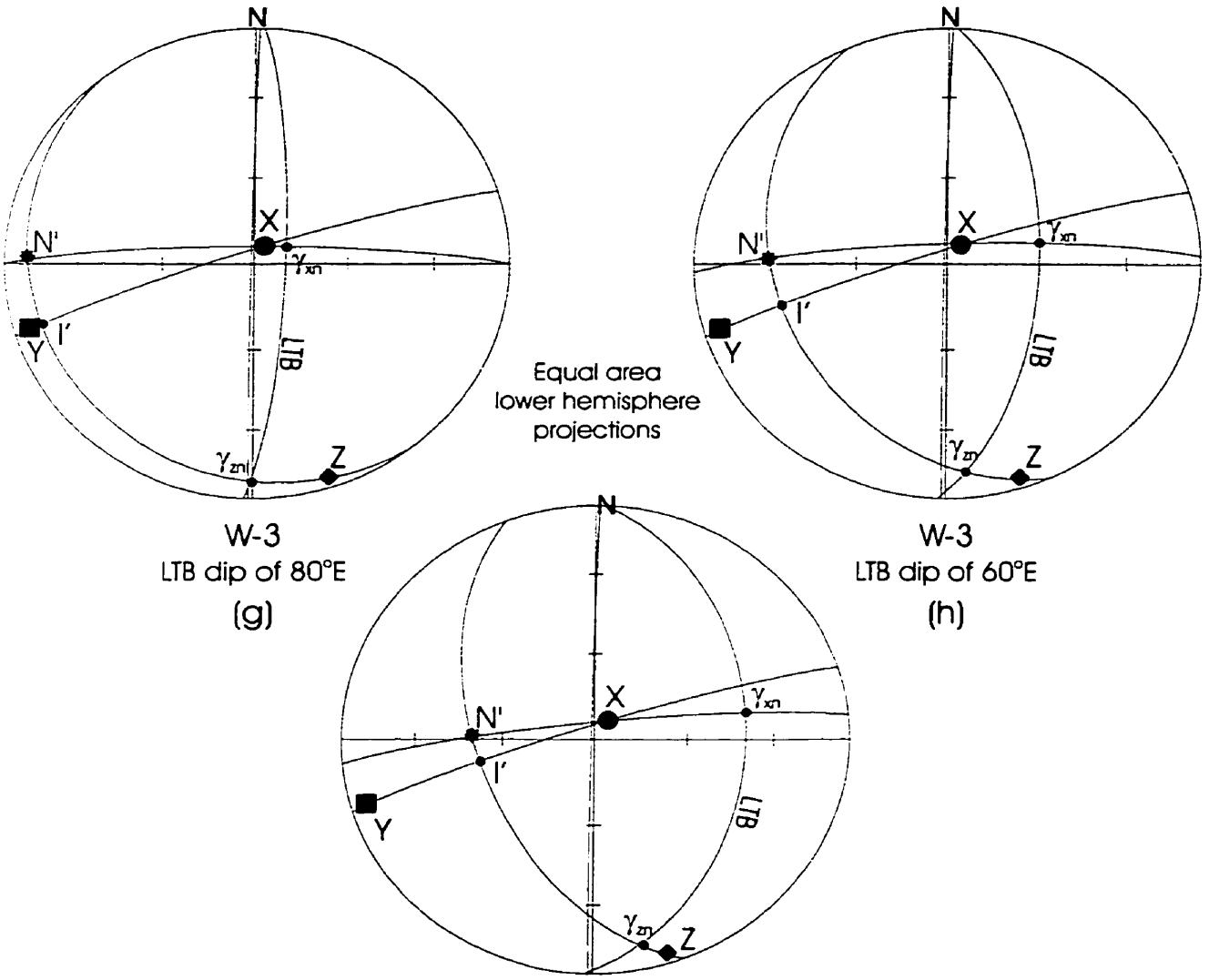

W-3
LTB dip of 80°E
(g)

W-3
LTB dip of 60°E
(h)

W-3
LTB dip of 40°E
(i)

Foot wall of Balmer-Woman assemblage boundary (LTB).
X, Y, Z= principal directions of total strain. N' = LTB normal,
γ_{xn} and γ_{zn} = directions of shear-strain components.
l' = long axis of section ellipse.

Figure 40 (g, h, i)

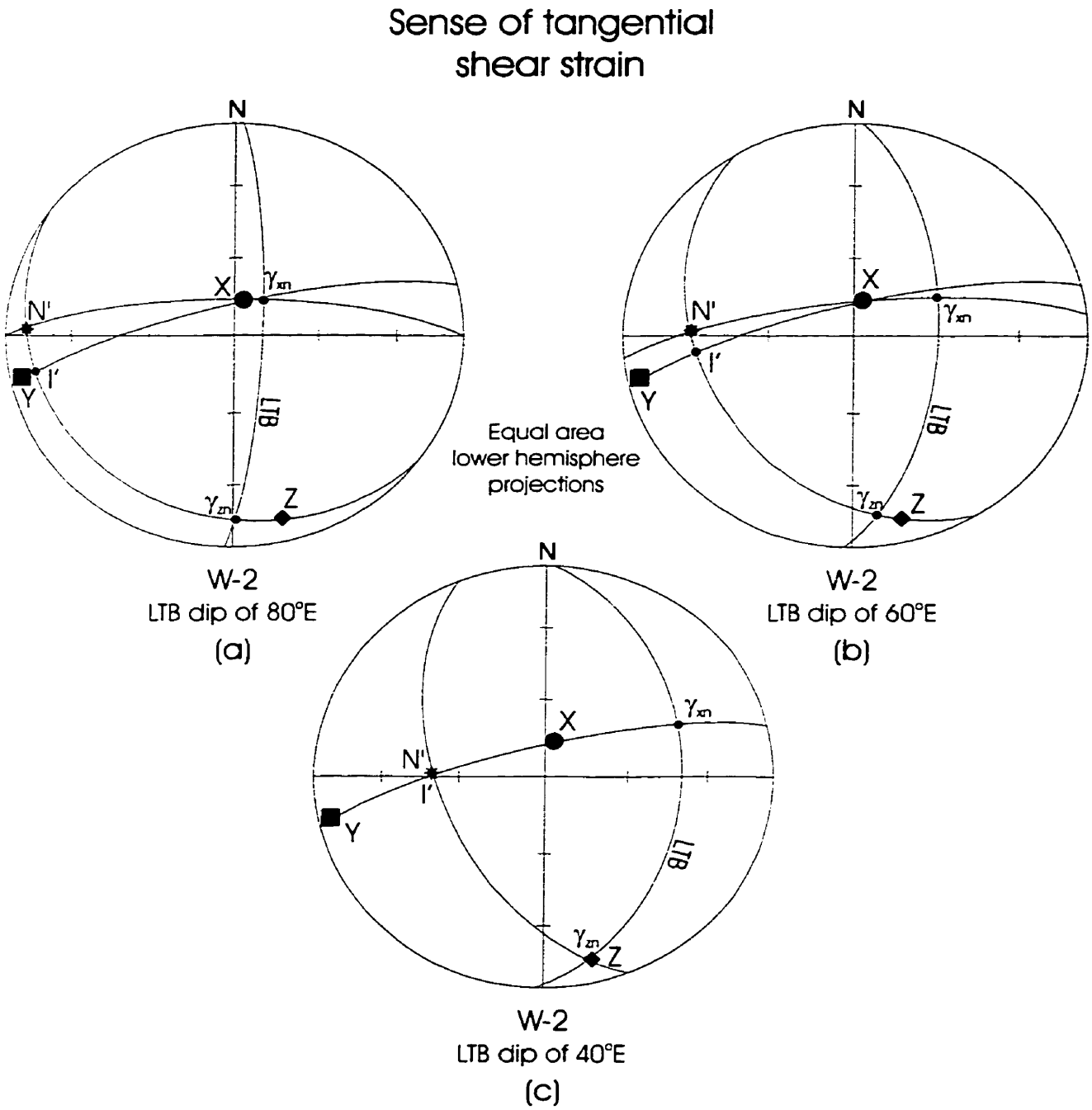

Hanging wall of Balmer-Woman assemblage boundary (LTB).
X, Y, Z= principal directions of total strain. N' = LTB normal,
γ_{xn} and γ_{zn} = directions of shear-strain components.
I' = long axis of section ellipse.

Figure 41 (a, b, c)

Sense of tangential shear strain

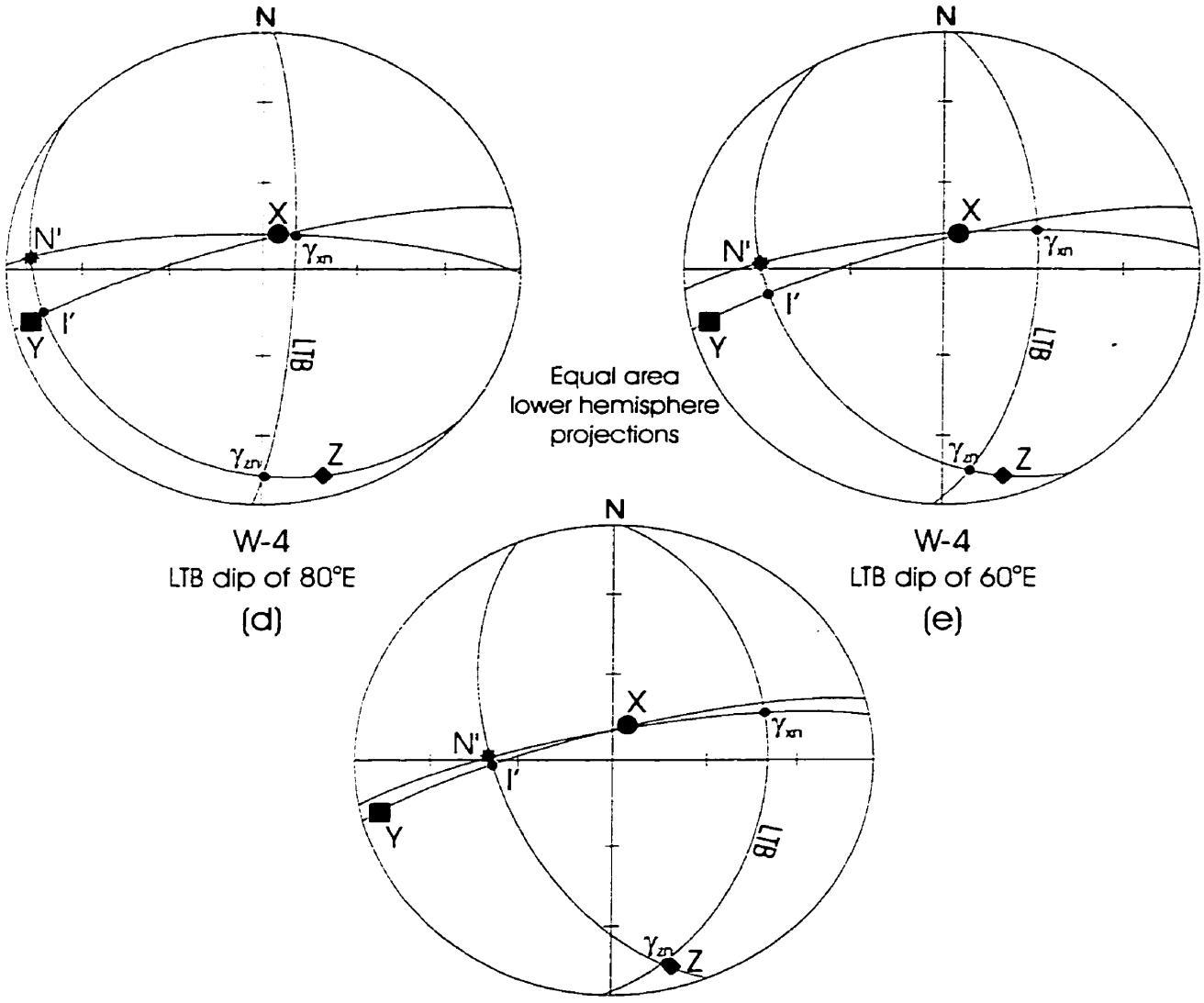

W-4
LTB dip of 80°E
(d)

W-4
LTB dip of 60°E
(e)

W-4
LTB dip of 40°E
(f)

Hanging wall of Balmer-Woman assemblage boundary (LTB). X, Y, Z= principal directions of total strain. N' = LTB normal, γ_{xn} and γ_{zn} = directions of shear-strain components. I' = long axis of section ellipse.

Figure 41 (d, e, f)

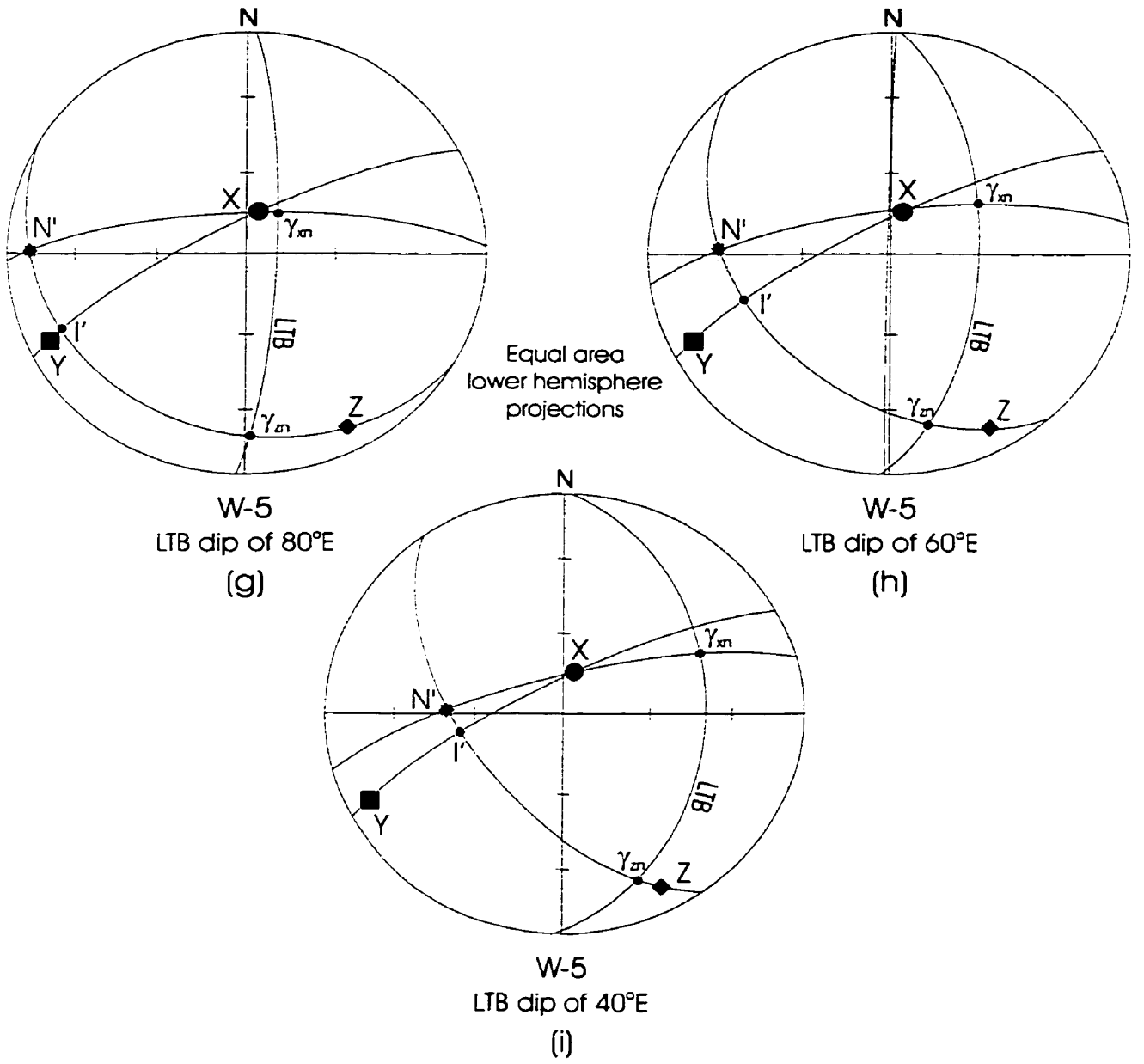

Hanging wall of Balmer-Woman assemblage boundary (LTB).
X, Y, Z= principal directions of total strain. N' = LTB normal,
γ_{xn} and γ_{zn} = directions of shear-strain components.
I' = long axis of section ellipse.

Figure 41 (g, h, i)

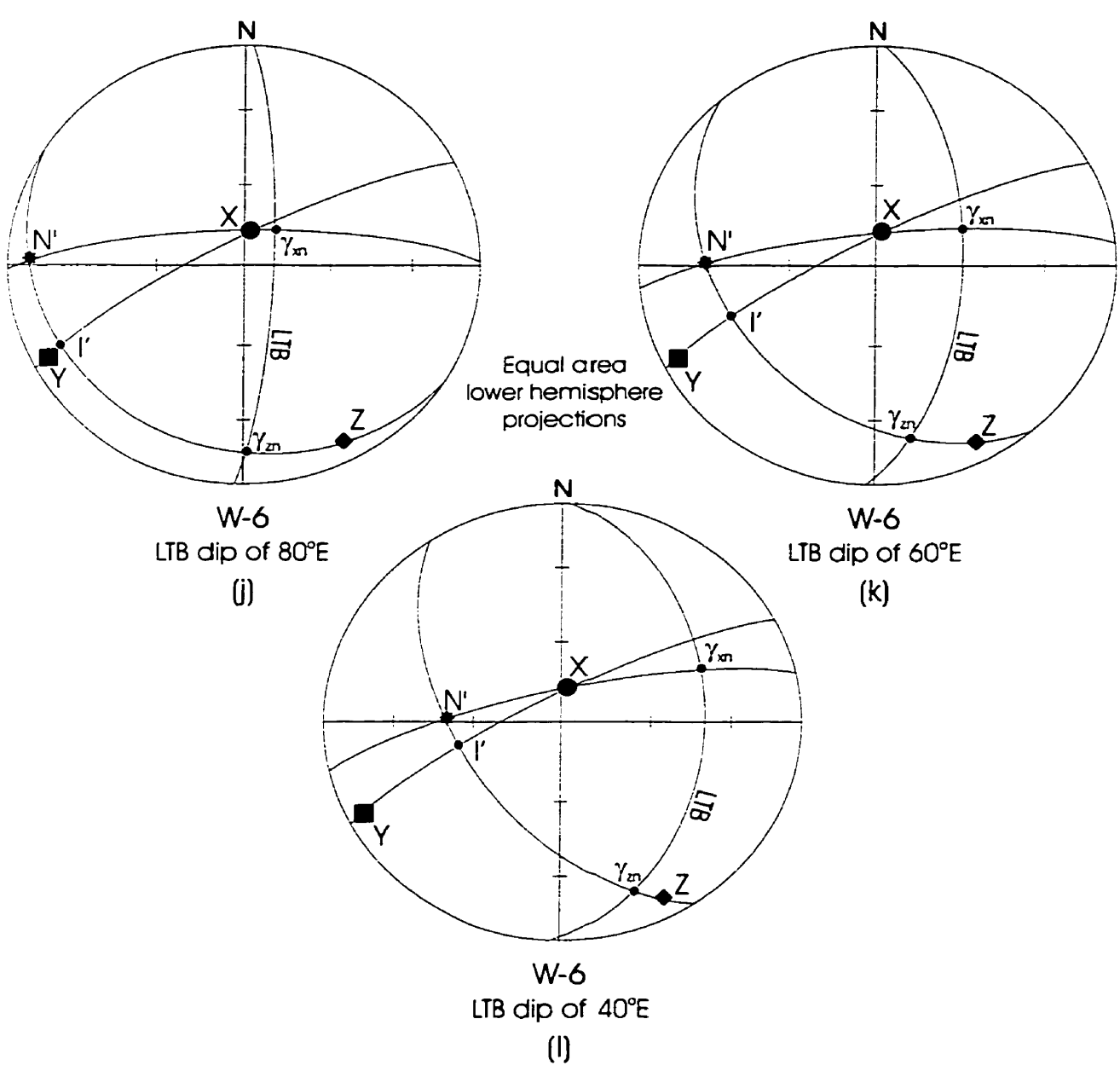

Hanging wall of Balmer-Woman assemblage boundary (LTB). X, Y, Z= principal directions of total strain. N' = LTB normal, γ_{xn} and γ_{zn} = directions of shear-strain components. I' = long axis of section ellipse.

Figure 41 (j, k, l)

8.2.3 Woman-Confederation Assemblage Boundary

The sense of tangential shear-strain was assessed at 4 localities in the walls of Woman-Confederation assemblage boundary (Figure 39). Figures 42 & 43 show the results of this assessment in the footwall and hanging wall, respectively (Figure 39). For an explanation of Figures 42 & 43, see text of subchapter 8.2.1. At most sites in both walls, the tangential shear-strain sense corresponds to that of thrust faults which have either a sinistral or dextral slip component (Figures 42 & 43). At site S97-238, the tangential shear-strain has either the sense of a pure thrust (γ_{xn}) or the sense of a sinistral thrust (γ_{zn}) for LTB dips of 60 and 40 degrees (Figures 39, 42). Shear strain with normal sense characterizes the hanging wall for the LTB dip option of 80°E (Figure 42). At site M26 in the hanging wall, $\gamma_{zn} = 0$ in the LTB dip option of 40°E, similar to sites in the hanging wall of the Balmer-Woman assemblage boundary (Figures 41, 43).

Although the tangential shear-strain sense was derived using Schwerdtner's (1998) method, the direction of the shear strain vector is difficult to fix within the acute range angle on the LTB surface (Figure 37). However, the local tangential shear strain direction can be determined if the ratios of principal strain are known (Table 1) and by applying Lisle's (1998) technique.

8.3 Lisle's Graphical Solution For The Direction of Tangential Shear Strain

8.3.1 Introduction

The direction of shear strain for a stretched material line is defined as " the direction of its projection on the plane that was originally perpendicular" (Lisle 1998). Lisle's technique is based on the same principles as Schwerdtner's (1998), but requires knowledge of strain ratios

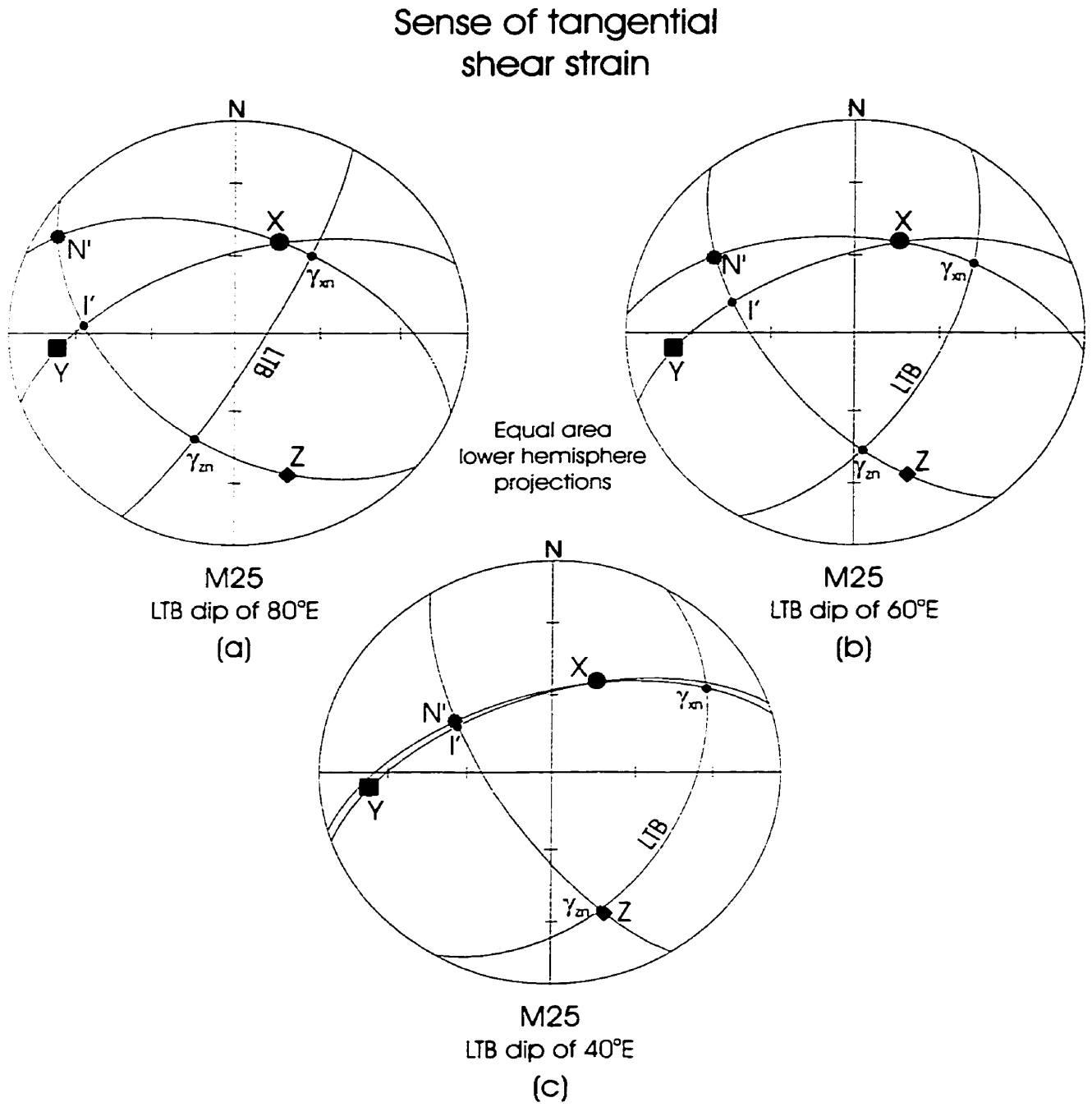

Foot wall of Woman-Confederation assemblage boundary (LTB). X, Y, Z= principal directions of total strain. N' = LTB normal, γ_{xn} and γ_{zn} = directions of shear-strain components. I' = long axis of section ellipse.

Figure 42 (a, b, c)

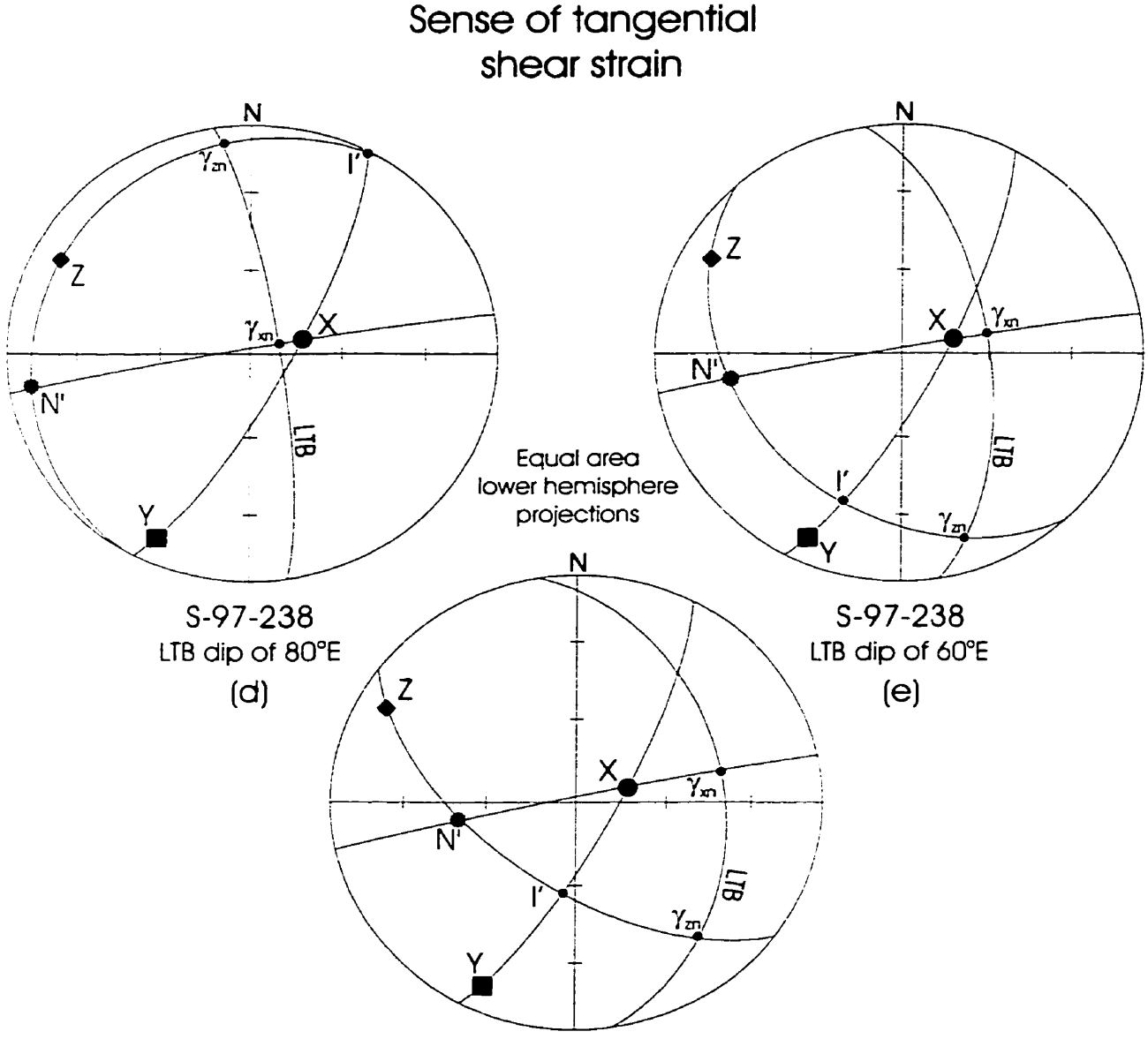

Foot wall of Woman-Confederation assemblage boundary (LTB).
X, Y, Z= principal directions of total strain. N' = LTB normal,
γ_{xn} and γ_{zn} = directions of shear-strain components.
I' = long axis of section ellipse.

Figure 42 (d, e, f)

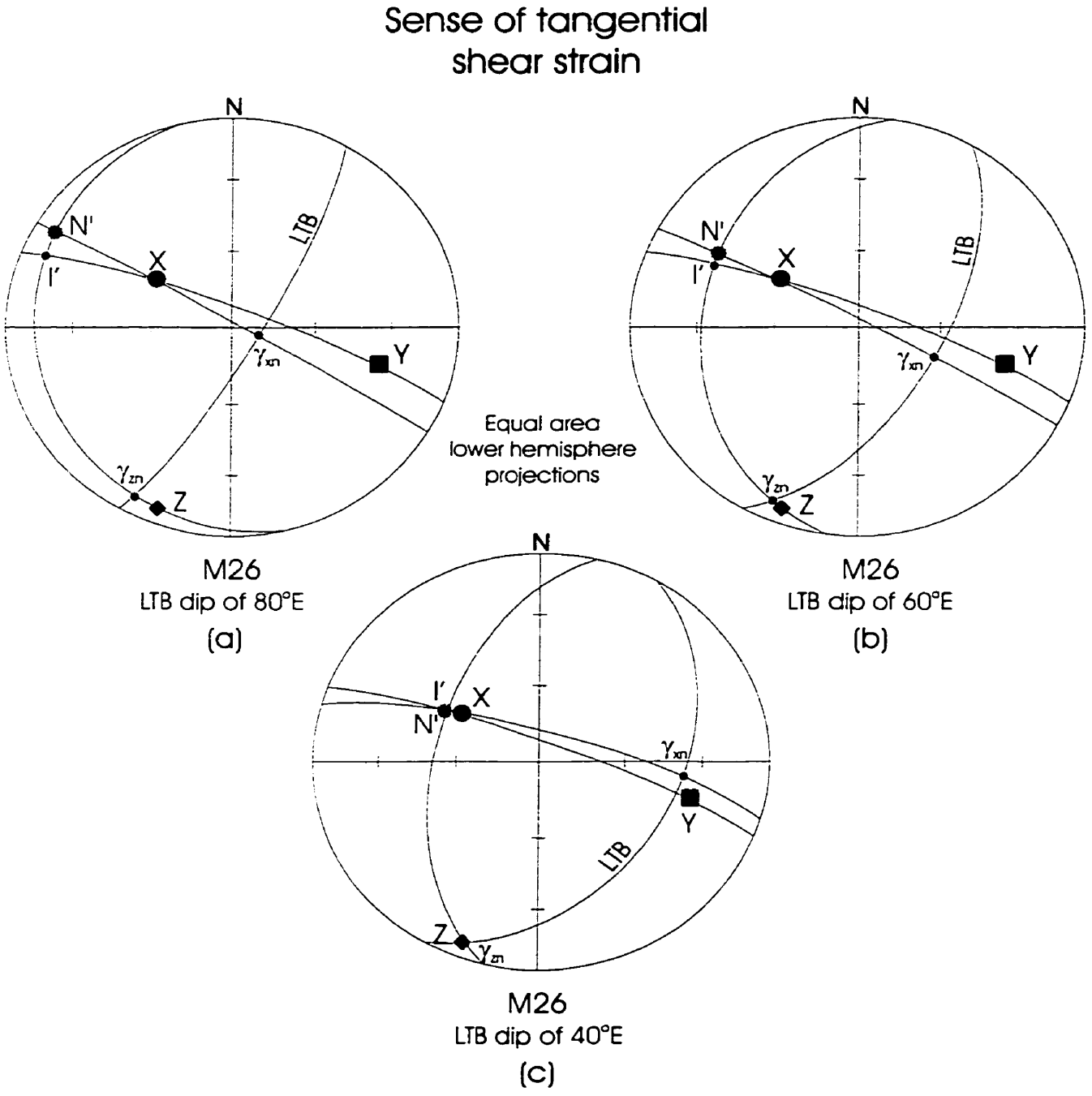

Hanging wall of Woman-Confederation assemblage boundary (LTB).
X, Y, Z= principal directions of total strain. N' = LTB normal,
γ_{xn} and γ_{zn} = directions of shear-strain components.
l' = long axis of section ellipse.

Figure 43 (a, b, c)

Sense of tangential
shear strain

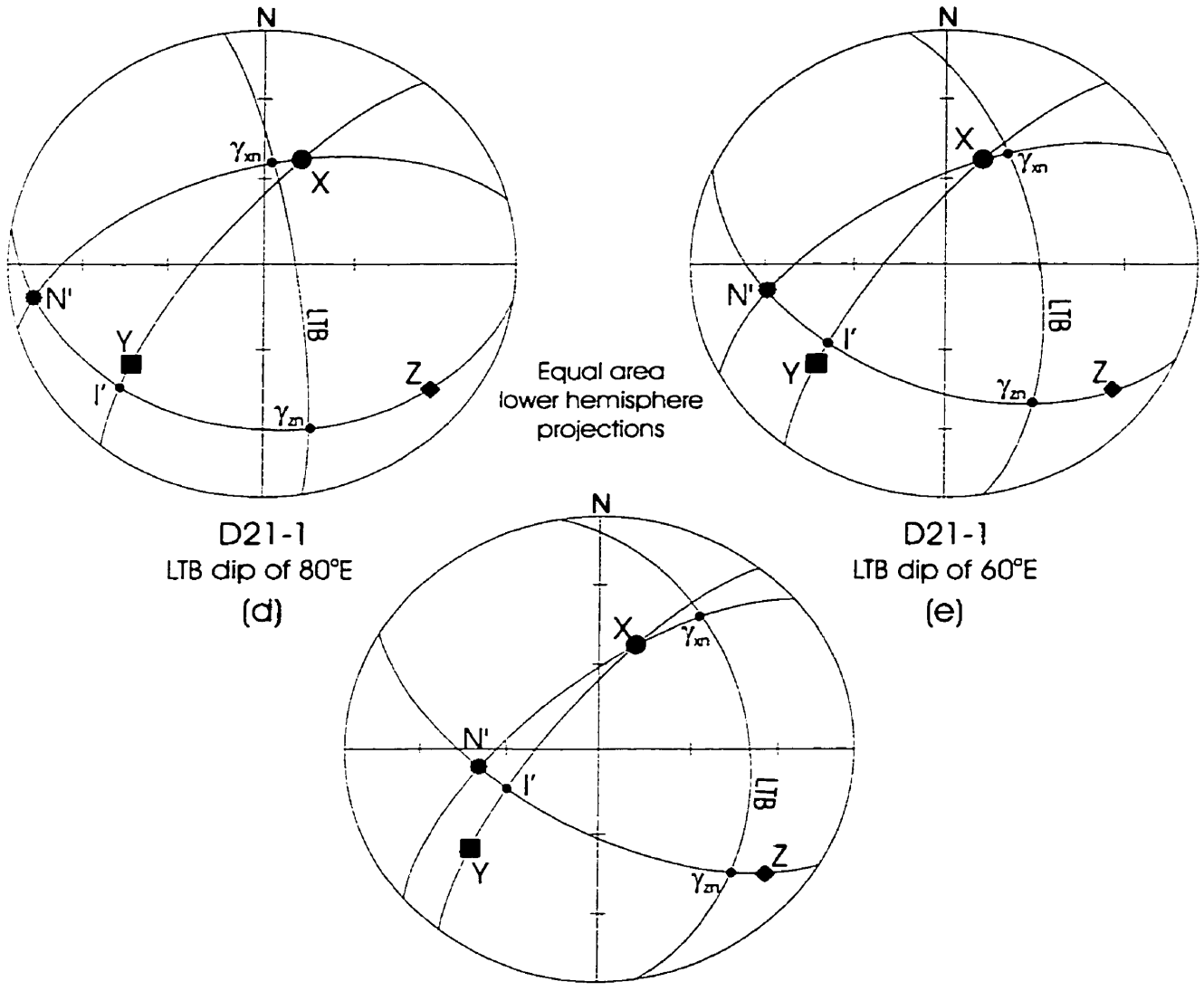

Hanging wall of Woman-Confederation assemblage boundary (LTB).
X, Y, Z= principal directions of total strain. N' = LTB normal,
γ_{xn} and γ_{zn} = directions of shear-strain components.
I' = long axis of section ellipse.

Figure 43 (d, e, f)

(Table 1). Such knowledge facilitates the determination of the local sense of distributed tangential shear-strain and the derivation of its direction. The strain-ratios permit estimation of the respective displacement of the hanging walls (Confederation and Woman assemblage masses) relative to the footwalls (Figures 23, 34).

In stereographic projection Lisle's (1998) technique (Figures 44, 45) leads to results similar to those of previous subchapter (Figures 42, 43). Added to Schwerdtner's (1998) stereoplot is the projection of line R', the deformed material line which was originally normal to the shear plane or LTB (Lisle 1998; line M of Figure 35). The orientation of R' on the schistosity is determined from:

$$\tan\theta_{R'} = \delta \tan\theta_{n'}$$

where $\theta_{R'}$ is the angle from the lineation (maximum principal direction (X)) to where R' is on the foliation plane and $\theta_{n'}$ is the angle between the lineation/X and the long axis of the strain ellipse in the Zn plane (n'; Figure 37). δ is the ratio of principal distortion values (A*, B*, C*: Table 1), which determines the direction of tangential shear strain. Once R' is found and plotted, a great circle (R'N') is generated. The intersection line between R'N' and the LTB surface constitutes the tangential shear-strain direction (γ) (Figures 44, 45). The components of γ_{xn} & γ_{zn} are parallel to the range limits for the shear direction (Schwerdtner 1998).

8.3.2 Balmer-Woman Assemblage Boundary

An assessment of the sense and direction of tangential shear strain was made of the Balmer-Woman assemblage at 2 locations (Figure 19). As with Schwerdtner's (1998) method, three possible dip values for the assemblage boundaries were used in applying Lisle's technique. Figure 44 shows the results of the shear-strain analysis, employing Lisle's technique on both walls of the Balmer-Woman assemblage boundary (Figure 19).

Direction and sense of tangential shear strain

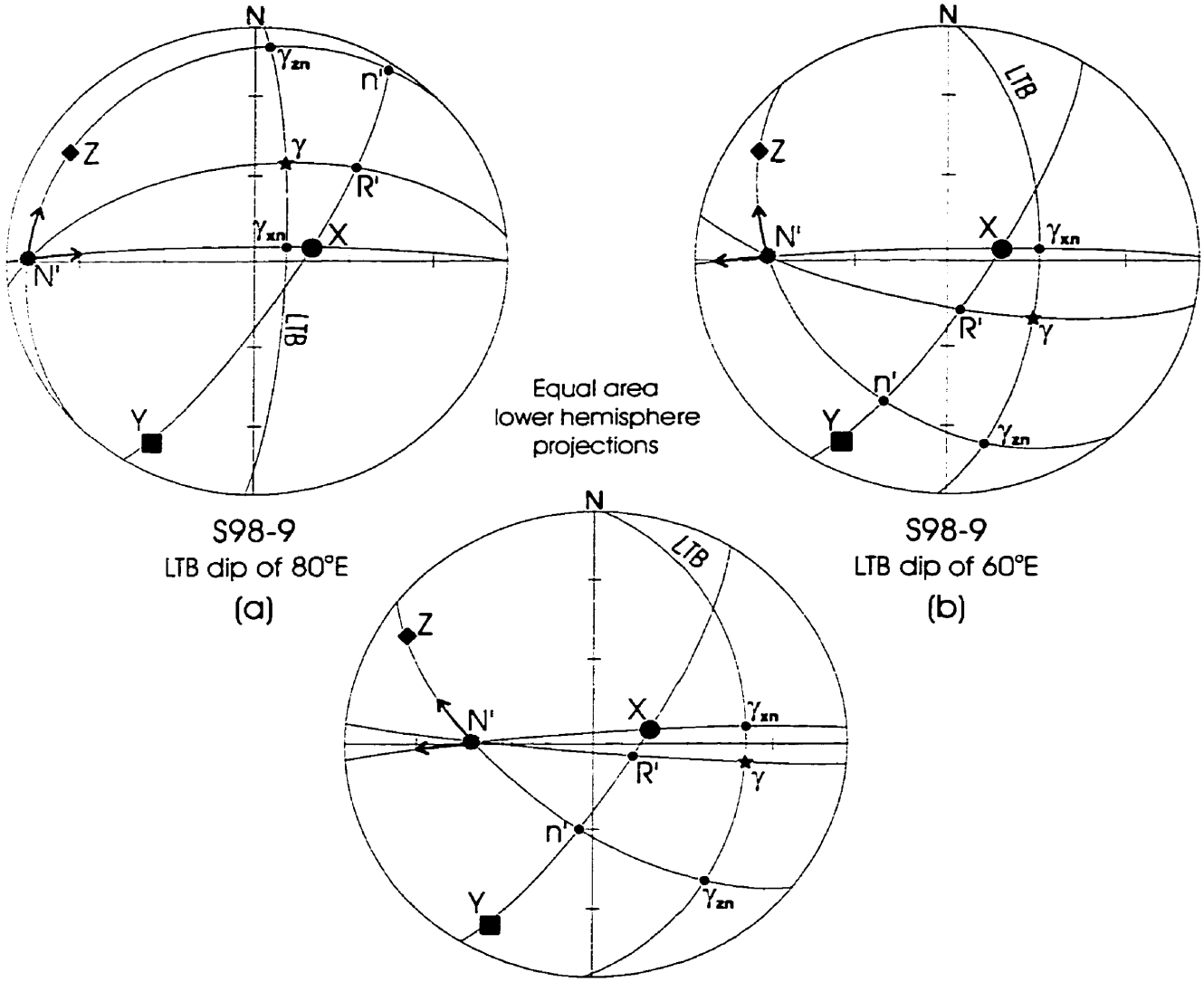

S98-9
LTB dip of 80°E
(a)

S98-9
LTB dip of 60°E
(b)

S98-9
LTB dip of 40°E
(c)

Foot wall of Balmer-Woman assemblage boundary (LTB). Arrows indicate displacement direction of hanging wall side. X, Y, Z= principal directions of total strain. N' = LTB normal, γ = shear-strain direction, γ_{xn} and γ_{zn} = directions of shear-strain components. Other symbols as used by Lisle (1998).

Figure 44 (a, b, c)

Direction and sense of tangential shear strain

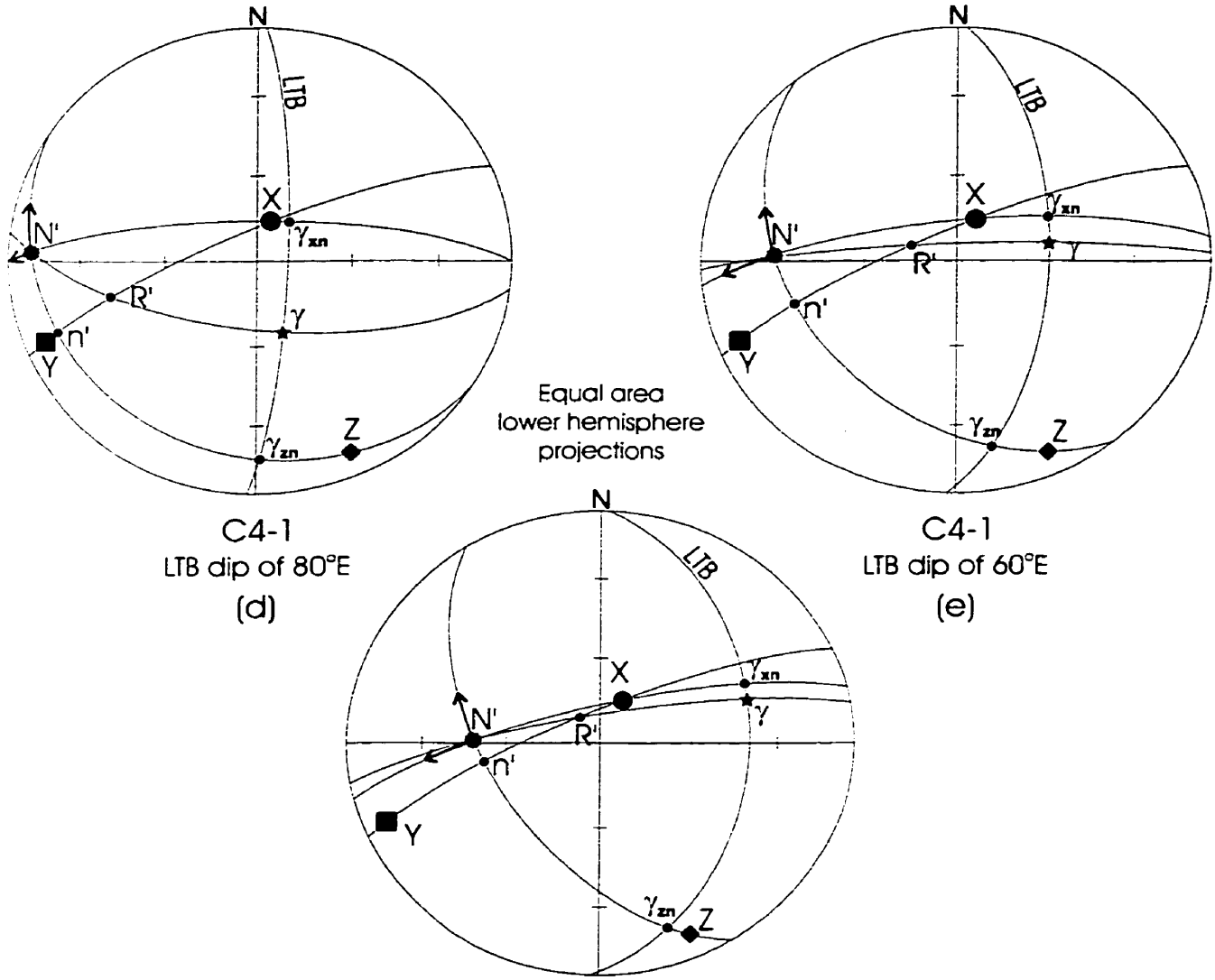

C4-1
LTB dip of 80°E
(d)

C4-1
LTB dip of 60°E
(e)

C4-1
LTB dip of 40°E
(f)

Hanging wall of Balmer-Woman assemblage boundary (LTB). Arrows indicate displacement direction of hanging wall side. X, Y, Z= principal directions of total strain. N' = LTB normal, γ = shear-strain direction, γ_{xn} and γ_{zn} = directions of shear-strain components. Other symbols as used by Lisle (1998).

Figure 44 (d, e, f)

The tangential shear strains in the walls of the Balmer-Woman assemblage boundary generally have the sense of thrust faults with small sinistral or dextral components (Figure 44). Only in the footwall of the LTB and the dip option of 80°, is the shear-strain sense like that on a normal fault (Figure 44).

Recall that a shear strain vector (γ) specifies the angle of relative rotation (ψ) of a straight line element that was initially normal to an element of a material plane which is also called a shear surface (Figure 35). LTBs (i.e. Balmer-Woman & Woman-Confederation assemblage boundaries) are shear surfaces that serve as a reference plane for shear-strain vectors.

In general, shear-strain vectors differ from vectors of point-displacement difference (DDV) that are referred to fixed geographic axes. If a boundary trace falls into a principal plane of strain and retains its orientation and length during deformation on the kilometre-scale, then the tangential shear strain becomes a set of DDVs whose magnitude increases linearly with distance from the boundary trace (Figure 24). This amounts to a transverse DDV gradient.

The DDV gradient at and transverse to, the Balmer-Woman assemblage boundary is seen mainly in subvertical cross-sections, which is close to a principal plane of total strain (cf. Chapter 7; Figure 23, 24). This is due largely to the fact that the sense of tangential shear strain is dominantly reverse (Figure 44). Accordingly, the upward displacement of a point 500m east of the boundary trace is ~312m (Figure 23). Contrary to what would be expected from thrusting, there is no gradual metamorphic change across the boundary. However, a marked metamorphic gradient may not be observable since the uplift is only a few hundred metres. Alternatively, no gradient would be seen if metamorphism occurred during or after the thrusting.

8.3.3 Woman-Confederation Assemblage Boundary

The sense and direction of tangential shear strain were analyzed at 3 localities in the boundary walls (Figure 19). Figure 45 shows the results of this analysis in both walls with the three boundary dip options (Figure 19).

For the 80° dip option, the tangential shear strain in the walls of the assemblage boundary proves to be mainly sinistral, although there is a small dip-shear component with reverse sense (Figure 45). However, for dip options of 40 and 60°E, the sense is dextral in the hanging wall. For steep LTB dips (i.e. 80°) the dip-shear component in both walls is normal (Figure 45). If one keeps the foot wall fixed and selects the 80° dip option, then the displacement differences can be shown in the horizontal plane of the strain ellipsoid (Y/Z; Figure 34). Assuming that the strain ratios estimated at two localities are representative of those in the entire hanging wall (S97-238, D21-1; Figure 19), a northward displacement of ~10 kilometres is obtained for the midpoint of the Confederation assemblage mass with respect to the foot wall (Figure 34).

Horizontal shear-strain vectors in an LTB wall are almost equivalent to point-displacement vectors if the material plane marking the present erosion level was horizontal at the onset of ductile deformation (Figure 25; cf. Chapter 7). This condition is effectively satisfied for the Woman-Confederation boundary because the horizontal plane is close to a principal plane of total strain (Figure 34). If strain is assumed to be homogeneous throughout the study area, then stretch or shortening components parallel to the assemblage boundaries (LTBs) will be constant throughout the assemblages (Figure 24).

Direction and sense of tangential shear strain

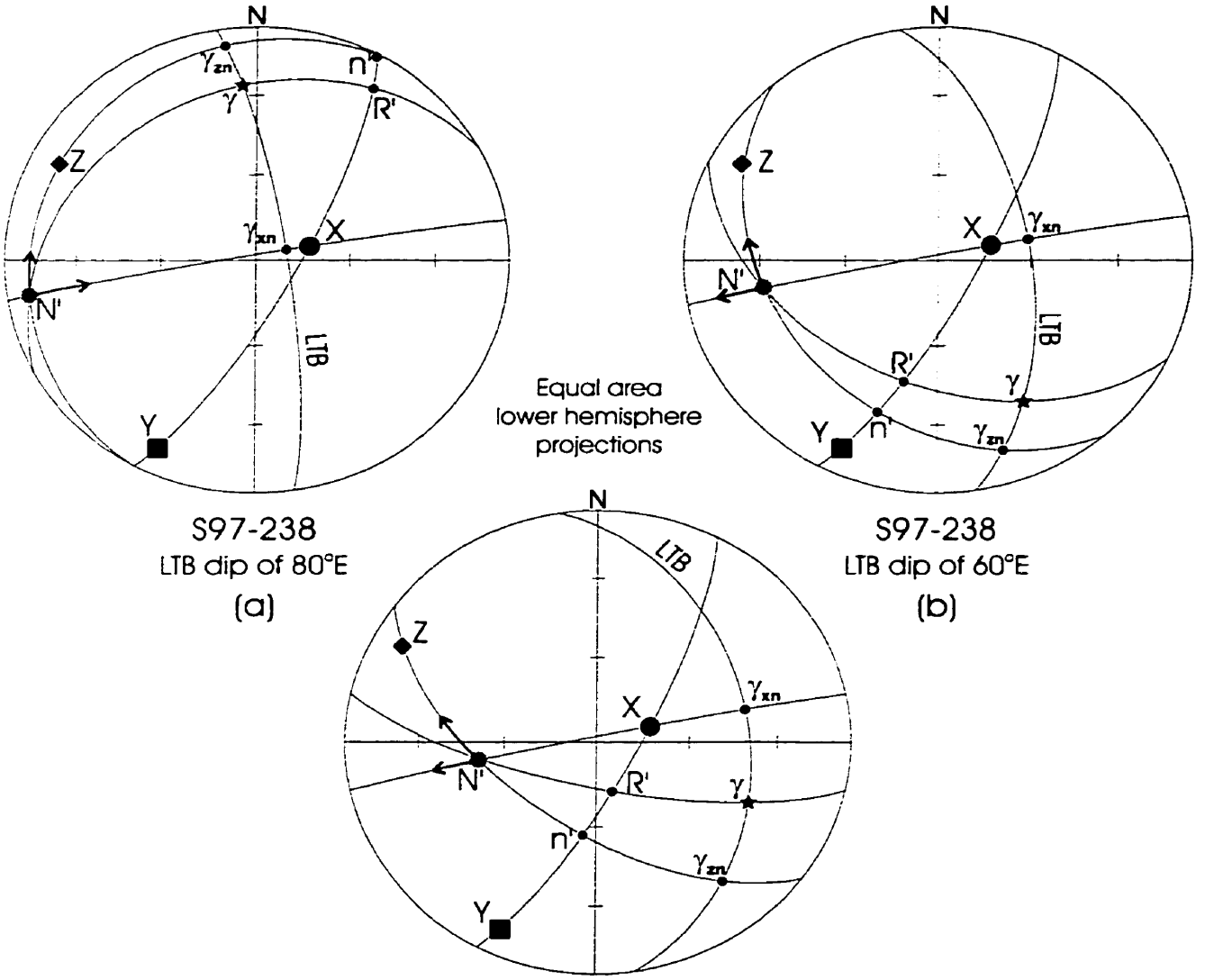

S97-238
LTB dip of 80°E
(a)

S97-238
LTB dip of 60°E
(b)

S97-238
LTB dip of 40°E
(c)

Foot wall of Woman-Confederation assemblage boundary (LTB). Arrows indicate displacement direction of hanging wall side. X, Y, Z= principal directions of total strain. N' = LTB normal, γ = shear-strain direction, γ_{xn} and γ_{zn} = directions of shear-strain components. Other symbols as used by Lisle (1998).

Figure 45 (a, b, c)

Direction and sense of tangential shear strain

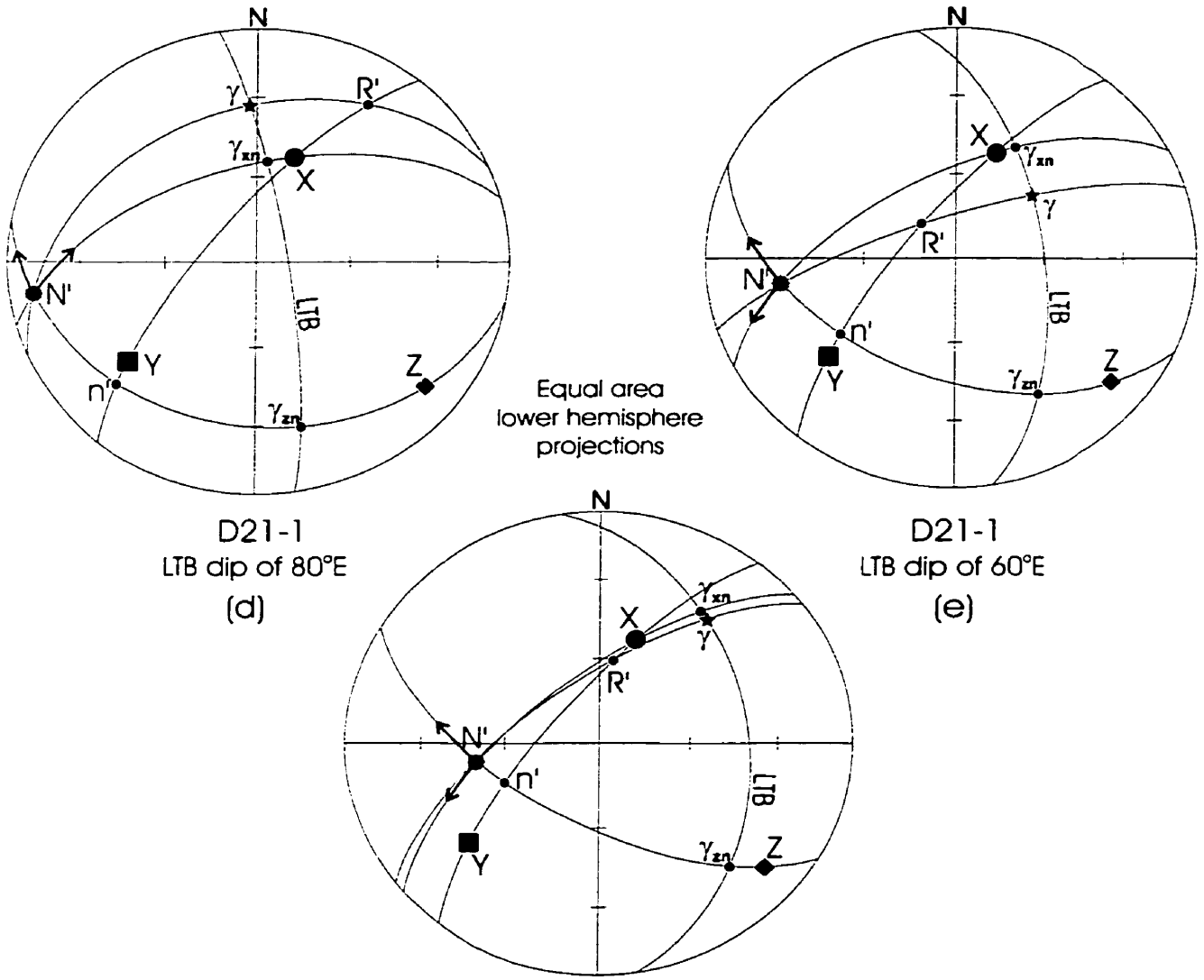

Hanging wall of Woman-Confederation assemblage boundary (LTB). Arrows indicate displacement direction of hanging wall side. X, Y, Z= principal directions of total strain. N' = LTB normal, γ = shear-strain direction, γ_{xn} and γ_{zn} = directions of shear-strain components. Other symbols as used by Lisle (1998).

Figure 45 (d, e, f)

Direction and sense of
tangential shear strain

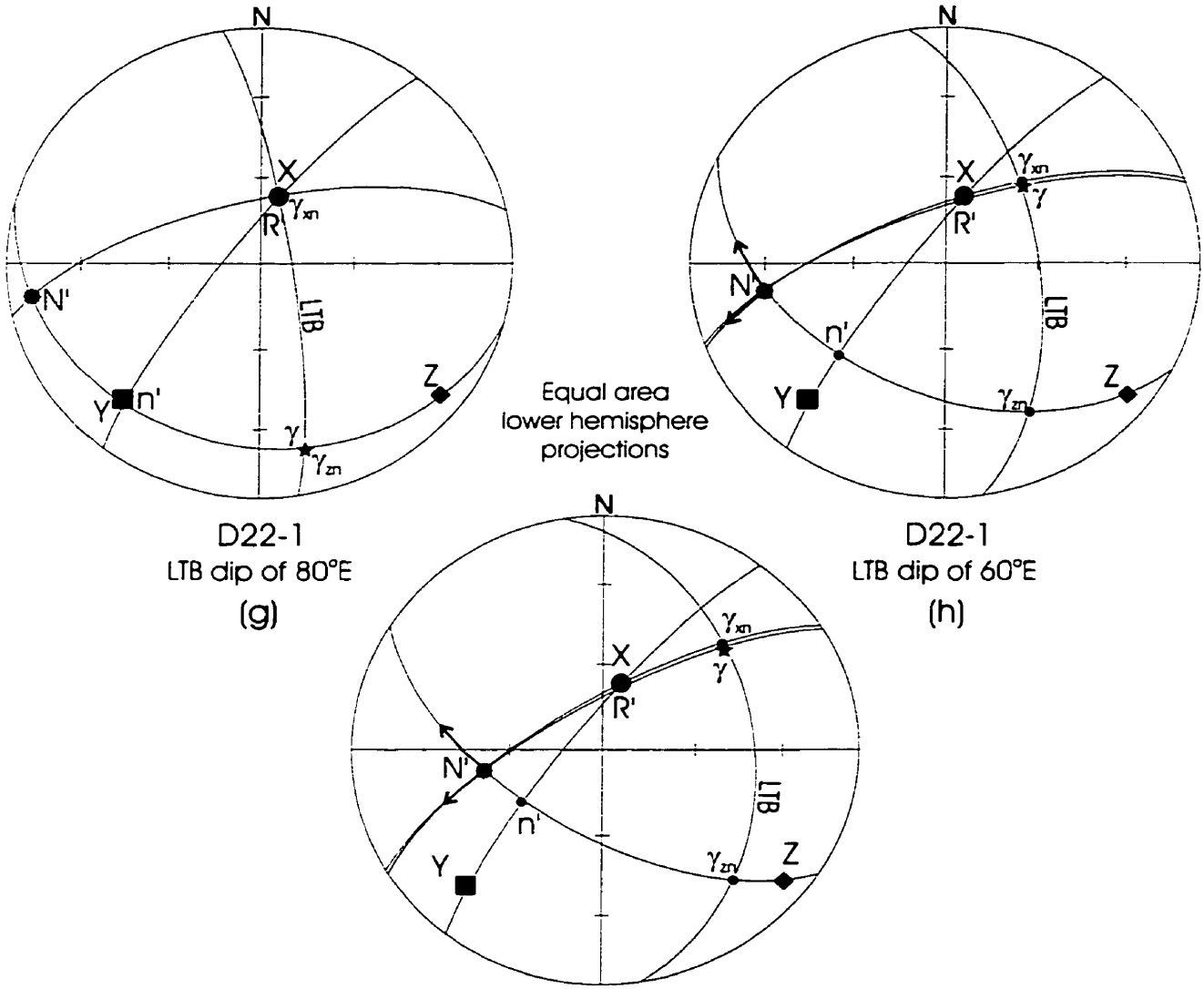

D22-1
LTB dip of 80°E
(g)

D22-1
LTB dip of 60°E
(h)

D22-1
LTB dip of 40°E
(i)

Hanging wall of Woman-Confederation assemblage boundary (LTB). Arrows indicate displacement direction of hanging wall side. X, Y, Z= principal directions of total strain. N' = LTB normal, γ = shear-strain direction, γ_{xn} and γ_{zn} = directions of shear-strain components. Other symbols as used by Lisle (1998).

Figure 45 (g, h, i)

8.4 Discussion and Summary

Attitudes of L-S fabrics defined by strained primary features and mineral aggregates suffice for approximating the direction and deriving the sense of tangential shear-strain components (Figures 40, 41, 42, 43). In order to determine the precise direction of tangential shear strain, however, both principal directions and principal ratios of strain are required for use of the graphic technique of Lisle (1998; Figures 44, 45).

The analysis of shear strain (total ductile deformation) depends critically on knowing the present attitude of assemblage boundaries (LTBs) on the kilometre-scale (Schwerdtner 1998). The attitude of the assemblage boundaries remains to be ascertained, however, the dip is expected to decrease with scale, a result of an observational bias in favour of steep bedding attitudes (cf. Chapter 4, Figure 21; Borowik *et al.* 1999).

The sinistral shear sense in the footwall of the assemblage boundaries is not affected by the choice of dip option (Figures 40, 41, 42, 43). However, the sense in the hanging walls of both assemblage boundaries, changes between different dip options (Figures 40, 41, 42, 43). In particular, the sense of the dip-shear component in both walls changes from normal sense for the 80° dip option to reverse sense for the 40° and 60° dip options (Figures 40, 41, 42, 43). One exception can be found in the hanging wall of the Balmer-Woman assemblage boundary where the thrust sense is independent of dip angle (Figure 44).

The centre of the Woman assemblage mass experienced a reverse tangential displacement of ~312 metres with respect to the Balmer assemblage mass (Figure 23). This supports Stott & Corfu's (1991) idea that the Woman assemblage rocks were thrust onto Balmer assemblage rocks (Figure 6). At the Woman-Confederation assemblage boundary the strike-shear is predominantly sinistral for the boundary dips considered. A northward displacement of ~10 kilometres for the

Confederation assemblage mass with respect to a fixed Woman assemblage mass is obtained (Figure 34). This is valid only if (i) the principal strain ratios used are close to the mean values for the western Birch-Uchi greenstone belt, and (ii) slip during ductile deformation is negligible on the assemblage boundary. No metamorphic grade change was discernible in the field across the Woman-Confederation assemblage boundary. This suggests that the displacement-difference vector for the interior of the Confederation assemblage mass may indeed be virtually horizontal (Figures 24, 25, 34).

Both the dominantly sinistral sense of tangential shear strain and the ~10 kilometre northward displacement of the Confederation assemblage mass, with respect to the Woman assemblage mass, accord with the northward transportation hypothesis of Stott & Corfu (1991).

CHAPTER IX

IMPLICATIONS OF ANALYTICAL RESULTS FOR THE BIRCH-UCHI GREENSTONE BELT

IX. IMPLICATIONS OF ANALYTICAL RESULTS FOR THE BIRCH-UCHI GREENSTONE BELT

9.1 Support For Northward Transportation Hypothesis

Stott & Corfu (1991) proposed a hypothesis that accounts for the geological map pattern by a northward displacement of the Confederation assemblage mass, with respect to the Woman assemblage mass to the west. This hypothetical relative displacement occurred on the scale of kilometres, during the Kenoran orogeny. Unlike in most other greenstone belts of the subprovince, the Birch-Uchi strata have a northerly strike. Moreover, in the eastern half of the belt, schistosity and bedding have a pronounced curvature (Thurston 1985, Stott & Corfu 1991, Schwerdtner *et al.* 1997). Large closures of Confederation assemblage rocks are observed in map view (Figure 2), in the northern portion of the eastern half (Stott & Corfu 1991). It was these geometric features of the greenstone belt that prompted Stott & Corfu (1991) to propose a northward tectonic transport of Confederation assemblage rocks, on the order of 10 kilometres.

One purpose of the present study was to test this hypothesis on the western side of the Confederation mass by using the results of shear strain analysis (cf. Chapter 8) at the Woman-Confederation assemblage boundary. Results of this analysis point to distributed, dominantly sinistral shear-strain in the map plane, i.e. northward relative displacement of Confederation assemblage rocks. The large S-fold in the assemblage boundary further supports a sinistral component of north-south shear strain (Schwerdtner *et al.* 1998, Borowik *et al.* 1999).

Principal strain ratios and tangential shear strain data obtained using Lisle's method (1998) permit estimates of the N-S displacement between the assemblage boundary and the midpoint of the Confederation assemblage mass (Table 1, Figure 34). This displacement is about 10 kilometres (Figures 24, 34; cf. Chapter 6). Therefore, both the sinistral sense and the magnitude of northward displacement determined at and along the Woman-Confederation

assemblage boundary support Stott & Corfu's (1991) suggestion of northward transportation. The displacement of the midpoint was caused by distributed tangential shear strain and was accompanied by a regional NNW-SSE shortening in the western central Birch-Uchi greenstone belt (Fyon & Lane 1985, Stott & Corfu 1991). Note that the shear-strain concept allows rotation of the assemblage boundary during ductile deformation. Therefore the boundary was more akin to a stretching fault than a translational dislocation in the shallow crust.

9.2 Kinematic History

The metavolcanics and associated metasediments of the Birch-Uchi greenstone belt are believed to have undergone repeated ductile deformation on the belt scale (Thurston & Breaks 1978, Fyon & Lane 1985, Fyon & O'Donnell 1986, Thurston 1985, Stott & Corfu 1991, van Staal 1998). The first deformation (D_1) may have resulted from compression induced by the emplacement of granitoid masses such as the Trout Lake batholith (Figure 8). Stott & Corfu (1991) consider an alternative according to which D_1 is a regional deformation associated with the northward transport of greenstone masses during collision between the Uchi-Sachigo and the Wabigoon-Winnipeg River superterranes. D_1 therefore created a northward striking schistosity conformable to bedding and subparallel to the assemblage boundaries and the belt as a whole (Figure 8). However, in this kinematic scenario why was the N-S boundary not rotated clockwise by oblique straining during D2?

The boundary would have retained its strike if the strain-induced rotation was cancelled out by an equal amount of counter-clockwise rigid-body rotation. Such stability, for example, is experienced by lines parallel to the direction of ideal simple shear, and, if true, would imply that the vertical assemblage boundaries were parallel to glide planes during horizontal simple shear

(D_2). However, this fails to explain the large S-folds supposedly created by D_2 and the subvertical elongation of rocks in the Woman Lake area.

Stott & Corfu (1991) proposed that the northward transportation of the Confederation assemblage mass started during D_1 and continued into D_2, a regional NNW-SSE shortening which produced the S-folds at both assemblage boundaries and the schistosity observed throughout the study area (Figures 12, 13). This required that most rocks in the study area (Figure 3) escaped significant straining during D_1. In western central parts of the belt, the mineral schistosity due to D_2 strikes NNE-SSW, and transects the bedding at oblique angles. (This contrasts with the north-south schistosity expected to have formed locally under the action of D_1.) Therefore, a single deformation accounts for the overall strain pattern observed in the study area. Further support for this idea comes from the discussion in Chapter 7 revealing that D2 could provide enough strain to produce the current structural configuration in the study area. However, if there is only one ductile deformation then the S-folds in bedding should not plunge at a steep angle.

D_1 fabrics may be present in the westernmost region of the Balmer assemblage (Figure 8), possibly enhanced by D_2 strain. The growing Trout Lake batholith may have strained parts of the Balmer assemblage, thereby generating the N-S fold set in close proximity to the batholith (Fyon & Lane 1985). The extent of apparent D_1 fabrics appears to be limited to a broad zone along the Trout Lake batholith (possibly equivalent to the strain aureole map zone?). The NNE-SSW striking D_2 fabric is seen throughout the study area and apparently coexists with D_1 fabrics nearer the Trout Lake batholith. NNE-SSW striking fabrics are also seen at the margin of the Trout Lake batholith and may have existed prior to, or at the onset of, the D_2 event (Fyon & Lane 1985). The mineral schistosity mapped in the study area may be axial planar to the S-folds at the

assemblage boundaries (Figures 12, 13). However, since a structural bias (cf. Chapter 4.6) prevents determination of the fold's true enveloping surfaces it remains uncertain if this is the case.

Planar fabrics for both deformation events diminish at a triple junction in Woman assemblage rocks where the fabric is dominantly linear (Figure 8). The origin of the triple junction is unknown presently, however, it may be a product of a passive interference effect between D_1 and D_2 strains.

In summary, the metavolcanic and metasedimentary rocks of the study area may have experienced at least two deformations, which produced the total strain pattern analysed (Fyon & Lane 1985, van Staal 1998, Schwerdtner *et al.* 1998). Such analysis is permissible even if the kinematics of D_1 and D_2 and other aspects of the deformation path are not well understood. Further structural, geochronological and geochemical studies need to be done throughout the greenstone belt in order to define better and understand the deformation history of rocks in the study area.

CHAPTER X

SUMMARY AND CONCLUSIONS

X. SUMMARY AND CONCLUSIONS

The Birch-Uchi greenstone belt is composed of three greenstone assemblage masses, which are thought to represent successive volcanic cycles and/or fault slices (Thurston 1985, Stott & Corfu 1991). Large jumps in protolith age are believed to occur at the boundaries between the assemblages, but geologists disagree about the position of the Woman-Confederation assemblage boundary. Stott & Corfu (1991) place the boundary at a unit of stromatolitic marble (Thurston 1985). Rogers *et al.* (1999), by contrast, put the southern part of the boundary in a brittle-ductile shear zone and the northern part of the boundary above a metaconglomerate unit. To establish the structural significance of the two assemblage boundaries and provide a better understanding of their mechanical behaviour during ductile deformation were important objectives of this thesis project. In particular, I tested the validity of the northward transportation hypothesis in the ductile realm (Stott & Corfu 1991). According to this hypothesis the Confederation assemblage mass moved north, with respect to older greenstone to the west.

Data presented in this thesis show that the strain intensity does not increase significantly at most localities, toward the assemblage boundaries (LTBs). Therefore, the boundaries were largely coherent during wall rock straining and the ductile deformation was not responsible for the apparent jump in protolith ages at the boundary surfaces. Nonetheless, the data are compatible with a modified version of the northward transportation hypothesis.

Schistosity trajectories do not refract across the assemblage boundaries. This indicates that the boundaries were largely coherent during ductile deformation. Measurement of the anisotropy of magnetic susceptibility in a metagabbro body transecting the Balmer-Woman

assemblage boundary suggests a slight strain gradient toward, or intermittent incoherence of the boundary surface during protracted gabbro emplacement and associated host-rock dilation.

Inspections of hand specimens and thin sections were made to assess the mineral fabric style for the main rock types of the field area. Typically, chlorite, sericite, amphiboles and various strained primary features (varioles, lapilli) define the schistosity (S) and lineation (L) observed macroscopically. Stronger fabrics are seen in mafic metavolcanics and intermediate metapyroclastics. A marble unit located in Woman Narrows at the Woman-Confederation assemblage boundary of Stott & Corfu (1991) was studied in thin section. Primary textural features are preserved and overprinted by pressure solution seams. Variable grain size of carbonates suggests that the fabric did not strongly recrystallize and that the rock is not a mylonite.

Two graphic techniques were utilized that permitted the determination of the direction and local sense of total tangential shear strain (γ) within the LTB walls. Both techniques use L-S fabrics defined by strained primary features and mineral grains. To find the precise direction of the γ-vector, at assemblage boundaries, principal ratios of total strain have to be known. The total strain is attributable to two ductile deformations (D_1, D_2), only one of which may have affected the rocks of the study area. If the assemblage boundaries acted as stretching faults (Means 1989) that were largely coherent (Cobbold 1983), then intermittent slip was driven by the same far-field stresses as the heterogeneous regional strain.

Results of the shear strain analysis indicate that, as part of the regional ductile deformation, the centre of the Woman assemblage mass experienced a reverse tangential displacement of ~312 metres with respect to the Balmer assemblage mass. Because of a large-scale curvature of schistosity trajectories, the walls of the Woman-Confederation assemblage

boundary have shear strain that is dominantly sinistral. A northward horizontal displacement of ~10-km is obtained for the centre of the Confederation assemblage mass with respect to a fixed Woman assemblage mass. This estimate assumes that (i) available principal strain ratios are representative of the entire western Birch-Uchi greenstone belt and (ii) no slip occurred on the assemblage boundary during ductile deformation.

NNW-SSE regional compression produced the strain pattern observed at the present erosion level. The compression also created km-scale S-folds at both assemblage boundaries. Because of an observational bias, neither the dip of the fold-enveloping surface nor the plunge of the fold axis is known at the km-scale.

Distortional strain components were estimated for material lines, parallel to (i) the strike of mineral schistosity and (ii) the trace of the enveloping surfaces to the S-fold at the Woman-Confederation assemblage boundary. The values for the components indicate that D_2 would provide enough distortion to account for the S-fold. Furthermore, the total distortion on the kilometre scale is nearly biaxial, with <23% extension parallel to schistosity trajectories at the Woman-Confederation assemblage boundary.

REFERENCES

REFERENCES

Anhausser, C.R., Mason, R., Viljoen, M.J., & Viljoen, R.P., 1969. A reappraisal of some aspects of Precambrian Shield geology. *Geological Society of America Bulletin*, **80**: 2175-2200.

Archanjo, C. J., Launeau, P., & Bouchez, J. L. 1995. Magnetic fabric vs. magnetite and biotite shape fabrics of the magnetite-bearing granite pluton of Gameleiras (Northeast Brazil). *Phys. Earth Planet. Inter.*, **89**: 63-75.

Arias, Z.G., and Helmstaedt, H., 1990. Structural evolution of the Michipicoten (Wawa) greenstone belt, Superior Province: Evidence for an Archean fold and thrust belt. Geoscience Research Grant Program Summary of Research 1989-1990. Ontario Geological Survey Miscellaneous Paper **150**: 107-114.

Ayres, L.D. 1978. Metamorphism in the Superior Province of northwestern Ontario and its relationship to crustal development. *In*: *Metamorphism in the Canadian Shield*, Geological Survey of Canada Paper **78-10**: 25-36.

Ayres, L.D. 1983. Bimodal volcanism in Archean Greenstone Belts as exemplified by greywacke composition, Lake Superior Park, Ontario. *Canadian Journal of Earth Sciences*, **20**: 1168-1194.

Ayres, L.D., & Thurston, P.C. 1985. Archean Supracrustal sequences in the Canadian Shield: An Overview. *In*: *Evolution of Archean Supracrustal Sequences*. Ayres, L.D., Thurston, P.C., Card, K.D., & Weber, W. (Eds.), Geol. Assoc. of Can. Special Paper **28**.

Ayres, L.D., & Corfu, F., 1991. Stacking of disparate volcanic and sedimentary units by thrusting in the Archean Favourable Lake Greenstone Belt, central Canada. *Precambrian Research*, **50**: 221-238.

Ayres, L.D., Halden, N.M., & Ziehlke, D.V., 1991. The Aulneau Batholith: Archean diapirism preceded by coalescence of granitoid magma at depth. *Precambrian Research*, **51**: 27-50.

Ayres, L.D., Lumbers, S.B., Milne, V.G., and Robeson, D.W., 1971. Exploratory text, legend, diagrams, time scale, for Ontario Geological Map; Ontario Department of Mines and Northern Affairs, Map **2196**.

Barlow, R.B., Gupta, V.K., & Wadge, D.R., 1976. Bouguer Gravity Map, Birch-Uchi-Confederation Lakes Area, District of Kenora (Patricia Portion). Ontario Division of Mines, Preliminary Map **P1186**.

Bateman, J.D., 1940a. Geology and gold deposits of the Uchi-Slate Lakes area; Ontario Department of Mines, *Annual Report 1939*, **48** pt.8, p.1-43.

Bateman, J.D., 1940b. Geology of the J.M. Consolidated Mine; Ontario Department of Mines, Annual Report 1939, **48** pt.8, p.44-52.

Beakhouse, G.P., 1989. Geology of the Western Birch Lake area, Kenora district, Patricia Portion. Ontario Geological Survey, Open File Report 5700, 106p.

Beakhouse, G.P., 1991. Winnipeg River Subprovince. *In: Geology of Ontario*, Ontario Geological Survey, Special volume **4**, Part 1, p. 279-301.

Beakhouse, G.P., Breaks, F.W., Stone, D., & Sutcliffe, R.H., 1989. Granitoid rocks and their significance for crustal evolution in the western Superior Province; In: Program with Abstracts, Geological Association of Canada-Mineralogical Association of Canada, **14**: A-8.

Benn, K. 1994. Overprinting of magnetic fabrics in granites by small strains: numerical modeling. *Tectonophysics*, **233**: 153-162.

Borowik, A., Crews, M.J., Schwerdtner, W.M., 1999. Northerly-directed shear strain within, and at the southern edge of, the Uchi Subprovince, Red Lake Region, Ontario: *Lithoprobe Report ##*, University of British Columbia, yy-zz, In Press.

Borradaile, G. J. 1987. Anisotropy of magnetic susceptibility: rock composition versus strain. *Tectonophysics*, **138**: 327-329.

Borradaile, G. J. 1988. Magnetic susceptibility, petrofabrics and strain. *Tectonophysics* **156**: 1-20.

Borradaile, G.J., 1991, Correlation of strain with anisotropy of magnetic susceptibility (AMS). *Pageoph.* **135**: 15-29.

Borradaile, G.J., and Mothersill, J.S., 1984. Coaxial deformed and magnetic fabrics without simply correlated magnitudes of principal values. *Phys. Earth and Planet. Int.* **35**: 294-300.

Borradaile, G.J., and Schwerdtner, W.M., 1984. Horizontal shortening of upward-facing greenstone structures in the southern Superior Province, Canadian Shield, *Can. J. Earth Sci.*, **21**: 611-615.

Borradaile, G., & Alford, C. 1987. Relationship between magnetic susceptibility and strain in laboratory experiments. *Tectonophysics*, **133**: 121-135.

Borradaile, G.J., & Dehls, J.F., 1993. Regional kinematics inferred from magnetic subfabrics in Archean rocks of Northern Ontario, Canada. *J. Structural Geology* **15(7)**: 887-894.

Borradaile, G.J., & Stupavsky, M., 1995. Anisotropy of magnetic susceptibility: measurement schemes. *Geophysical Res. Letters* **22(15)**: 1957-1960.

Bruce, E.L., 1929. Gold deposits of Woman, Narrow and Confederation Lakes, District of Kenora (Patricia Portion). Ontario Department of Mines, Annual Report for 1928, **37** Pt.4 p.1-51.

Burke, K., 1997. Forward. *In: Greenstone Belts*, edited by de Wit, M.J., & Ashwal, L.D., Clarendon Press, London, p.v-vii.

Burwash, E.M., 1920. A geological reconnaissance into Patricia. Ontario Department of Mines, Annual Report for 1920, **29** Pt.1 p.157-192.

Cañón-Tapia, E. 1996. Single-grain versus distribution anisotropy: a simple three-dimensional model. *Phys. Earth Planet. Inter.*, **94**: 149-158.

Capes, C., 1999. Study of large geologic strain in the western part of the Birch-Uchi-Confederation Greenstone Belt, Northwestern Ontario. Unpublished B.Sc. Thesis, University of Toronto.

Card, K.D., 1990. A review of the Superior Province of the Canadian Shield, A product of Archean accretion. *Precambrian Research*, **48**: 99-156.

Card, K.D., & Ciesielski, A., 1986. DNAG#1: Subdivisions of the Superior Province of the Canadian Shield. *Geoscience Canada*, **13**: 5-13.

Cobbold, P.R., 1983. Kinematic and mechanical discontinuity at a coherent interface. *Journal of Structural Geology* **5**: 341-350.

Cogné, J. P. & Perroud, H. 1988. Anisotropy of magnetic susceptibility as a strain gauge in the Flamanville granite, NW France. *Phys. Earth Planet. Inter.* **51**: 264-270.

Condie, K.C., 1976. *Plate Tectonics and Crustal Evolution*. Pergamon Press, New York, N.Y., 288p.

Condie, K.C., 1981. *Archean Greenstone Belts*. Elsevier Scientific Pub. Co., New York, 434p.

Condie, K.C., 1997. *Plate Tectonics and Crustal Evolution*. 4th ed., Butterworth Heineman, 282p.

Corfu, F. and Wallace, H., 1986. U-Pb zircon ages for magmatism in the Red Lake greenstone belt, Northwestern Ontario. *Can. J. Earth Sci.* **23(1)**: 27-42.

Corfu, F., & Andrews, A.J., 1987. Geochronological constraints on the timing of magmatism, deformation and gold mineralization in the Red Lake Greenstone belt, northwestern Ontario. *Can. J. Earth Sci.*, **24**: 1302-1320.

Corfu, F. and Stott, G.M.,, 1993a. Age and petrogenesis of two late Archean magmatic suites, Northwestern Superior Province, Canada: Zircon U-Pb and Lu-Hf isotopic relations. *J. of Petrology* **34(4)**: 817-838.

Corfu, F. and Stott, G.M., 1993b. U-Pb geochronology of the central Uchi subprovince, Superior province. *Can. J. Earth Sci.* **30(6)**:1179-1196.

Coward, M.P., 1976. Archean deformation patterns in southern Africa. *Phil. Trans. P. Soc. Lond.* **A283**: 313-331.

Coward, M.P., and James, P.R., 1974. The deformation patterns of 2 Archean greenstone belts in Rhodesia and Botswana. *Precambrian Research*, **1**: 235-258.

Crews, M.J., and Schwerdtner, W.M., 1997. Structural analysis at tectonic assemblage boundaries in western Confederation Lake (Birch-Uchi) Greenstone Belt, Red Lake Region, Northwest Ontario; *Lithoprobe Report* **63**, University of British Columbia.

Crews, M.J., Hanley, J.J., Moslehi, H., Schwerdtner, W.M., 1998. Structural analysis at tectonic assemblage boundaries in Western Confederation Lake (Birch-Uchi) Greenstone Belt, Western Superior Province, Red Lake Region, Ontario. *Lithoprobe Report* **65**, University of British Columbia, p.8-11.

Crews, M.J., Capes, P.C., Moslehi, H., Schwerdtner, W.M., 1999. Crude estimation and practical use of principal-strain ratios in western Birch-Uchi Greenstone belt, Red Lake Region: Lithoprobe Report ##, University of British Columbia, yy-zz, In Press.

Cruden, A.R., Davis, D.W., Menard, T., & Robin, P.-Y.F., 1997. Structural and geochronological relationships between the Winnipeg River & Wabigoon Subprovinces: Implications for the Terrane Accretion Model. *Lithoprobe Report* **63**: 18-26.

Cruden, A.R., Davis, D.W., Melnyk, M., Robin, P.-Y.F., Menard, T., 1998. Structural and geochronological observations at Kenora: Implications for the style and timing of deformation during the Kenoran Orogeny, NW Ontario. *Lithoprobe Report* **65**: 54-62.

Cruden, A.R., & Robin, P.-Y.F., 1998. New models for Archean gneiss domes and greenstone belts. E.O.S. Transactions, American Geophysical Union 1998 Spring Meeting, **79(17)**: S343.

Cruden, A.R. & Hynes, A. 1999. Western Superior Lithoprobe seismic lines 2a and 2b: Comparison with surface geology and preliminary interpretations. Western Superior Transect, *Lithoprobe Report* xx, University of British Columbia, yy-zz, In Press.

Davis, D.W., 1997. Accretion of the Superior Province by collapse of an arc/back-arc/continent margin system: Evidence from comparison of U-Pb Ages in Western Superior and Abitibi Lithoprobe Transects. *Lithoprobe Report* **63**: 92-94.

Davis, D.W. 1998. Speculations on the formation and crustal structure of the Superior Province from U-Pb geochronology. *Lithoprobe Report* **65**: 21-28.

Davis, D.W. and Corfu, F., 1990. Evolution of the Superior province, constraints and inferences based on U-Pb geochronology. *In: Greenstone gold and crustal evolution*, NUNA conference volume, Val d'Or, PQ. Geological Survey of Canada. p. 151-152.

Devaney, J.R., 1997. Sedimentological studies of the Birch Lake Area, western Uchi Subprovince. In Summary of Field Work and Other Activities 1997, Ontario Geological Survey, *Miscellaneous Paper* **168**: 44-47.

Devaney, J.R., 1999. Tectonic hypotheses regarding the late orogenic history of the Birch-Uchi Greenstone Belt. Ontario Geological Survey, *Miscellaneous Paper* **169**: p.113-118.

de Wit, M.J., 1998. On Archean granites, greenstones, cratons and tectonics: Does the evidence demand a verdict? *Precambrian Research*, **91**: 181-226.

de Wit, M.J., & Ashwal, L.D., 1997. *Greenstone Belts*. Clarendon Press Oxford.

Dowling, D.B., 1896. Report on the country and the vicinity of Red Lake and Part of the Basin of Berens River, Keewatin. Geological Survey of Canada, *Annual Report for 1894*, **7F** 54p.

Eskola, P.E., 1948. The problem of mantled gneiss domes. *Quart. J. Geol. Soc. London*, **104**: 461-476.

Flinn, D., 1962. On folding during 3-D progressive deformation. *Quart. J. Geol. Soc. London*. **181**: 385-433.

Fyon, A.J. and Lane, L., 1985. Structural geology and alteration patterns related to gold mineralization in the Confederation Lake area; *In:* in Summary of Field Work and Other Activities 1985, Ontario Geological Survey. *Miscellaneous Paper* **126**: 201-209.

Fyon, A.J. and O'Donnell, L., 1986. Regional strain state and alteration patterns related to gold mineralization in the Uchi-Confederation-Woman lakes area; in Summary of Field Work and other Activities 1986. Ontario Geological Survey, *Miscellaneous Paper* **132**: 266-275.

Gabrielse, H., & Yorath, C.J., 1989. DNAG#4: The Cordilleran Orogen in Canada. *Geoscience Canada*, **16**: 67-83.

Gay, N.C., 1969. The analysis of strain in the Barberton Mountain Land, eastern Transvaal, using deformed pebbles. *Journal of Geology*. **77**: 377-396.

Gelinas, L., Brooks, C., Trzcienski, W.E. Jr., 1976. Archean variolites-quenched immiscible liquids. *Can. J. Earth Sc.* **13**: 210-230.

Glikson, A.Y., 1971. Premature Archean element distribution patterns: Chemical evidence and geotectonic significance. *Earth Plant. Sci. Lett.*, **12**: 309-320.

Glikson, A.Y., 1972. Early Precambrian evidence of a primitive ocean crust and island nuclei of sodic granite. *Bull. Geol. Soc. Amer.*, **83**: 3323-3344.

Good, D.J., 1988. Geology of the east half of the Birch Lake area, District of Kenora, Patricia Portion. Ontario Geology Survey, *Open File Report* **5685**, 131p.

Goodwin, A.M., 1967. Volcanic studies in the Birch-Uchi Lakes Area of Ontario. Ontario Department of Mines, *Miscellaneous Paper* **6**, 96p.

Goodwin, A.M. 1978. Archean crust in the Superior Geotraverse Area: Geologic Overview. *In*: Smith, I.E.H., & Williams, J.G. (Eds.), *Archean Geochemistry conference*, p.73-106.

Goodwin, A.M., 1991. *Precambrian Geology*: London, Academic Press, 666p.

Goodwin, A.M., 1996. *Principles of Precambrian Geology*. London, Academic press, 327p.

Grégoire, V., de Saint Blanquat, M., Nedelec, A., & Bouchez, J. L. 1996. Shape anisotropy Versus magnetic interactions of magnetic grains: experiments and application to AMS in granitic rocks. *Geophys. Res. Lett.*, **22**: 2765-2768.

Greig, J.W., 1928. Woman and Narrow Lakes Area, District of Kenora (Patricia Portion). Ontario Department of Mines, *Annual Report for 1927*, **36** Pt. 3 p.85-110.

Gupta, V.K., & Wadge, D.R., 1978. Bouguer gravity and generalized geologic Map, Red Lake Area, District of Kenora (Patricia Portion). Ontario Geological Survey, Preliminary Map **P1248**.

Gupta, V.K., & Ramani, N., 1980. Some aspects of regional-residual separation of gravity anomalies in a Precambrian terrain. *Geophysics*, **45**: 1412-1426.

Gupta, V.K., & Wadge, D.R., 1980. Gravity study of the Birch-Uchi and Red Lakes Area, District of Kenora (Patricia Portion). Ontario Geological Survey, *Open File Report* **5278**, 249p.

Gupta, V.K., Thurston, P.C., & Dusanowskyj, T.H., 1982. Constraints upon models of greenstone belt evolution by gravity modeling, Birch-Uchi Greenstone Belt, northern Ontario. *Precambrian Research* **16**: 233-255.

Gupta, V.K., & Wadge, D.R. 1986. Gravity study of the Birch, Uchi, and Red Lakes area, District of Kenora (Patricia Portion), *Ontario Geological Survey report* **252**, 98p. Accompanied by Maps 2492, 2493, 2494 and 2495. Scale 1:250,000.

Gupta, V.K., & Wadge, D.R. 1986. Bouguer gravity, Red Lake-Birch Lake, District of Kenora, Ont. Geol. Surv., Map 2492, Geophysical/Geochemical Series, Scale 1:250,000. Survey 1976,1977.

Hall, D.H., & Hajnal, Z. 1968. Crustal structure of Northwestern Ontario: Refraction Seismology. *Can. J. Earth Sci.* **6**: 81-107.

Hall, D.H., & Brisbin, W.C. 1982. Overview of regional geophysical studies in Manitoba and northwestern Ontario. *Can. J. Earth Sci.* **19**: 2049-2059.

Hamilton, W.B., 1998a. Archean tectonics and magmatism. *International Geology Review*, **40**: 1-39.

Hamilton, W.B., 1998b. Archean magmatism and deformation were not products of plate tectonics. *Precambrian Research*, **91**: 143-179.

Harding, W.D., 1936. Geology of the Birch-Springpole Lakes Area. Ontario Department of Mines, *Annual Report for 1936*, **45** Pt.4 p.1-33.

Hargraves, R. B., Johnson, D. & Chan, C. Y. 1991. Distribution anisotropy: the cause of AMS in Igneous rocks? *Geophys. Res. Lett.* **18**: 2193-2196.

Hirt, A. M., Lowrie, W., Clendenen, W. S., & Kligfield, R. 1988. The correlation of magnetic anisotropy with strain in the Chelmsford Formation of the Sudbury Basin, Ontario. *Tectonophysics*, **145**: 177-189.

Hoffman, P.F., 1989. Precambrian Geology of North America - An Overview, Geological Society of America, *The Geology of North America*, **A**: 447-512.

Hofmann, H.J., Thurston, P.C., and Wallace, H., 1985. Archean stromatolites from Uchi Greenstone Belt, Northwestern Ontario; *In:* Evolution of Archean supracrustal sequences (edited by L.D. Ayres, P.C. Thurston, K.D. Card and W. Weber), Geological Association of Canada, *Special Paper* **28**: 125-132.

Holman, R.H.C., 1963. A regional geochemical reconnaissance of bedrock in the Red Lake-Lansdowne House area of Ontario: p.28-39 in Eight Papers on Regional Geochemistry in Canada. *Geological Survey of Canada Paper* **63-23** 46p.

Hossack, J.R., 1968. Pebble deformation and thrusting in the Bygdin area, S. Norway. *Tectonophysics* **5**: 315-339.

Hossack, J.R., 1978. The correction of stratigraphic sections for tectonic finite strain in the Bygdin Area, Norway. *J. Geol. Soc. Lond.* **135**: 229-241.

Hrouda, F., 1982. Magnetic anisotropy and its application in geology and geophysics, *Geophysical Survey*, **5**: 37-82.

Hrouda, F. 1992. Separation of a component of tectonic deformation from a complex magnetic fabric. *J. Struct. Geol.*, **14**: 65-71.

Hudleston, P.J., 1976. Early deformational history of Archean rocks in the Vermilion District, northwestern Minnesota. *Can. J. Earth Sci.*, **13**: 579-592.

Hudleston, P.J., Schultz-Ela, D., & Sothwick, D.L., 1988. Transpression in an Archean Greenstone belt, northern Minnesota. *Can. J. Earth Sci.*, **25**: 1060-1068.

Hudleston, P.J., and Schwerdtner, W.M., 1997. Strain: *In Greenstone Belts*. de Wit, M. J., & Ashwal, L. D. (editors), Clarendon Press, Oxford, p.296-308.

Hunter, D.P., & Stowe, C.W., 1997. A historical review of the origin, composition, and setting of Archean Greenstone belts (Pre-1980): *In: Greenstone Belts*: edited by de Wit, M.J., and Ashwal, L.D., Clarendon Press, Oxford, p.5-29.

Innes, M.J.S., 1960. Gravity and isostasy in northern Ontario and Manitoba. *Dominion Observatory Publication*, **21(6)**: 263-338.

Innes, D. 1964. The state of gravity mapping in Canada, November 1964. *In:* Gravity anomalies - Unsurveyed areas. *Am. Geophys. Union Geophys. Mon. Ser.* **9**: 26-27.

Jaeger, J.C., 1969. *Elasticity, fracture & flow with engineering and geological applications*; 3rd edition, Methuen & Company Ltd., London, 268p.

Jelinek, V., 1973. Precision AC bridge set for measuring magnetic susceptibility of rocks and its anisotropy. *Studia. geoph. et. geod.*, **17**: 3b.

Jelinek, V., 1981. Characterization of the magnetic fabric of rocks. *Tectonophysics*, **79**: T63-T67.

Khan, M.S. 1982. Paleomagnetism of Archean rocks from the English River and Uchi subprovinces, northwestern Ontario and polar wandering path for North America. Unpublished M.Sc. thesis, University of Manitoba.

Krogh, T.E., & Davis, G.L., 1971. Zircon U-Pb Ages of Archean metavolcanic rocks in the Canadian Shield. *Carnegie Institution, Washington D.C. Yearbook* **70**: 241-242.

Krogh, T.E., Davis, D.W., & Corfu, F. 1984. Implications of precise U-Pb dating for the geological evolution of Superior province. Geological Association of Canada, *Program with Abstracts* **9**: p. 79.

Langford, F.F. & Morin, J.A. 1976. The development of the Superior province of northwestern Ontario by merging island arcs. *American Journal of Science*, **276**: 1023-1034.

Lisle, R.J., 1998. Graphic derivation of the local sense of shear strain components in stretched walls of lithotectonic boundaries. *Journal of Structural Geology*, **20**: 957-967.

Macgregor, A.M., 1951. Some milestones in the Precambrian of Southern Rhodesia. *Proc. Geol. Soc. S. Africa.* **54**: 27-71.

Marachal, J.-C., & West, G.F., 1980. A model for Archean tectonism. Part 2 Numerical models of vertical tectonism in greenstone belts. Cdn. J. Earth Sci. **17**: 60-71.

Means, W.D., 1989. Stretching faults. *Geology*, **17**: 893-896.

Moslehi, H., 1998. Quantitative estimates of principal strain ratios in metaconglomerates and fragmental volcanic rocks of the Birch-Uchi Greenstone Belt, Uchi Subprovince. Unpublished B.Sc. Thesis, University of Toronto.

Moxham, R.L., 1965. Distribution of minor elements in coexisting hornblende and biotites. *Canadian Mineralogist*, **8**: 204-240.

Noble, S.R., 1989. Geology, geochemistry and isotope geology of the Trout Lake Batholith and the Uchi-Confederation Lakes Greenstone Belt, Northwestern Ontario, Canada; Unpublished PhD thesis, University of Toronto, Toronto, Ontario, 288p.

Noble, S.R., Krogh, T.E., & Evensen, N.M., 1989. U-Pb age constraints on the evolution of the Trout Lake-Uchi-Confederation Lakes granite-greenstone terrane, Superior Province, Canada. Geological Association of Canada-Mineralogical Association of Canada, Joint Annual Meeting, *Program with Abstracts*, **14**: A56.

Nunes, P.D. and Thurston, P.C., 1980. Two hundred and twenty million years of Archean evolution: a zircon U-Pb age stratigraphic study of the Uchi-Confederation Lakes Greenstone Belt; *Canadian Journal of Earth Sciences*, **17**: 710-721.

Observatories Branch, Department of Energy, Mines and Resources,
1970. Gravity Map Series #29,
1973. Gravity Map Series #100 & 101.

Ontario Geological Survey, 1992. Tectonic assemblages of Ontario, west central sheet; Ontario Geological Survey, Map **2576**.

Peach & Lisle, R.J., 1979. A fortran program for the analysis of tectonic strain using deformed elliptical markers. *Computers & Geosciences*, **5**: 325-334.

Percival, J.A., & Williams, H.R., 1989. Late Archean Quetico accretionary complex, Superior Province, Canada. *Geology*, **17**: 23-25.

Percival, J.A., Stern, R.A., Skulski, T., Card, K.D., Mortenson, J.K., & Bégin, N.J., 1994. Minto Block, Superior Province, missing link in deciphering assembly of the craton at 2.7 Ga.. *Geology*, **22**: 839-842.

Platt, J.P., 1980. Archean Greenstone belts: A structural test of tectonic hypotheses. *Tectonophysics*, **65**: 127-150.

Pryslak, A.P., 1970. Mitchell Township, District of Kenora (Patricia Portion); Ontario Department of Mines and Northern Affairs, *Preliminary Map* **P.593**.

Pryslak, A.P., 1971a. Corless Township, District of Kenora (Patricia Portion); Ontario Department of Mines and Northern Affairs, *Preliminary Map* **P.634**.

Pryslak, A.P., 1971b. Knott Township, District of Kenora (Patricia Portion); Ontario Department of Mines and Northern Affairs, *Preliminary Map* **P.635**.

Ramberg, H., 1981. *Gravity, deformation and the Earth's crust*, 2nd ed.: Academic Press, London, pp.452.

Ramsay, J.G., 1967. *Folding and Fracturing of Rocks*. McGraw-Hill, New York, N.Y., 68pp.

Ramsay, J.G., and Huber, M.I., 1983. *The Techniques of Modern Structural Geology, V 1: Strain Analysis*. Academic Press, New York, N.Y., 307pp.

Rathore, J. S. and Henry, B. 1982. Comparison of strained magnetic fabrics in Dalradian rocks from the southwest Highlands of Scotland. *J. Struct. Geol.*, **4**: 373-384.

Rochette, P. 1987. Magnetic susceptibility of the rock matrix related to magnetic fabric studies. *J. Struct. Geol.* **9**: 1015-1020.

Rochette, P., Jackson, M. and Aubourg, C. 1991. Rock magnetism and the interpretation of anisotropy of magnetic susceptibility. *Reviews of Geophysics*, **30**: 209-226.

Richter, C. 1992. Particle motion and the modelling of strain response in magnetic fabrics. *Geophys. J. Int.*, **110**: 451-464.

Richter, C., van der Pluijm, B. A., Housen, B. A. 1993. The quantification of crystallographic Preferred orientation using magnetic anisotropy. *J. Struct. Geol.* **15**: 113-116.

Richter, C., & van der Pluijm, B. A. 1994. Separation of paramagnetic and ferrimagnetic Susceptibilities using low temperature magnetic susceptibilities and comparison with high field methods. *Phys. Earth Planet. Inter.*, **82**: 113-123.

Robin, P-Y.F., 1977. Determination of geologic strain using randomly oriented strain markers of any shape. *Tectonophysics*, **42**: T7-T16.

Rogers, N., van Staal, C.R., & McNicoll, V., 1999. Recent advances in the geology and structure of the Confederation Lake region, northwestern Ontario. Geological Survey of Canada, *Current Research* **1999-C**: 187-195.

Runnalls, R.J. 1978. Gravity modeling, Red Lake region, N.W. Ontario. Unpublished M.Sc. Thesis, University of Toronto.

Schärer, U., 1989. Age, origin and metamorphic overprint of volcanic and plutonic rocks in the Central Uchi Subprovince, Superior Province, Canada. Geological Association of Canada-Mineralogical Association of Canada, *Program with Abstracts*, **14**: A55.

Schwerdtner, W.M., 1973. Schistosity and penetrative mineral lineation as indicators of paleostrain directions. *Can. J. Earth Sci.*, **10**: 1233-1243.

Schwerdtner, W.M., 1977. Distortion and dilatation in paleostrain analysis. *Tectonophysics*, **40**: T9-T13.

Schwerdtner, W.M., 1995. Local displacement of diapir contacts and its importance to pluton emplacement study. *Journal of Structural Geology*, **17**: 907-910.

Schwerdtner, W.M., 1997. Construction and prospective use of displacement-difference vectors (DDVs) in vertical sections across shear belts: outline of a new method. *In:* Evolution of Geological Structures in Micro- to Macro-scales. Edited by S. Sengupta, Chapman & Hall, London, p.237-242.

Schwerdtner, W.M. 1998. Graphic derivation of local sense of shear strain components in stretched walls of lithotectonic boundaries, *J. Struct. Geol.* **20**: 957-967.

Schwerdtner, W.M., Bennett, P.J., Janes, T.W., 1977. Application of L-S fabric scheme to structural mapping and paleostrain analysis. *Can. J. Earth Sci.*, **14:** 1021-1032.

Schwerdtner, W.M., Morgan, J., Osadetz, K., Stone, D., Stott, G., & Sutcliffe, R.H. 1978. Structure of Archean rocks in Western Ontario. *In:* Smith, I.E.H., & Williams, J.G. (Eds.), *Archean Geotraverse conference*, p.107-126.

Schwerdtner, W.M., Stone, D., Osadetz, K., Morgan, J., & Stott, G.M. 1979. Granitoid complexes and the Archean tectonic record in the southern part of northwestern Ontario. *Can. J. Earth Sci.* **16**: 1965-1977.

Schwerdtner, W.M., Borowik, A., Crews, M.J., Coté, M.L. & Shanks, W.S. 1997. Sense of shear strain components near deformed lithotectonic boundaries imaged by geophysical methods, *Lithoprobe Report* **63**: 67-82.

Schwerdtner, W.M., Crews, M.J., Gaudette, J., Hanley, J.J., Moslehi, H., 1998. Structural analysis at the Woman-Confederation assemblage boundary, western Birch-Uchi Greenstone belt: Progress Report. Ontario Geological Survey, *Miscellaneous Paper* **168:** 57-58.

Schwerdtner, W.M., Crews, M.J., Moslehi, H., 1998. Strain patterns of large Greenstone Belts of Northwestern Ontario and the Archean tectonics controversy: abstract *In: Abstracts with Programs*, 1998 Geological Society of America Annual Meeting, Toronto, **30(7):** A395.

Schwerdtner, W.M., Capes, C., Crews, M.J., Moslehi, H., 1999. Pattern of total strain in western parts of Birch-Uchi Greenstone belt, Northwestern Ontario. ***In:*** Summary of Field Work & Other Activities 1998, Ontario Geological Survey, *Miscellaneous Paper* **169:** 104-108.

Spheristat v.2.0 1995. *Orientation analysis and plotting for MSDOS® computers.* Pangea Scientific Software, Brockville, Ontario, Canada.

Stettler. E.H., de Beer, J.H., Eberle, D., Ludden, J., & Mareschal, M., 1997. Chapter 4.1, Geophysics and Deep Structures. *In: Greenstone belts.* Edited by de Wit, M.J., & Ashwal, L.D., Clarendon Press, Oxford, p.339-375.

Stix, J., and Gorton, M.P., 1989. Physical and chemical processes of Archean subaqueous pyroclastic rocks; in Geoscience Research Grant Program, Summary of Research 1988-1989, Ontario Geological Survey, *Miscellaneous Paper* **143**: 231-238.

Stockwell, C.H., 1973. Revised Precambrian time scale for the Canadian Shield. *Geological Survey of Canada Paper* **72-52**: 4p.

Stott, G.M., 1997. The Superior Province, Canada: *In: Greenstone Belts*, edited by de Wit, M.J., & Ashwal, L.D., Clarendon Press, London, p.480-507.

Stott, G.M. & Corfu, F. 1988. Whither the Kenoran orogeny? *In*: GAC-MAC, Annual Meeting, *Program with abstracts* **13**: A120.

Stott, G.M., Corfu, F., Breaks, F.W. & Thurston, P.C. 1989. Multiple orogenesis in the northwestern Superior Province. *In*: GAC-MAC, annual meeting, *Program with abstracts* **14**: 56.

Stott, G.M., and Corfu, F., 1991. Uchi Subprovince; *In: Geology of Ontario*, Ontario Geological Survey, Special volume **4**, Part 1, p.145-236.

Stowe, C.W., 1974. Alpine-type structures in the Rhodesian Basement Complex at Selukwe. *Q. J. Geol. Soc. Lond.*, **130**: 411-425.

Sun, W., Hudleston, P.J., & Jackson, M., 1995. Magnetic and petrofabric studies in the multiply deformed Thomson Formation, east-central Minnesota. *Tectonophysics* **249**: 109-124.

Talbot, C.J., 1973. A plate tectonic model for the Archean crust. *Philosophical Transactions of the Royal Society of London*, series A, **273**: 413-427.

Tarling, D.H., and Hrouda, F., 1993. *The magnetic anisotropy of rocks*. Chapman & Hall, New York, N.Y., 217pp.

Themistocleous, S.G., & Schwerdtner, W.M., 1977. Estimates of distortional strain in mylonites from the Grenville Front Tectonic Zone, Tomiko area, Ontario. *Can. J. Earth Sci.*, **14**: 1708-1720.

Thomson, J.E., 1939. The Uchi Lake Area. Ontario Department of Mines, *Annual Report for 1938*, **47** Pt.3 p.65-82.

Thurston, P.C., 1978. Geology of the Earngey-Costello Area, District of Kenora (Patricia Portion). Ontario Geological Survey, *Open File Report* **5240**: 210p.

Thurston, P.C., 1980. Subaerial volcanism in the Archean Uchi-Confederation volcanic belt. *Precambrian Research*, **12**: 79-80.

Thurston, P.C. 1981. No.2 western Uchi Sub-Province Synoptic Project. Precambrian-Superior Province. *In*: *Summary of field work* OGS MP **100**: 8-11.

Thurston, P.C., 1981. Volcanology and trace element geochemistry of cyclic volcanism in the Archean Confederation Lake Area, northwestern Ontario. Unpublished PhD Thesis, University of Western Ontario, London, Ontario 553p.

Thurston, P.C., 1985. Physical volcanology and stratigraphy of the Confederation Lake area, District of Kenora (Patricia Portion). *Ontario Geological Survey Report* **236**: 117p. Accompanied by Map 2498.

Thurston, P.C., 1991. Geology of Ontario: Introduction. *In: Geology of Ontario*, Special Volume 4, Part 1, Ontario Geological Survey p.3-25.

Thurston, P.C., Raudsepp, M., & Wilson, B.C., 1974. Earngey Township & Part of Birkett Township, District of Kenora (Patricia Portion). Ontario Division of Mines, *Preliminary Map* **P932**.

Thurston, P.C., & Breaks, F.W. 1978. Metamorphic and tectonic evolution of the Uchi-English River subprovince; *In*: Metamorphism in the Canadian Shield, Geol. Surv. of Can. Paper **78-10**: 49-62.

Thurston, P.C., and Fryer, B.J., 1983. The geochemistry of repetitive cyclical volcanism from basalt through rhyolite in the Uchi-Confederation Greenstone Belt. *Contributions to Mineralogy and Petrology*, **83**: 204-226.

Thurston, P.C., Ayres, L.D., Edwards, G.R., Gélinas, L., Ludden, J.N., & Verpaelst, P. 1985. Archean bimodal volcanism. *In*: Ayres, L.D., Thurston, P.C., Card, K.D., & Weber, W. (Eds.), *Evolution of Archean Supracrustal Sequences*, Geol. Assoc. of Can. Special Paper **28**.

Thurston, P.C., Osmani, I.A., & Stone, D., 1991. Northwestern Superior Province: Review and terrane analysis. *In: Geology of Ontario*, Special Volume 4, Part 1, Ontario Geological Survey p.80-142.

Thomson, J.E., 1939. The Uchi Lake area; Ontario Department of Mines, *Annual Report*, 1939, **47**, pt.3, p.65-82.

Tipper, H.W., Woodsworth, G.J., & Gabrielse, H., 1981. Tectonic assemblage map of the Canadian Cordillera. *Geological Survey of Canada Map* **1505A**.

van Staal, C.R., 1998. Some notes on the assemblage boundaries and internal structure of the Uchi-Confederation greenstone belt, northwestern Ontario; *In: Current Research 1998-C*, Geological Survey of Canada, Paper **98-1C:** 107-114.

Wallace, H., Thurston, P.C., and Corfu, F. 1986. Developments in stratigraphic correlation: Western Uchi Subprovince; in volcanology and mineral deposits, Ontario Geological Survey, *Miscellaneous Paper* **129**: 88-102.

West, G.F., 1976. Geophysics in the geotraverse; p17-21; in Geotraverse Conference, 1976, University of Toronto.

White, D., Forsyth, D., Ndemovic, M., Perron, G., Carroll, P., van der Velden, A., Hall, K., Harrap, R., 1998. 1997 Seismic reflection data acquisition in the Western Superior Transect. *Lithoprobe Report* **65**, University of British Columbia, p.79.

White, D., Forsyth, D., Ndemovic, M., Perron, G., Carroll, P., van der Velden, A., Hall, K., Harrap, R., 1999. 1998 Seismic reflection data acquisition in the Western Superior Transect. Lithoprobe Report ##, University of British Columbia, yy-zz, In Press.

Williams, H.R., 1990. Subprovince accretion area tectonics in the south-central Superior Province. *Canadian Journal of Earth Sciences*. **27**: 570-581.

Williams, H.R., 1991. Variation in Tectonic Style in the Wawa Subprovince. *In: Program with Abstracts*, Geological Association of Canada, Annual Meeting, **16**: A132.

Williams, H.R., Stott, G.M., Thurston, P.C., Sutcliffe, R.H., Bennett, G., Easton, R.M., & Armstrong, D.K., 1991. Tectonic Evolution of Ontario: Summary & Synthesis. *In: Geology of Ontario*, Ontario Geological Survey, Special Volume 4, part 2 p.1255-1332.

Windley, B.F., 1993. Uniformitarianism Today - Plate Tectonics is the Key to the Past. *J. Geol. Soc. Lond.* **150**: 7-19.

Wood, D.S., Oertel, G., Singh, J., and Bennett, H.F., 1976. Strain and Anisotropy in Rocks. *Phil. Trans. R. Soc. Lond.* **A283**: 27-42.

APPENDIX A

A.1 INTRODUCTION

Appendix A contains thin section descriptions of various rock types collected from the western central Birch-Uchi Greenstone Belt (Figure 3). A discussion of the mineralogical and fabric observations listed here can be found in Chapter III. Photographs of relevant features mentioned in appendix A are located in Plates 1 to 8.

A.2 Ultramafic and Mafic metavolcanic rocks

A.3 Metagabbros

A.4 Intermediate metavolcanic and pyroclastic rocks

A.5 Felsic metavolcanic and pyroclastic rocks

A.6 Metasedimentary rocks

SUMMARY OF THIN SECTION PETROGRAPHY

Rock sample localities are shown in Figure 4, Chapter I.

A.2 Ultramafic and Mafic metavolcanic rocks

C3-1
Ultramafic rock

45% carbonate, 40% talc, 10% magnetite, 5% chlorite.

- sparry (dog-tooth) growth of carbonate grains on large carbonate grains with a transition to talc.
- pseudomorphs of magnetite grains - aligned parallel with schistosity trace (lineation).
- talc and smaller carbonate grains are elongate parallel with schistosity (also elongate larger carbonate grains).
- zones perpendicular to schistosity trace with primarily talc (tension gashes? Can see these features in hand specimen).
- penetrative schistosity observable in hand specimen.

A15-1 (A & B)
Mafic metavolcanic

27% quartz, 35% carbonate, 25% chlorite, 10% amphibole, 2% opaques.

- recrystallized quartz throughout (fine grain)
- alternating layers of chlorite rich, chlorite poor with quartz and carbonate define the fabric
- elongate pods of carbonate aggregate - pseudomorphs
- opaque minerals elongate and parallel with fabric (located dominantly with chlorite rich areas
- series of chlorite filled fractures with iron staining throughout
- veinlets of coarse grained quartz subparallel to fractures
- quartz has irregular boundaries and undulose extinction

C8-1A
Mafic metavolcanic

36% plagioclase, 31% amphibole 10% opaques, 12% chlorite, 2% carbonate, 4% sericite, 3% epidote, 2% quartz.

-overall massive igneous texture
- several fracture containing carbonate, epidote and chlorite
- chloritization of amphibole grains
- sericitization of plagioclase grains
- very weak alignment of plagioclase and mafic grains define a weak schistosity
- fractures are subparallel to schistosity

D14-1A
Mafic metavolcanic

10% quartz, 44% carbonate, 13% chlorite, 18% plagioclase, 4% opaques, 11% sericite.

- very fine grained rock
- carbonate, quartz, and opaques are coarser grained in veins and pods
- quartz grains exhibit undulose extinction with sutured grain boundaries
- quartz is cataclastic in veins
- chlorite and sericite and coarse grained carbonate define the schistosity and lineation
- very similar in appearance to C3-1

D12-1A
Mafic metavolcanic

22% sericite, 20% plagioclase, 15% amphibole, 15% chlorite, 10% quartz, 8% opaques, 5% carbonate, 3% biotite, 2% epidote.

- carbonate filled voids
- amphibole grains are both short euhedral grains or long fibrous grains that parallel schistosity.
- long amphibole grains have carbonate and opaques filled fractures that are perpendicular to schistosity, possibly a response to the schistosity producing strain
- chlorite and biotite grains fill voids of previous minerals
- highly sericitized plag. and quartz with chlorite (matrix) define the schistosity.

A.3 Metagabbros

A7
Metagabbro

30% amphibole, 25% clinozoisite, 18% chlorite, 6% plagioclase, 4% epidote, 5% garnet, 4% clinopyroxene, 3% quartz, 3% carbonate, 2% talc, 1% opaques.

- massive orientation of grains
- pods of fine grained quartz and calcite
- intracrystalline deformation of quartz - undulose extinction
- fractures criss-crossing across the slide - filled with chlorite
- interstitial chlorite is fibrous
- quartz is replaced by epidote
- relic plagioclase twins observed
- rock is relatively unstrained
- clinozoisite has undergone garnetization

A6-4A (A4-5A, A2-5A, A1-2A, A6-4A, A7)
Metagabbro

25 (22-30)% clinozoisite, 22 (18-22)% amphibole, 17 (10-17)% plagioclase, 22 (22-32)% chlorite, 3 (3-8)% quartz, 6 (<1-6)% clinopyroxene, 2 (<1-8)% carbonate, 2 (<1-3)% epidote, <1% opaques.

- no observed preferred orientation
- amphiboles chloritized
- plagioclase altered to clinozoisite, partially and completely in areas
- amphibole grains dilated with quartz and chlorite infill (a few grains with a sinistral offset
- quartz recrystallized, in "pods" & interstitial to large grains
- carbonate located with quartz aggregates and are parallel to fracture planes

A5-A
Metagabbro

35% clinozoisite, 24% chlorite, 11% plagioclase, 8% amphibole, 15% clinopyroxene, 4% carbonate, 3% quartz, 1% opaques.

- quartz is dominantly graphic quartz (grew last in remaining space)
- plag grains altered to clinozoisite
- clinozoisite and amphibole grains heavily sericitized
- a few amphibole grains are fresh, unaltered
- fractures run through slide, filled with chlorite
- weakly strain

D19-1A
Quartz-metagabbro

50% amphibole, 20% plagioclase, 15% epidote, 10% quartz, 5% magnetite

- magnetite preferentially follows coarse amphibole grains
- spaced schistosity - weakly aligned amphibole and opaques
- fabric is enhanced by deformation of large grained quartz (undulose extinction - recovery produced slightly elongate grains)
- graphic quartz last to crystallize
- amphibole grains have rims

B1-1A
Metagabbro

50% amphibole, 35% plagioclase, 10% sericite, 4% opaques, <1% quartz.

- no apparent preferred orientation of grains
- opaques located near/in amphibole grains
- fine grained opaques follow amphibole cleavage
- large phenocrystic amphibole and fine grained amphibole aggregates constitute the amphibole presence
- weakly strained

A.4 Intermediate metavolcanic and pyroclastic rocks

F1-2A (A & B)
Intermediate metavolcanic (crystal tuff?)

- carbonate grains scattered throughout matrix
- amygdules of carbonate and fine grained quartz, elongate and parallel to lineation
- sericitized pseudomorphs of plagioclase porphyroblasts
- carbonate is twinned throughout, quartz - undulose extinction
- chlorite and sericite define the schistosity (weak to moderate strain) and pass through both the matrix and phenocrysts

A17-A
Lapilli Tuff

25% sericite, 20% quartz, 15% chlorite, 10% carbonate, 8% plagioclase, 15% feldspar, 7% sphene.

- fractures iron stain and run parallel to fabric trace
- lapilli clasts are aligned and define the strain fabric
- chlorite grains inside lapilli run parallel with schistosity
- quartz vein parallel with lapilli and carbonate
- quartz boundaries are highly sutured indicating late-stage deformation event, grain boundary migration

A.5 Felsic metavolcanic and pyroclastic rocks

F7-1A
Felsic metavolcanic

40% quartz, 20% sericite, 18% plagioclase, 11% feldspars, 4% carbonate, 3% epidote, 2% chlorite, 2% opaques.

- euhedral quartz phenocrysts and fine grained recrystallized quartz
- recrystallized spherulites containing feldspars and quartz
- calcite grains are cut by quartz veins
- primary layering defined by layers of fine grained quartz and darker layers of altered plagioclase
- dark laminae of sericite between quartz grains further define the foliation, possible bedding parallel pressure solution seams

F14-1A
Felsic metavolcanic

38% quartz, 26% sericite, 18% feldspars, 11% amphibole, 5% opaques, 2% epidote, <1% muscovite.

- "zones" and veins of sericite filled grains
- feldspar grains in matrix are sericitized
- quartz has sutured grain boundaries
- recrystallized phenocrysts - quartz, previously plagioclase define a weak foliation
- opaques restricted to quartz rich amygdules

B4-1A
Felsic metavolcanic

28% plagioclase, 25% quartz, 17% feldspars, 13% sericite, 10% chlorite, 5% muscovite, 2% epidote

- fine grained matrix contains quartz, plag, k-spar, chlorite and sericite
- foliation defined by chlorite, quartz and feldspars in matrix and large quartz grained phenocrysts, also locally abundant muscovite
- dark fractures throughout parallel foliation
- cross-cutting set of microfractures run oblique to main set of fractures
- cataclastic texture with coarse quartz grains
- large quartz vein (5mm wide) slightly boudinaged and folded at one end

F13-2A
Felsic metavolcanic

42% quartz, 18% sericite, 18% feldspars, 11% carbonate, 8% chlorite, 3% opaques

- opaques locally abundant
- carbonate is interstitial to quartz

A.6 Metasedimentary rocks

E6-1 (A &B, E2-1)
Marble

84% carbonate, 15% quartz, <1% micas.

- alternating layers define bedding: variable grain sizes
  - coarse grained carbonate
  - fine grained carbonate
- quartz and carbonate grains have sutured boundaries
- coarse carbonate grains are mechanically twinned
- dark laminae parallel to bedding (pressure solution seams)
- seams concentrated between coarse grained carbonate and quartz aggregates
- dilating carbonate veins oblique to seams
- preserved primary features

E7-1
Metasediment

42% sericite, 38% epidote, 15% chlorite, 5% opaques, <1% rutile (brookite)

- fractures parallel with bedding
- elongate epidote grains follow the fractures
- primary layering defined by epidote dominant layers and sericite, epidote-poor layers